2007

Hexaaluminate catalysts for the partial oxidation of middle distillate fuels

Todd H. Gardner
West Virginia University

HEXAALUMINATE CATALYSTS FOR THE PARTIAL OXIDATION OF MIDDLE DISTILLATE FUELS

by

Todd H. Gardner

**Dissertation submitted to the College of Engineering and Mineral Resources
at West Virginia University
in partial fulfillment of the requirements
for the degree of**

**Doctor
of
Philosophy**

Approved by

**Edwin L. Kugler, Ph.D., Chair
Dady Dadyburjor, Ph.D.
Daniel Driscoll, Ph.D.
Charter Stinespring, Ph.D.
Richard Turton, Ph.D.**

Department of Chemical Engineering

**Morgantown, West Virginia
2007**

Keywords: Hexaaluminate, Catalyst, Reforming, Diesel, Nickel, Cobalt, Iron

ABSTRACT

Hexaaluminate Catalysts for the Partial Oxidation of Middle Distillate Fuels

Todd H. Gardner

Studies were conducted on active metals (i.e., Co, Fe and Ni) substituted into the lattice of hexaaluminate compounds to reform liquid hydrocarbon fuels into H_2-rich synthesis gas for fuel cell applications. Both the concentration of active metals substituted into the lattice and the different mirror cations, (i.e., Ba, La and Sr) were investigated for their effect on the catalytic properties of the hexaaluminate compound. In these studies, n-tetradecane was used as a model middle distillate fuel. The synthesized catalysts were characterized by a series of techniques including: N_2 BET surface area, powder XRD, TPR, H_2 pulse chemisorption, bulk elemental analysis by ICP, and surface analysis by XPS.

The catalysts were shown to exhibit $P6_3/mmc$ crystal symmetry which was indicative of the hexaaluminate structure. TPR experiments on the catalysts indicated that the substitution of cobalt, iron and nickel cations into the lattice stabilized their reducibility. The reduction temperature for the nickel series of catalysts correlated with the type of mirror cation substituted into the lattice. H_2 pulse chemisorption performed on reduced nickel hexaaluminate catalysts confirmed that the number of active nickel sites that were reduced in the lattice was influenced by the mirror cation. XPS analysis of $LaNi_{0.4}Al_{11.6}O_{19-\delta}$, $SrNi_{0.4}Al_{11.6}O_{19-\delta}$ and $BaNi_{0.4}Al_{11.6}O_{19-\delta}$ catalysts indicated that the

variation in the nickel surface concentration of the oxide catalysts also correlated with the mirror cation.

The activity of the synthesized catalysts toward the partial oxidation of n-tetradecane was examined by temperature programmed reaction between 750 to 900°C. Iron substituted into the hexaaluminate lattice was shown to exhibit relatively poor catalytic activity and selectivity at all concentrations during the temperature programmed reaction with n-tetradecane. Cobalt substituted into the hexaaluminate lattice at concentrations of $y \leq 0.8$ ($LaCo_yAl_{12-y}O_{19-\delta}$) exhibited equally poor catalytic activity and selectivity. However, the $LaCoAl_{11}O_{19-\delta}$ catalyst exhibited equilibrium CO and H_2 yields.

The $LaNi_yAl_{12-y}O_{19-\delta}$ (y = 0.2, 0.4, 0.8 and 1.0) series and the $M_INi_{0.4}Al_{11.6}O_{19-\delta}$ (M_I = Ba, La and Sr) series of catalysts possessed the greatest H_2 and CO activity and selectivity over the temperature region examined. Both the $LaNi_{0.2}Al_{11.8}O_{19-\delta}$ and the $BaNi_{0.4}Al_{11.6}O_{19-\delta}$ catalysts exhibited sharp increases in H_2 yield at 850 and 875°C, respectively. The increase in H_2 yield in this region corresponded to a decrease in CH_4 yield indicating that the additional H_2 produced was derived from CH_4.

The role that the mirror cation produced on nickel substituted hexaaluminate stability during n-tetradecane isothermal partial oxidation was also examined. Nickel catalysts with Ba^{2+} and Sr^{2+} mirror cations exhibited greater stability during n-tetradecane partial oxidation than did the La^{3+} cation. The catalytic behavior induced by the mirror cation suggested that its influence on controlling carbon deposition was structural.

ACKNOWLEDGEMENTS

I would like to express my thanks to Dr. Edwin L. Kugler, my major professor for his guidance and suggestions throughout the course of this work. Thanks to Dr. Dady Dadyburjor, Dr. Daniel Driscoll, Dr. Charter Stinespring and Dr. Richard Turton, for their service as my doctoral committee members. I would also like to thank the following National Energy Technology Laboratory employees: Mr. Donald Floyd for his valuable encouragement and assistance with this work, Mr. Jim Poston for his assistance with the XPS investigation and Mr. Brett Howard for his assistance with the XRD investigation.

Special thanks go to my wife, Beth, for helping me to realize my dreams. I would like to express my thanks and appreciation for their encouragement to my Father, Dr. Aubrey Gardner, my Mother, Mrs. Anne Lindgren, my Father-in-law, Dr. Thomas Bower and my Mother-in-law Dr. Annabel Bower.

I am so much thankful to my children, Matthew, Brianna, and Grant for their presence around me and giving me the joyful times that make my life more beautiful. To my lovely wife and children, I dedicate this work.

TABLE OF CONTENTS

LIST OF FIGURES

LIST OF TABLES

1.0 INTRODUCTION

This is the era in which air pollution and excessive energy consumption are major problems around the world. A significant source of this problem is distributed power generation systems. Fuel cell power generation technology offers the potential to minimize these effects through ultra-high efficiency energy conversion in compact, high power density systems. An existing market for this technology exists in the light-duty and heavy-duty vehicle transportation markets. However, the use of fuel cell technology for this application requires that they operate on existing middle distillate fuels; such as, diesel and military logistic fuels. The technology issues involved in reforming middle distillate has stimulated research into many different areas of catalysis and, in general, the actual number of catalytic approaches to solve the fuel reforming issues.

An early entry market for long-haul truck transportation has been identified as the diesel-fueled auxiliary power unit (APU). The idling of heavy-duty diesel engines is a common practice in the trucking industry with long distance trucking runs typically including rest periods of between 6 to 8 hours per day. During these periods, the engine remains running at idle to provide heating and cooling for the cab and sleeper compartment, heat to keep the engine warm in cold weather and electricity to power on-board equipment and appliances. The Environmental Protection Agency (EPA) estimates that 500,000 to 1,000,000 trucks will consume a total of 1.2 billion gallons of diesel fuel during rest period idle conditions (1, 2). Engine idling is very inefficient (<10%), which

contributes to the problem. This results in a cost of $1.8 billion in wasted energy, produces 11 million tons of carbon dioxide (CO_2) and approximately 150,000 tons nitrogen oxides (NO_x) per year (2). Fuel cells offer a high efficiency, low emission, and low-noise alternative that would supplant the need for truck engine idle. At efficiencies approaching 50%, fuel cell APUs could dramatically reduce fuel consumption, cost, and pollution emissions.

The reforming catalyst is a crucial component of the APU and must be able to provide a clean, tailored synthesis gas to the fuel cell stack for long-term operation. Key characteristics desired for the APU include low cost, high efficiency, maximum thermal integration, low maintenance intervals and acceptable startup and transient response features. There are several catalytic barrier issues that must be overcome to achieve these characteristics including the reforming of carbon deposition prone fuels, less reactive aromatic compounds and trace concentrations of organic sulfur compounds.

Industrially, catalysis has proven to be the most effective passive system to reform hydrocarbon feedstocks. Its use to directly reform middle distillates is an area of active research and study. Presently, there are catalyst development efforts in industry at Delphi, Johnson-Matthey and Sud-Chemie and at research laboratories including Argonne National Laboratory, National Energy Technology Laboratory, the University of Minnesota and West Virginia University.

The technology of carbon deposition resistance in catalysts has logically followed these pathways:

- The incorporation of alkali (e.g., K, Li) and/or alkaline earth (e.g., Ca, Mg) elements into the structure or on the surface of the support to increase water and CO_2 adsorption and to titrate acidic sites (3, 4);
- The development of bi-metallic alloys (e.g., Pt-Sn) to atomically disperse the catalytically active sites in lower coordination thereby reducing the number of active sites that are responsible for rapidly adsorbing and stabilizing hydrocarbons through multi-point mechanisms (5, 6);
- An increase in the active metal dispersion that imparts electron deficient character to the active metal when in contact with an electron deficient support (11, 51);
- The use of oxygen-ion conducting supports (e.g., CeO_2) that increase the gasification of carbon deposits (7, 8); and
- The use of highly active metals that have fast surface reactions and are intrinsically less prone to forming carbon deposits (e.g., Rh, Ru) (9, 60).

APUs must operate with relatively dry feed since they are mobile and require compactness. Therefore, partial oxidation is preferred over steam reforming or autothermal reforming. The partial oxidation reaction is a self-sustaining exothermic chemical reaction between oxygen and an oxidizable hydrocarbon fuel where the fuel contains C-H-S. The reaction products are heat, hydrogen, carbon monoxide, carbon dioxide and water vapor. Hydrogen sulfide may also be formed from the organic sulfur compounds reacting with oxygen and hydrogen in the feed. Certainly, the reaction and

products are influenced by fuel composition, temperature, pressure and the catalysts employed.

Catalysts which have been designed for partial oxidation influence the reaction by lowering the activation barriers that lead to increased reaction rates, conversions and altered product compositions, including carbon. Both carbon formation and inactive metal sulfide formation have been linked to active sites of high coordination and low dispersion (10, 11, 12, 13). Therefore, the design of a carbon deposition resistant catalyst for middle distillate partial oxidation would have to have active sites that are not only well dispersed, but of low coordination. Macroscopically, these effects are relatively well understood; however, the design of materials that can implement these effects at such severe conditions as those found in partial oxidation is far from complete.

Solid oxide compounds, known as 'hexaaluminates,' have found application industrially, as combustion catalysts (14, 15, 16, 17). Their crystal structure suppresses internal mass diffusion resulting in a refractory oxide that possesses an unusually high resistance to thermal degradation (16, 17). This unique property has resulted in a variety of applications for hexaaluminates which have included nuclear-waste disposal (18), host laser crystals (19), combustion catalysts and catalyst supports (20, 21).

These properties may prove useful in the design of middle distillate partial oxidation catalysts. If transition metals can be doped directly into the structure of hexaalumina, its refractory properties may produce strong interactions between the support and the metal

minimizing sintering and vaporization at high temperatures. If the transition metals are atomically dispersed within its structure, then both carbon deposition resistance and sulfur tolerance may be achieved. A number of simple, inexpensive transition metals may prove to be acceptable high-temperature partial oxidation catalysts when doped into the hexaaluminate structure. These promising and less costly alternatives to noble metals include cobalt, nickel and iron.

2.0 BACKGROUND

2.1 Partial Oxidation Reforming

2.1.1 Catalytic Partial Oxidation

Catalytic partial oxidation is an attractive option for H_2 and CO production from liquid hydrocarbon fuels when compact or mobile fuel processing systems are desirable. This process has the advantage of inherently rapid reforming kinetics with rapid light-off characteristics. Since there is no need to feed water, as in autothermal reforming and steam reforming, partial oxidation reactors are easily integrated into transportation–based, onboard fuel reforming systems. Two major issues that distinguish higher hydrocarbon partial oxidation from methane partial oxidation are the propensity to form coke products on the catalyst, and the presence of residual organic sulfur compounds, such as dibenzothiophene, that are not easily removed through hydrodesulfurization.

In industry, the partial oxidation of heavy liquid petroleum feedstocks is carried out thermally, without the use of a catalyst at temperatures between 1,250 and 1,500°C, and at pressures between 2.5 and 8 Mpa (22). In smaller systems, the introduction of a catalyst is necessary for operational stability, and to reduce the operating and light-off temperatures.

The reactions occurring in the partial oxidation of liquid hydrocarbons are extremely complex. However, overall catalytic partial oxidation reaction can be described by the simple reaction (1):

$$C_nH_m + \frac{n}{2}O_2 \rightarrow nCO + \frac{m}{2}H_2 \quad (1)$$

This is followed by the WGS reaction (2) and methanation reaction (3):

$$CO + H_2O \leftrightarrow CO_2 + H_2 \quad (2)$$

$$CO + 3H_2 \leftrightarrow CH_4 + H_2O \quad (3)$$

The associated temperature rise from reaction (1) also results in the fragmentation of the heavier molecular weight hydrocarbons into lighter ones. These fragments react, in turn, with the steam and carbon dioxide formed by reaction (2) and (3) to form CO and H_2:

$$C_nH_m + nH_2O \rightarrow nCO + \left(n + \frac{m}{2}\right)H_2 \quad (4)$$

$$C_nH_m + nCO_2 \rightarrow 2nCO + 2\left(n + \frac{m}{2}\right)H_2 \quad (5)$$

To avoid excessive fragmentation of the feed, which could result in the formation of unsaturated hydrocarbons and carbon deposits on the catalyst, reactor feed preheat temperatures for liquid fuels must be kept to a minimum. Reaction temperatures are typically in the range of 700 to 900°C. If organic sulfur is present in the feed, then the reactor is typically operated at higher temperatures where metal sulfides are less stable.

The oxygen in the feed initially converts the organic sulfur compounds in the feed into SO_2 that is less detrimental to the catalyst than H_2S.

2.1.2 Thermodynamics

Thermodynamic calculations on the reformate product distribution and carbon formation characteristics for n-tetradecane (n-$C_{14}H_{30}$), a model diesel fuel compound, were examined over the temperature range, 700 to 900°C, and over an O/C ratio of 1 to 1.5 using the Gibbs free energy minimization routine provided in the HSC Chemistry software package (23). The equilibrium amount of each species formed was normalized on the basis of one mole of n-$C_{14}H_{30}$ fed to the reactor.

2.1.2.1 Effect of O/C ratio

The effect that the O/C ratio has on equilibrium carbon formation and product distribution for n-$C_{14}H_{30}$ partial oxidation is shown in Figure 1. The calculation was performed at 850°C and 1 atm. Conversion of n-$C_{14}H_{30}$ was complete over the range of O/C ratios. Thermodynamically, carbon formation is avoidable with O/C ratios greater than 1.1. At an O/C of 1.05, H_2 and CO yields are at their maximum. As the O/C ratio is increased above 1.1, the carbon formation propensity decreases in addition to the methane selectivity which is essentially zero at an O/C of 1.4. The selectivity toward combustion products, CO_2 and H_2O, also increases with a corresponding decline in the selectivity toward H_2 and CO.

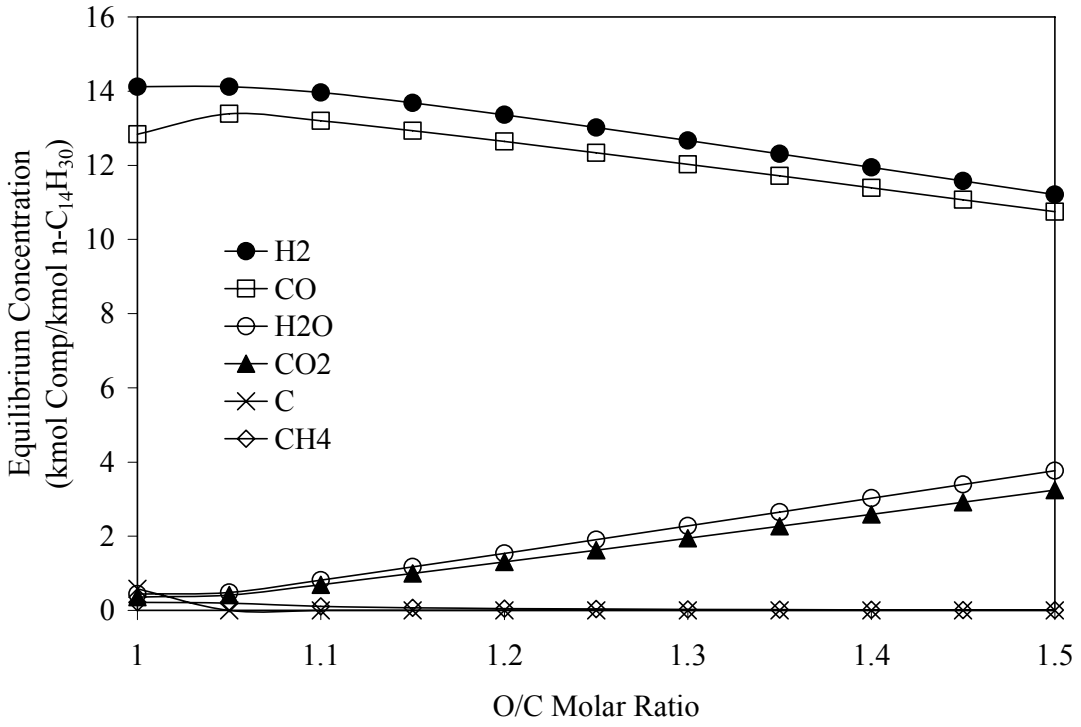

Figure 1. Equilibrium product distribution for the partial oxidation of n-tetradecane at 850°C and 1 atm.

2.1.2.2 Effect of temperature

Figure 2 shows the effect of temperature on n-$C_{14}H_{30}$ partial oxidation, over a temperature range of 700 to 900°C, at an O/C of 1.2, and a pressure of 1 atm. At all temperatures, n-$C_{14}H_{30}$ conversion was complete. H_2 and CO selectivity increases from 700 to 750°C, where a nearly constant selectivity is reached from 750 to 900°C. Carbon formation is avoided by operation above 750°C. From 700 to 750°C, selectivity toward H_2O and CO_2 diminishes. Selectivity toward CH_4 also diminishes from 700 to 825°C, where it essentially reaches zero.

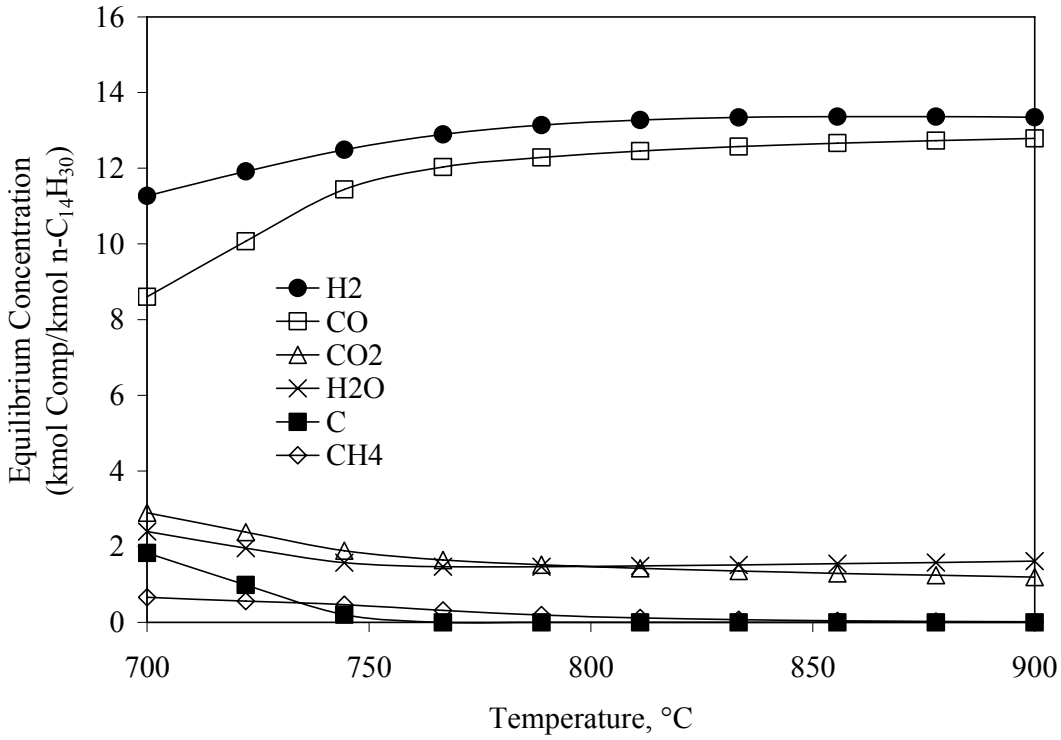

Figure 2. Equilibrium product distribution for the partial oxidation of n-tetradecane at an O/C = 1.2 and P = 1 atm.

2.1.3 Catalysts

This review of the literature encompasses catalysts that have been developed specifically to reform liquid hydrocarbon fuels into synthesis gas.

2.1.3.1 Nickel catalysts

n-Heptane partial oxidation was studied over NiLiLa/γ-alumina by Ran et al. (24). The catalyst was tested over the temperature range of 700 and 850°C at an O/C = 1 and a GHSV of 38,000 $cm^3/g/h$. The LiLa promoter was added to both disperse the nickel over the surface of the catalyst and to titrate active Lewis acid sites on the catalyst surface. This catalyst converted 100% of the n-heptane in the feed and produced 93% hydrogen selectivity over a period of 4 hours. Similar results were obtained from n-heptane POx when the catalyst LiLaNiO/γ-Al_2O_3 was combined with a dense oxygen permeation membrane $Ba_{0.5}Sr_{0.5}Co_{0.8}Fe_{0.2}O_3$ that supplied pure O_2 for the reaction (25). The hydrogen selectivity of Ni/γ-alumina, also tested in this study, dropped to 30% after 4 hours (24). It was also mentioned that the nickel-based catalysts maintained their stability under harsh conditions over time.

2.1.3.2 Noble Metal Catalysts

Rh-based catalysts have been investigated on different supports, resulting in different H_2 and CO yields. Gasoline and naphtha partial oxidation over a supported Rh catalyst

were reported by Fujitani et al. (26). For γ-alumina supported Rh catalyst, maximum yields of 96% of both H_2 and CO were reported with 0.2 wt% Rh loading at 700°C, an air equivalence ratio (i.e., the ratio of the fuel-to-oxidizer ratio to the stoichiometric fuel-to-oxidizer ratio) of 0.41, and liquid hourly space velocity (LHSV) of 2 h^{-1}. Whereas, 0.05 wt% Rh supported on zirconia yielded 98% H_2 and 85% CO at 725 °C, an equivalence ratio of 0.41, and a LHSV of 2 h^{-1}. However, 0.1 wt% Rh loaded on a honeycomb structure of α-alumina-magnesia gave the highest yield of H_2 and CO (both 98%) at 820°C, air equivalence ratio of 0.41, and a LHSV of 2 h^{-1}. Furthermore, carbon deposition was not observed with these supported Rh catalysts.

Tanaka et al. (27) have reported that gasoline partial oxidation over Rh, Pt, and Pt-Rh is promoted by alkali metals (Li) and alkaline earth metals (Ba, Ca, K) supported on magnesium aluminate spinel. The catalysts were tested isothermally at 800°C at an air to fuel ratio of 5.1, and a GHSV of 50,000 h^{-1}. Li, Mg and MgLi promoters were added to Pt supported on $MgAl_2O_4$ spinel. All catalysts produced similar H_2 and CO reformate concentrations of 23 vol% and 25 vol%, respectively. There was a discernable difference in the carbon deposition. The unpromoted Pt catalyst showed carbon levels of 0.02 wt% carbon, where the alkali and alkaline earth promoted Pt catalysts had carbon levels of 0.01 wt%.

In another study by the same group (27), K, Ca and CaK promoters were added to Rh supported on $MgAl_2O_4$ spinel. The modified catalysts and the unmodified catalysts produced similar H_2 and CO reformate concentrations of 23 vol% and 25 vol%,

respectively. The different modifiers did produce an effect on carbon formed on the catalyst. The un-promoted Rh catalyst showed carbon levels of 0.03 wt% carbon, whereas the RhK catalyst had 0.02 wt% carbon, the RhCa catalyst had 0.015 wt% carbon and the RhCaK catalyst had the lowest concentration of carbon at 0.01 wt%. Bi-metallic PtRh with Li, Ba and LiBa modifiers supported on $MgAl_2O_4$ spinel were also examined for H_2 and CO selectivity and carbon formation resistance. There was no significant difference in H_2 and CO yields. The unpromoted PtRh catalyst produced 22 vol% H_2; the promoted catalysts produced 23 vol% H_2 concentrations. Carbon monoxide levels for all catalysts tested were 25 vol%. The different modifiers did affect carbon formed on the catalyst. The unpromoted PtRh catalyst showed carbon levels of 0.01 wt% carbon, where the promoted PtRh catalysts all showed reduced coking levels of 0.005 wt%.

The partial oxidation reaction has also been studied using reactors with very short contact times. Cyclohexane, n-hexane, n-octane, n-decane, n-hexadecane, isooctane, toluene, naphthalene, and gasoline partial oxidation has been studied over Rh-based monolithic catalysts at millisecond contact times (28, 29, 30, 31). Several factors affect the conversion and selectivity of these fuels. The mean cell density, typically defined as pores per inch (ppi) for foam materials [e.g., 40 ppi corresponds to a mean cell diameter of ~0.6 mm], significantly affected the syngas selectivities, but the gas space-velocity did not. The density of the catalytic pores within the monolith were shown to significantly affect syngas selectivity. The higher density 80-pore per inch (ppi) washcoated alumina monolith containing 5 wt% Rh catalyst was proved to be the best for the partial oxidation of hydrocarbons. A higher conversion of fuels (>95%) and syngas yields >90% were

obtained even at higher space velocities (3,000,000 h^{-1}). The partial oxidation of commercial grade gasoline yielded 75% CO_x selectivity to CO, but the sulfur and metal contaminants present in gasoline poisoned the catalyst over time. Partial oxidation of a 75% isooctane / 25% toluene blend was conducted to simulate the aromatics contained in fuels. The lower conversion of toluene compared to isooctane was attributed to the absence of secondary or tertiary C-H bonds that facilitate adsorption and reaction. The transient light-off experiments showed that the steady state temperature can be attained from ambient conditions in less than 5 seconds in these millisecond catalytic partial oxidation reactors using homogeneous combustion to rapidly heat the catalyst.

Krummenacher et al. (32) have reported syngas selectivities greater than 80% with greater than 99% conversion of hydrocarbons from the catalytic partial oxidation of diesel components, n-decane and n-tetradecane, over a Rh-coated monolith at 5 to 25 millisecond contact times. Partial oxidation of a high grade diesel fuel (10 ppmw sulfur, 8% aromatics, 90% alkanes) produced syngas at greater than 98% fuel conversion. Maximum selectivities of H_2 and CO observed were 70% and 80%, respectively, at an O/C ratio of 1.4 and a 25 millisecond contact time.

2.2 Catalytic Materials

2.2.1 Hexaaluminate Catalysts

Hexaaluminate related materials are of importance in many application fields, such as supersonic conductors (33), host crystals for fluorescence lasers (19), nuclear waste storage (19) and as catalyst supports (20, 21). Recently, these materials have attracted considerable attention for the combustion of methane due to their heat resistance in high temperature applications (16, 17). Hexaaluminate compounds can be divided into two types, i.e., magnetoplumbite and β-alumina, according to the ionic configuration of the mirror plane. Both structures possess similar physico-chemical properties. Ideal magnetoplumbite and β-alumina are shown in Figure 3 (32). Hexaalumina has the general formula $M_IO{\cdot}6(Al_2O_3)$. The substitution of a variety of transition metals into the hexaaluminate lattice has been reported (33, 34, 35). Substitution can occur at the mirror plane cation, M_I, or at the aluminum site, M_{II}. When the lattice is doped at both the M_I and M_{II} site, the general formula may be expressed as $M_I(M_{II})_yAl_{12-y}O_{19-\delta}$.

The structure of hexaalumina is comprised of alternative stacks of Al-O 'spinal blocks' that are four oxide layers thick and are stacked in a cubic stacking sequence. Adjacent spinel blocks are separated by a fifth layer that is oxygen-deficient. This monatomic layer is the mirrored plane in which larger cations that charge balance the spinel block reside. Mono-, di- and tri-valent mirror cations can be accommodated. The oxygen atoms within this plane are less tightly bound than oxygen present in the spinel

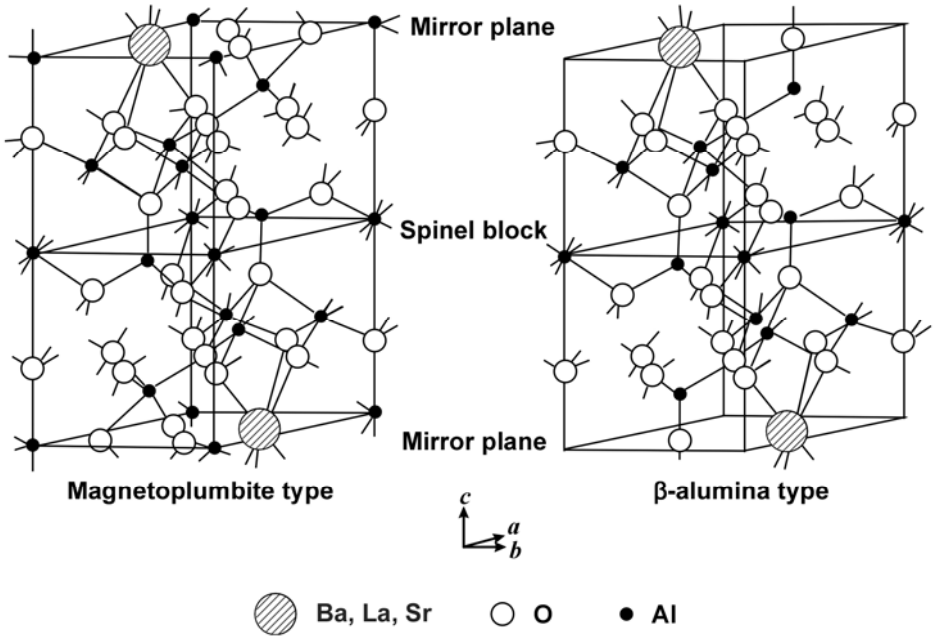

Figure 3. Ideal unit cell structure of magnetoplumbite and β–alumina.

block (37). Anisotropy in oxygen diffusion has been shown to occur in the c-direction within this plane (37). This property is responsible for the evolution of a planar morphology in the β-alumina crystals which retains a high surface area at high temperatures (38).

It is likely that the suitability of an active transition metal substituted solid oxide, as a reforming catalyst, lies in its unique crystalline structure. It is anticipated that the introduction of transition metals into the hexaaluminate lattice will result in well dispersed active sites that are less susceptible to sintering, vaporization and carbon deposition.

2.2.2 Physico-Chemical Properties of Hexaaluminate Constituents

The physico-chemical properties (23, 40) of hexaaluminate catalyst constituents are given in Tables 1 and 2. The spinel block components consist of catalytically active metals: nickel, cobalt and iron and the structural components: aluminum and oxygen. The properties of the mirror plane cations are given in Table 2. Transition metals that are reported in the literature as incorporating into the hexaaluminate lattice are either di-valent or tri-valent. In the present work, it was anticipated that iron will substitute into the lattice as Fe^{3+} which suggests that two O^{2-} anions will need to be stripped from the lattice for iron to achieve a reduced state. However, Co^{2+} and Ni^{2+} are not multivalent cations and require the loss of only one O^{2-} anion to achieve a reduce state.

To be soluble in the hexaaluminate lattice, transition metal cations must possess ionic radii which are comparable to that of Al^{3+}. In this study, the catalytically active transition metal cations selected possess ionic radii which range between 0.69 and 0.72 Å and are all greater than Al^{3+}. For a cation to substitute into the mirror plane position, its ionic radius must be significantly larger than that of Al^{3+}. In this study, mirror cations were selected based on their valence state and ionic radii.

Table 1. Physico-chemical properties of spinel block components.

Property	**Al**	**O**	**Co**	**Fe**	**Ni**
F.W. (g/g·mol)	26.98	16.00	58.93	55.84	58.69
Most stable oxidation state	3+	2-	2+	3+	2+
Ionic Radii (Å)	0.51	1.36	0.72	0.74	0.69

Table 2. Physico-chemical properties of mirror cations.

Property	**La**	**Ba**	**Sr**
F.W. (g/g·mol)	138.91	137.33	87.62
Most stable oxidation state	3+	2+	2+
Ionic Radii (Å)	1.02	1.34	1.12

2.3 Middle Distillate Fuel Composition and Properties

2.3.1 Middle Distillate Composition

Diesel fuel contains literally hundreds of hydrocarbon components. To determine a suitable model diesel fuel compound, a representative low sulfur No. 2 diesel fuel (mfr: Conoco-Phillips) was analyzed by GC-MS to determine its major organic components. The concentrations of the major organic components are reported in Table 3 by their organic group.

No. 2 diesel fuel was determined to contain: 76.76 wt% paraffin, with the highest concentration occurring as normal paraffin in the C_{14} range; 13.63 wt% mono-aromatic, with the high concentrations in both benzene and tetralin in the C_{12} range; and 8.79 wt% di-aromatic compounds, with high concentrations in both napthalenes and acenaphthenes in the C_{12} to C_{15} range. Overall, n-tetradecane was present in the highest concentration above other diesel constituents. From this analysis, n-tetradecane was selected as the most appropriate No. 2 diesel fuel model compound.

2.3.2 Physico-Chemical Properties of n-Tetradecane

The physico-chemical properties of n-tetradecane are given in Table 4 (40). These properties were crucial to the research effort. n-Tetradecane density was utilized in the

calculation of HPLC pump flow rates and the reactor preheat temperature was set well above the n-tetradecane boiling point to ensure proper fuel vaporization.

Table 3. Diesel fuel composition.

Organic Group	**Concentration (wt%)**
Paraffins:	38.13
Cyclo-paraffins:	38.63
Mono-aromatics:	13.63
Di-aromatics:	8.79
Tri-aromatics:	0.82
Total	100.00

Table 4. Physico-chemical properties of n-tetradecane.

Property	**n-Tetradecane**
Chemical Formula	n-$C_{14}H_{30}$
F.W. (g/g mol)	198.40
Density (g/mL)	0.7628
Boiling point (°C)	253.7

3.0 RESEARCH OBJECTIVE

The objective of this research was to investigate the catalytic properties of hexaaluminate catalysts for the partial oxidation of middle distillate fuels using n-tetradecane as a model fuel compound.

The goal was to prepare catalysts that exhibited useful catalytic activities for the partial oxidation reaction and to achieve a fundamental understanding of catalyst structure and surface properties and how they relate to observed activity, selectivity and carbon deposition resistance. The control variables investigated were: catalytic metal type, the concentration of catalytic metal substitution and the mirror cation type.

The following topics have been investigated in this work:

1. The feasibility of using transition metal substituted hexaaluminate catalysts for the partial oxidation of middle distillate fuels using n-tetradecane as a model compound.

2. The cobalt, iron and nickel substituted hexaaluminate catalysts were characterized by phase, surface and bulk techniques.

3. The relationship between key chemical and physical properties of cobalt, iron and nickel substituted lanthanum hexaaluminate catalysts and their activity as expressed by H_2, CO, CO_2 and CH_4 yields for the temperature programmed partial oxidation of n-tetradecane.

4. The relationship between the mirror cation (M_I = Ba, La and Sr) and $M_INi_{0.4}Al_{11.6}O_{19-\delta}$ catalyst stability as expressed by H_2, CO, CO_2 and CH_4 yields.

5. The relationship between the type of mirror cation and carbon deposition over $M_INi_{0.4}Al_{11.6}O_{19-\delta}$ catalysts as expressed by the carbon present on the catalyst surface and the temperature programmed oxidation burn-off profiles.

4.0 EXPERIMENTAL METHODS

4.1 Catalyst Synthesis

Transition metal substituted hexaaluminate catalysts have been reported in the literature as having been synthesized using a variety of liquid phase techniques including: co-precipitation (41), the alkoxide method (42) and solid-state mixing of carbonate powders (43). Generally, liquid phase synthesis techniques have proven quite effective in achieving a homogeneous dispersion of each element at the atomic level.

In this investigation, a liquid phase technique known as co-precipitation was utilized to synthesize the hexaaluminate catalyst samples. Catalysts were prepared by first dissolving nitrate precursor salts in 300 mL of de-ionized water at 60°C. In a separate beaker, a sufficient amount of ammonium carbonate was added to 300 mL of de-ionized water to neutralize the nitrates. The ammonium carbonate solution was then heated and maintained at 60°C. Once both solutions had reached 60°C, the nitrate solution was then added drop wise, over the course of 30 minutes, to the ammonia carbonate solution under vigorous mixing conditions.

The initial pH of the ammonia carbonate solution and the nitrate solutions was 8.5 to 9.0 and 1 to 2, respectively. The nitrate solution was then added to the ammonia carbonate solution until a pH of 7.5 was achieved. The resultant gel was then aged at 60°C under vigorous mixing for six hours. After aging, the gel was then separated by

vacuum filtration and rinsed three times with deionized water to remove excess nitrate. The filtered gel was then dried overnight at 110°C, crushed and finally calcined. Samples were calcined at a temperature of 1250°C for two hours.

With the synthesis method utilized here, the metal nitrate solution was added to a mild basic solution containing ammonium carbonate. This procedure proved useful since it avoided the sequential precipitation which was observed to have occurred when the ammonium carbonate solution was added to the acidic metal nitrate solution. Additionally, the use of a mild base has proved useful from the standpoint that Ni^{2+} cations have been reported as having a wide solubility over a range of pH (44). Co-precipitating with a strong base and at high pH would likely have resulted in incomplete nickel precipitation.

Four different series of hexaaluminate, $M_I(M_{II})_yAl_{12-y}O_{19-\delta}$, catalysts were prepared. The first three series were synthesized with M_I = La at four levels of M_{II} (M_{II} = Co, Fe, Ni) substitution, y = 0.2, 0.4, 0.8 and 1.0. The final series examines the effect of M_I cation type, at a fixed level of M_{II} = Ni substitution, y = 0.4.

4.2 Catalyst Characterization

The hexaaluminate catalysts were subjected to a variety of characterization techniques.

4.2.1 BET Surface Area

N_2 BET surface area was determined using a Quantachrome Surface Area Analyzer 2000. The surface areas were measured after varying calcination time and temperature.

4.2.2 Phase Analysis by Powder X-ray Diffraction

Powder X-ray diffraction (XRD) was used to identify the phases present in each of the catalyst samples. The instrument used was a PANalytical X'Pert PRO model XRD, utilizing filtered monochromatic CuK_α radiation. The XRD instrument was operated at 50 kV and 30 mA. The spectra were scanned between 5 and 75° (2θ) at a rate of 2.4° per minute. Sample preparation consisted of mild grinding in an agate mortar and pestle prior to mounting the samples on a glass sample cell.

4.2.3 Temperature Programmed Reduction

Temperature programmed reduction was utilized to characterize the reductive stability of the hexaaluminate catalysts. The instrument used was a Micromeritics ASAP 2910 automated catalyst characterization system. The catalysts, as prepared in their oxide state, were heated from ambient to 1100°C at a rate of 10°C per min in a binary gas mixture containing 5.15 vol% H_2 and argon (Ar). The reductive stability of each catalyst was assessed by reporting the reduction peak temperature.

4.2.4 Catalyst Dispersion by H_2 Pulse Chemisorption

The number of reduced nickel sites present in each catalyst was determined by H_2 pulse chemisorption measurements. The instrument used was a Micromeritics ASAP 2910 automated catalyst characterization system. The $LaNi_{0.4}Al_{11.6}O_{19-\delta}$, $SrNi_{0.4}Al_{11.6}O_{19-\delta}$ and $BaNi_{0.4}Al_{11.6}O_{19-\delta}$ catalysts were heated from ambient to 1000°C at a rate of 15°C/min in a 50 sccm flow of 5.15 vol% H_2 in Ar to reduce nickel present in the hexaaluminate lattice. The sample was held at 1000°C until a stable baseline was achieved. After reduction, the reaction cell was immediately purged with 50 sccm of Ar while bringing the sample to 1050°C. This additional heating of the sample to 1050°C in the Ar purge gas was performed to clean the catalyst surface of any remaining adsorbed H_2. The sample was then held at 1050°C until a stable baseline was achieved before cooling to 50°C. Next, H_2 pulse chemisorption was performed to determine the volume

of H_2 adsorbed. The volume of H_2 adsorbed was taken to be proportional to the number of reduced nickel sites present in the lattice.

4.2.5 Catalyst Bulk Composition by Inductively Coupled Plasma Emission Spectroscopy

Inductively Coupled Plasma (ICP) Emission Spectroscopy was utilized to determine the bulk composition of the hexaaluminate catalysts. The instrument used was a Perkin Elmer Optima 3000 ICP spectrometer. Analyte standards were obtained from Alfa Aesar. Samples were first digested by mixing 0.1 gram of sample with 1.0 gram of lithium tetraborate and heating in a platinum crucible at 950°C for 20 minutes. The crucibles were then cooled to room temperature and submerged in a dilute HCl solution to dissolve the melt. The solution was taken to volume with water to give a clear sample solution. This procedure was performed in duplicate with the average taken as the final value. Sample precision was determined to be within ± 2% for all samples.

4.2.6 Catalyst Surface Composition by X-ray Photoelectron Spectroscopy

X-ray photoelectron spectroscopy (XPS) spectra were recorded with a cylindrical mirror analyzer with a 15 kV X-ray source (Perkin-Elmer TNBX). The system consisted of separately pumped preparation and detection chambers which were operated within a pressure range of 10^{-9} to 10^{-8} Torr. The detector angle used was 54.7°. The instrument was calibrated by using the following photo emission lines: $E_B(Cu\ 2p_{3/2}) = 932.4$ eV,

$E_B(Au\ 4f_{7/2})$ = 83.3 eV. The binding energies were referenced to the C(1s) level at 284.6 eV for adventious carbon. Spectra were recorded at low X-ray fluxes both at 15 kV and 22 mA and 12 kV and 10 mA in order to avoid X-ray induced reduction. The sensitivity factors for the elements under study are given in Table 5 (45).

Table 5. Sensitivity factors for hexaaluminate constituents.

Element	Sensitivity Factor
Al^{3+}	0.234
La^{3+}	9.122
Ba^{2+}	7.469
Sr^{2+}	1.843
Ni^{2+}	4.044

4.3 Reaction Studies

4.3.1 Reaction System

Reaction studies were carried out in a micro-reactor (Autoclave, Model No. BTRS-Jr) equipped with an 8 mm I.D. reaction cell made of Incoloy 800 HT. Nitrogen and air feed gases were delivered by thermal mass flow controllers (Brooks, Model No. 5890E). Liquid feed was delivered by a high accuracy HPLC metering pump (Dionex, Model No. P 680A HPG). Gas phase product identification was made by a scanning magnetic sector mass spectrometer (ThermoOnyx, Model No. VG Prima). A process flow diagram of this reaction system setup is shown in Figure 4.

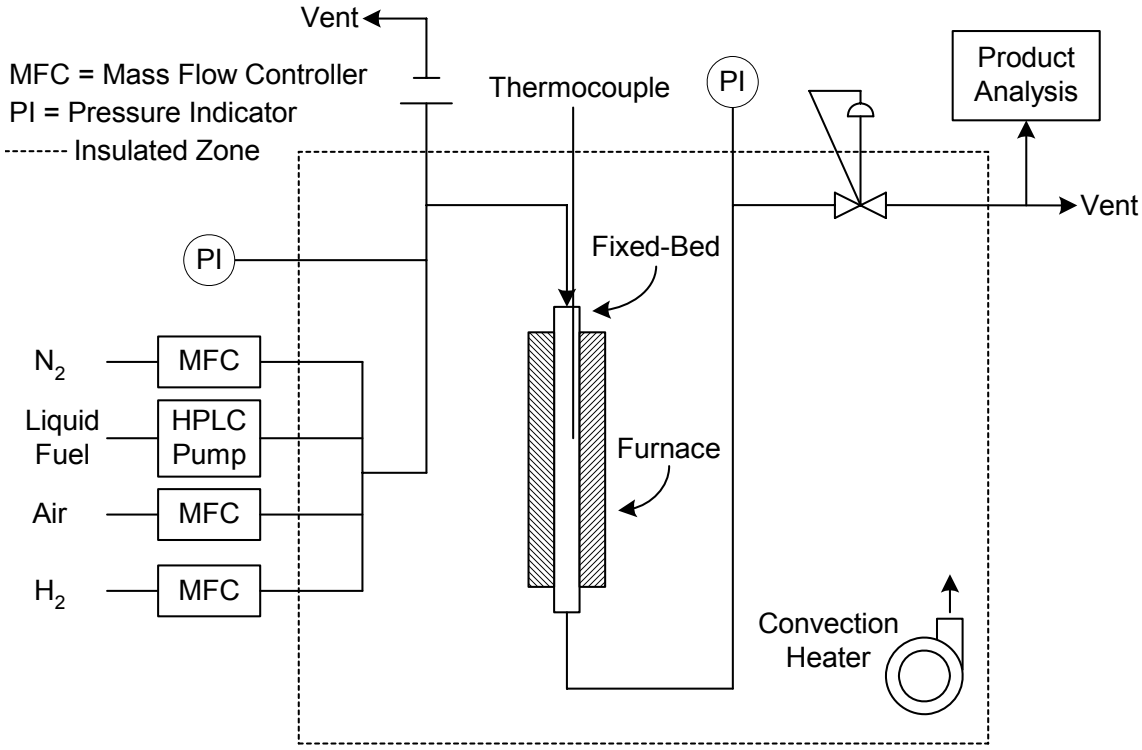

Figure 4. Process flow diagram of reaction system.

5.0 CATALYST CHARACTERIZATION

5.1 Introduction

In order to relate catalyst structure to performance, a number of analytical techniques were employed to fully characterize the synthesized transition-metal-substituted hexaaluminate catalysts.

5.2 Experimental

The experimental details for characterization of the hexaaluminate catalysts are given in Section 4.2. The analyses performed on these catalysts include: N_2 BET surface area, average pore size, phase analysis by powder XRD, reduced metal sites by H_2 pulse chemisorption, temperature programmed reduction, surface composition by XPS and bulk composition by ICP spectroscopy.

5.3 Results and Discussion

5.3.1 Surface Area and Average Pore Size

Two of the most fundamental properties of a catalyst are its surface area and average pore size. The textural properties of the synthesized hexaaluminate catalysts are given in Table 6. The surface area of hexaaluminate compounds is derived from the formation of

crystals with planar morphology that is evolved from oxygen diffusion through the mirrored planes during the heat treatment process (37). The planar morphology of the compound is responsible for their excellent high temperature stability (37). In hexaalumina, the specific surface area has been shown to correspond well to the aspect ratio (width/thickness) of the crystallite (38). Several variables influence the final surface area of the calcined hexaaluminate catalysts including: 1) the gel aging process during co-precipitation, 2) oxygen diffusion within the mirror plane of the catalyst as well as 3) the substitution of catalytic metals into the lattice which influences the packing structure in the spinel block. The obtained surface areas are within a narrow range from 9.9 to 26.3 m^2/g. There is no discernable trend between the concentration of metal substituted into the lattice or metal type. However, the nickel hexaaluminate catalysts that were substituted with divalent mirror cations, Ba^{2+} and Sr^{2+}, did produce noticeably lower surface areas than the trivalent mirror cation, La^{3+}, catalyst.

The pore structure that evolved during calcination of the catalysts was also examined. The BJH average pore diameters for the $LaCoAl_{11}O_{19-\delta}$, $LaFeAl_{11}O_{19-\delta}$, $LaNiAl_{11}O_{19-\delta}$ catalysts, as reported in Table 6, were between 522 and 564 Å. The distribution was narrow between the samples. The data suggested that both meso- and macro-pores were predominantly formed during the heat treatment process which was used to produce the hexaaluminate phase.

Table 6. Textural properties of $M_I(M_{II})_yAl_{12-y}O_{19-\delta}$ catalysts calcined at 1250°C for 2 hours.

Catalyst	Surface Area (m^2/g)	BJH Average Pore Diameter (Å)
$LaCo_{1.0}Al_{11}O_{19-\delta}$	13.2	-
$LaCo_{0.8}Al_{11.2}O_{19-\delta}$	26.3	-
$LaCo_{0.4}Al_{11.6}O_{19-\delta}$	21.2	-
$LaCo_{0.2}Al_{11.8}O_{19-\delta}$	23.8	-
$LaFe_{1.0}Al_{11}O_{19-\delta}$	11.6	522
$LaFe_{0.8}Al_{11.2}O_{19-\delta}$	13.3	-
$LaFe_{0.4}Al_{11.6}O_{19-\delta}$	20.1	-
$LaFe_{0.2}Al_{11.8}O_{19-\delta}$	25.4	-
$LaNi_{1.0}Al_{11}O_{19-\delta}$	9.9	564
$LaNi_{0.8}Al_{11.2}O_{19-\delta}$	15.7	-
$LaNi_{0.4}Al_{11.6}O_{19-\delta}$	22.6	-
$LaNi_{0.2}Al_{11.8}O_{19-\delta}$	21.4	-
$BaNi_{0.4}Al_{11.6}O_{19-\delta}$	14.3	-
$SrNi_{0.4}Al_{11.6}O_{19-\delta}$	16.2	-

5.3.2 Phase Analysis by Powder X-ray Diffraction

The formation of the hexaaluminate phase is of prime concern. The literature reports a number of powder XRD studies that have been performed to determine the effect of the mirror cation and active metal on the formation of the hexaaluminate phase (46, 47). Changes in the crystalline phase of hexaalumina that were induced by the substitution of various cations into the mirror plane have been reported by Inoue et al. (48). However, relatively little work has been reported on the effect of the substitution of different active metals and their concentration within the hexaaluminate lattice.

In this study, the predominant phases present within the synthesized catalysts were identified. The effect of increasing the substitution of active metals into the hexaaluminate lattice on crystalline phase formation was examined. Also examined, was the effect that the substitution of different mirror cations into the lattice produced on crystalline phase formation. The compounds under study included: $La(M_{II})_yAl_{12-y}O_{19-\delta}$ (M_{II} = Co, Fe and Ni with y = 0.2, 0.4, 0.8 and 1.0) and $M_INi_{0.4}Al_{11.6}O_{19-\delta}$ (M_I = Ba and Sr) catalysts. All samples were calcined at the same conditions, for exactly 2 hours at 1250°C, to normalize the comparison between samples.

Figures 5, 6 and 7 give the powder XRD patterns for $LaCo_yAl_{12-y}O_{19-\delta}$, $LaFe_yAl_{12-y}O_{19-\delta}$ and $LaNi_yAl_{12-y}O_{19-\delta}$ at the different active metal (y = 0.2, 0.4, 0.8 and 1.0) substitutions. Phase identification of the hexaaluminate compounds was made based on the reference peak positions obtained from [JCPDS: 33-0699] for $LaAl_{11}O_{18}$ which

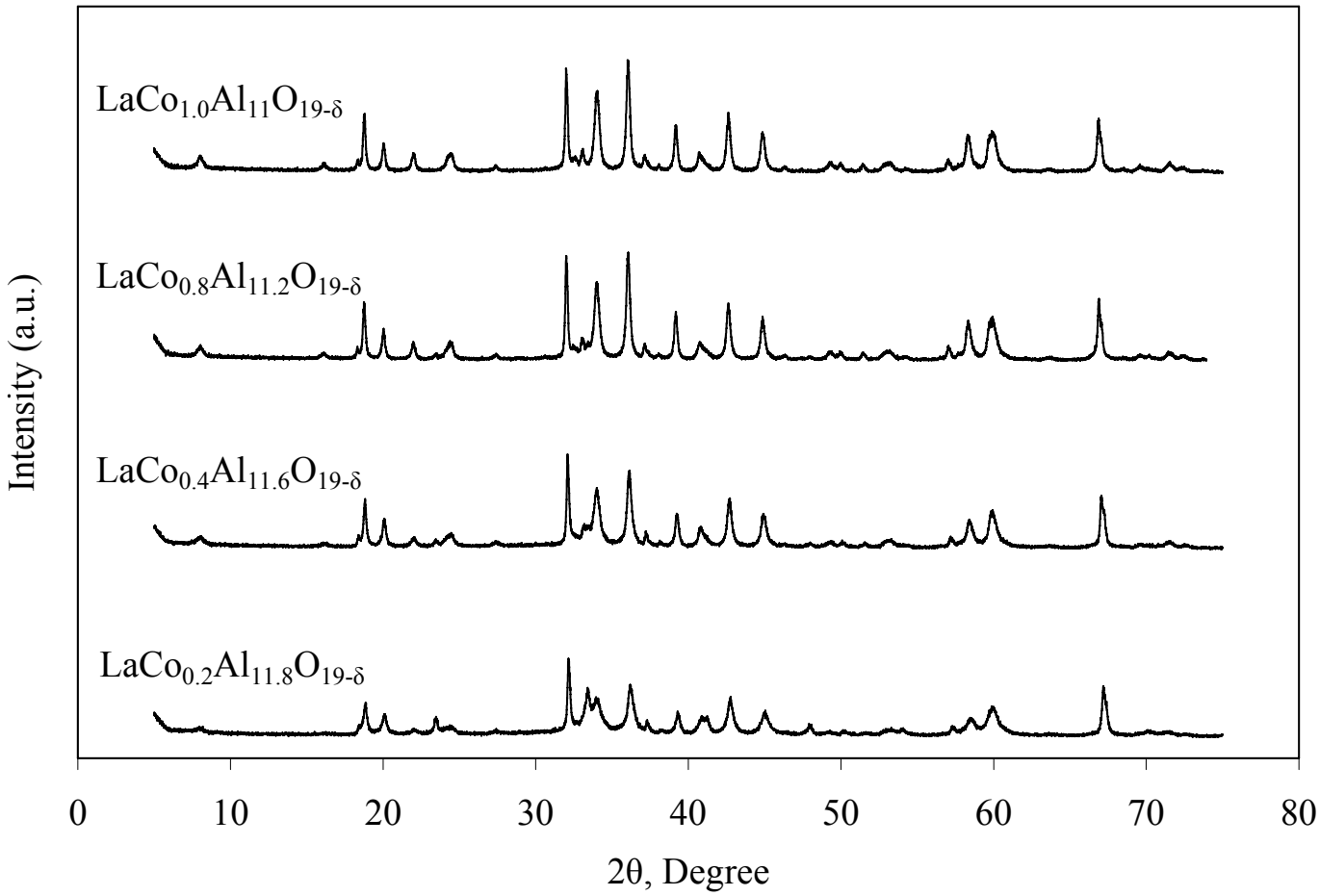

Figure 5. Powder XRD spectra of $LaCo_yAl_{12-y}O_{19-\delta}$ (y = 0.2, 0.4, 0.8 and 1.0). The effect of cobalt substitution on phase formation.

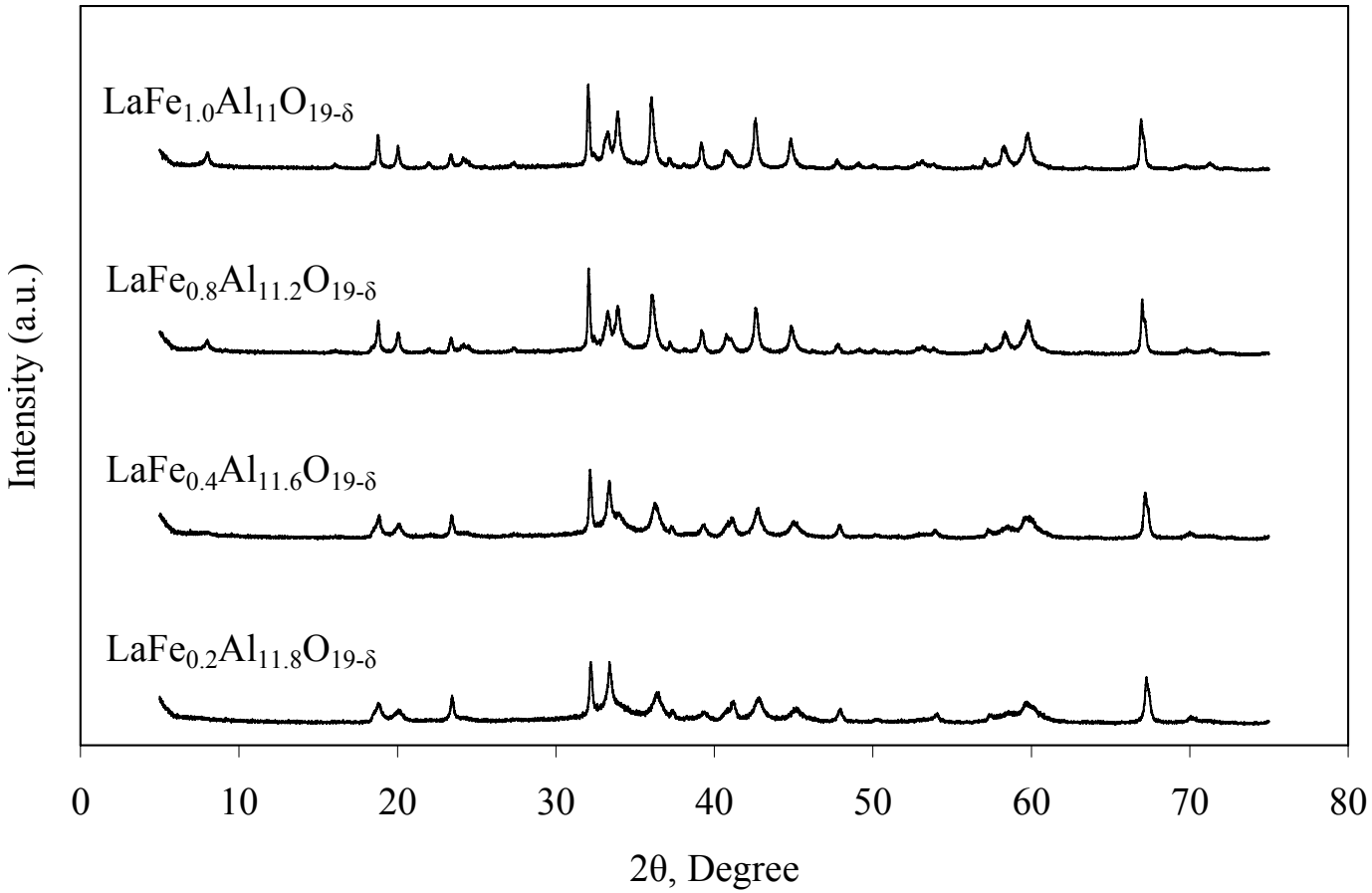

Figure 6. Powder XRD spectra of $LaFe_yAl_{12-y}O_{19-\delta}$ (y = 0.2, 0.4, 0.8 and 1.0). The effect of iron substitution phase formation.

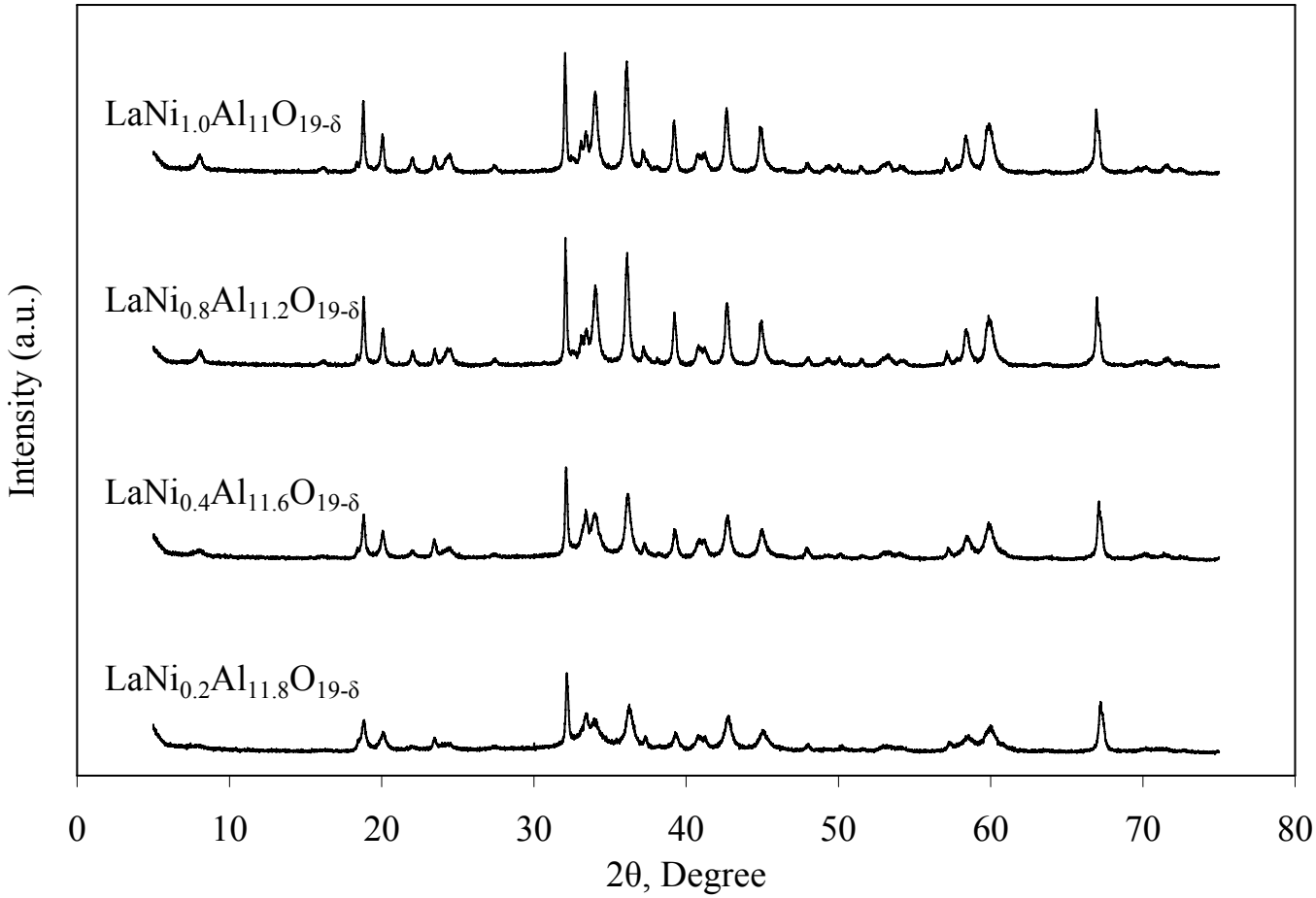

Figure 7. Powder XRD spectra of $LaNi_yAl_{12-y}O_{19-\delta}$ (y = 0.2, 0.4, 0.8 and 1.0). The effect of nickel substitution on phase formation.

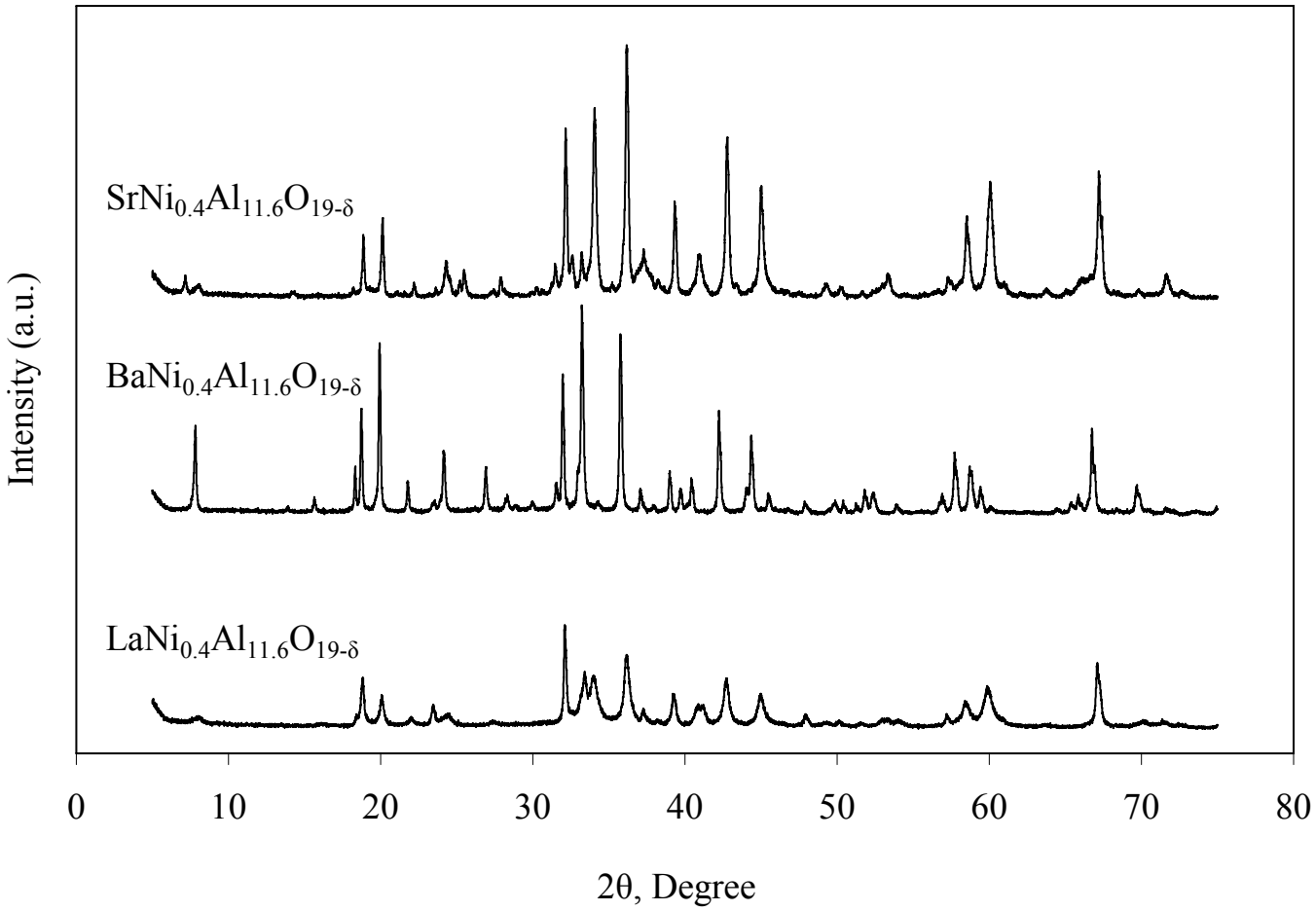

Figure 8. Powder XRD spectra of $M_INi_{0.4}Al_{11.6}O_{19-\delta}$ (M_I = Ba, Sr and La). The effect of mirror cation on phase formation.

possessed $P6_3/mmc$ crystal symmetry. Characteristic hexaaluminate peaks for the $LaCo_yAl_{12-y}O_{19-\delta}$ series of catalysts were located at 2θ = 18.8, 20.0, 24.5, 32.0, 33.1, 34.0, 36.1, 39.2, 42.6, 44.8, 58.3 and 66.86°. A minor unidentified phase was observed to be located at 2θ = 51.5°. The $LaFe_yAl_{12-y}O_{19-\delta}$ series of catalysts exhibited characteristic hexaaluminate peaks located at 2θ = 8.0, 18.8, 20.0, 32.0, 33.3, 33.9, 36.0, 39.2, 40.7, 42.6, 44.8 and 66.9°. Minor unidentified phases were observed to be located at 2θ = 47.9, 54.0, 70.0°. Finally, characteristic peaks for the $LaNi_yAl_{12-y}O_{19-\delta}$ catalyst series were located at 2θ = 18.8, 20.0, 22.0, 23.5, 24.5, 32.0, 33.1, 34.0, 36.1, 37.2, 39.2, 42.6, 44.9, 58.3, 59.7 and 66.9°. Minor unidentified phases were observed to be located at 2θ = 23.5, 48.0 and 51.5°. The relative low intensity of the minor phases indicated that they were present in low concentration. The presence of transition metal oxides of CoO, Fe_2O_3 and NiO phases were not observed.

The effect of increasing metal substitution was similar with all active metals (i.e., Co, Fe and Ni) substituted into lattice. A refinement in the crystallinity of the sample was observed when the ratio of the intensity of the peak located at 36.161° in the sample was greater relative to the intensity of this peak from the reference sample. The peak located at 36.161° was one of the most intense spectral lines for the $LaAl_{11}O_{18}$ compound. The reference sample peak used was the sample substituted at y = 0.2 within each series in all cases.

The $LaCo_yAl_{12-y}O_{19-\delta}$ series of catalysts exhibited a discernable peak at this location for the sample substituted at y = 0.2. The crystallinity of the cobalt doped $LaAl_{11}O_{18}$

compound was observed to increase incrementally with increasing cobalt substitution into the lattice. For the $LaFe_yAl_{12-y}O_{19-\delta}$ series of catalysts, the sample reference peak located at 36.161° was not broad which suggested that this sample was poorly crystallized. However, as the iron substitution was increased to $y \geq 0.4$, this peak narrowed. The crystallinity of the iron doped $LaAl_{11}O_{18}$ compound was observed to increase incrementally with increasing iron substitution into the lattice. For the $LaNi_yAl_{12-y}O_{19-\delta}$ series of catalysts, the sample crystallinity was observed to substantially increase with nickel substitution into the lattice.

Increasing the substitution of active metals into the hexaaluminate lattice was observed to produce an improvement in the crystallinity of the $LaAl_{11}O_{18}$ compound due to coarsening. Crystalline structure refinement was apparent by both increased intensities and narrower peaks. Therefore, the substitution of active metals into the lattice produced the effect of improving the rate of solid state reaction to form the $P6_3/mmc$ crystalline structure. Such a change in the annealing rate suggested that not simply the catalytic properties of the $LaAl_{11}O_{18}$ compound had been altered, but also the microstructure and likely a number of physico-chemical properties.

The effect of different mirror cations on crystalline phase was also examined. Powder XRD patterns for three catalyst systems $BaNi_{0.4}Al_{11.6}O_{19-\delta}$, $LaNi_{0.4}Al_{11.6}O_{19-\delta}$ and $SrNi_{0.4}Al_{11.6}O_{19-\delta}$ are presented in Figure 8. Similar to the $LaAl_{11}O_{18}$ compound, the $BaAl_{12}O_{19}$ and $SrAl_{12}O_{19}$ compounds also exhibit $P6_3/mmc$ crystal symmetry. Phase identification of $BaNi_{0.4}Al_{11.6}O_{19-\delta}$ and $SrNi_{0.4}Al_{11.6}O_{19-\delta}$ was made based on the reference

peak positions obtained from [JCPDS: 26-0135 and 26-0976] for $BaAl_{12}O_{19}$ and $SrAl_{12}O_{19}$, respectively. $NiAl_2O_4$ phase formation was not discernable in the samples. Minor phases were observed in each catalyst. Their relatively low intensity indicated that these phases were present in low concentration. The presence of NiO was not observed in the catalyst samples.

Characteristic $P6_3/mmc$ crystal symmetry was observed at 2θ = 18.3, 18.7, 19.9, 21.8, 24.2, 26.9, 32.0, 33.2, 35.8, 42.2, 44.4, 55.8 and 66.8° for $BaNi_{0.4}Al_{11.6}O_{19-\delta}$. Minor unidentified phases were observed to be located at 2θ = 13.9, 15.7, 23.5, 28.3, 28.9, 30.0, 34.3, 38.0, 51.3, 60.1, 64.4, 68.4 and 71.6°. Similarly, $P6_3/mmc$ crystal symmetry was observed in $SrNi_{0.4}Al_{11.6}O_{19-\delta}$ as indicated by peaks located at 2θ = 18.9, 20.1, 24.3, 24.6, 25.2, 32.2, 32.6, 34.1, 36.2, 39.3, 42.8, 45.0, 58.5, 60.1 and 67.2 °. Minor unidentified phases were observed to be located at 2θ = 8.1, 14.2, 18.2, 21.1, 22.2, 23.6, 25.5, 27.9, 30.2, 31.5, 43.4, 65.1, 71.6, 69.7, 71.6 and 72.7°.

5.3.3 Temperature Programmed Reduction

A key property of solid oxide catalysts is the reduction temperature of the metals that are substituted into the lattice. The temperature programmed reduction (TPR) technique was used to indicate the relative strength with which metal-oxygen bonds present in the lattice were held. For high temperature applications such as reforming, maximizing the metal stability toward aggregation and a loss of dispersion is important. In hexaaluminate catalysts, the oxygen in the mirror plane has been reported as being less

tightly bound (37), which suggests that the reduction of metal-oxygen bonds is affected by how tightly oxygen is held in and around the mirror cation. The TPR profiles for $LaCo_yAl_{12-y}O_{19-\delta}$, $LaFe_yAl_{12-y}O_{19-\delta}$, $LaNi_yAl_{12-y}O_{19-\delta}$ (y = 0.2, 0.4, 0.8 and1.0) and $M_INi_{0.4}Al_{11.6}O_{19-\delta}$ (M_I = Ba and Sr) are given in Figures 9 through 11. Their reduction peak temperature assignments are given in Table 7.

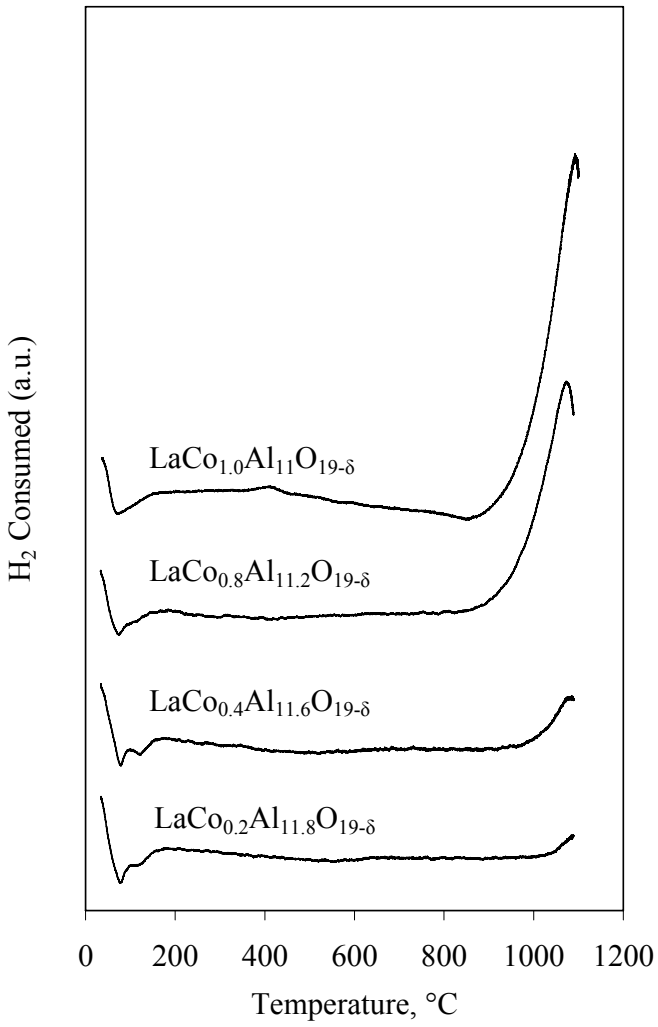

Figure 9. Temperature programmed reduction profile of $LaCo_yAl_{12-y}O_{19-\delta}$. The effect of cobalt substitution.

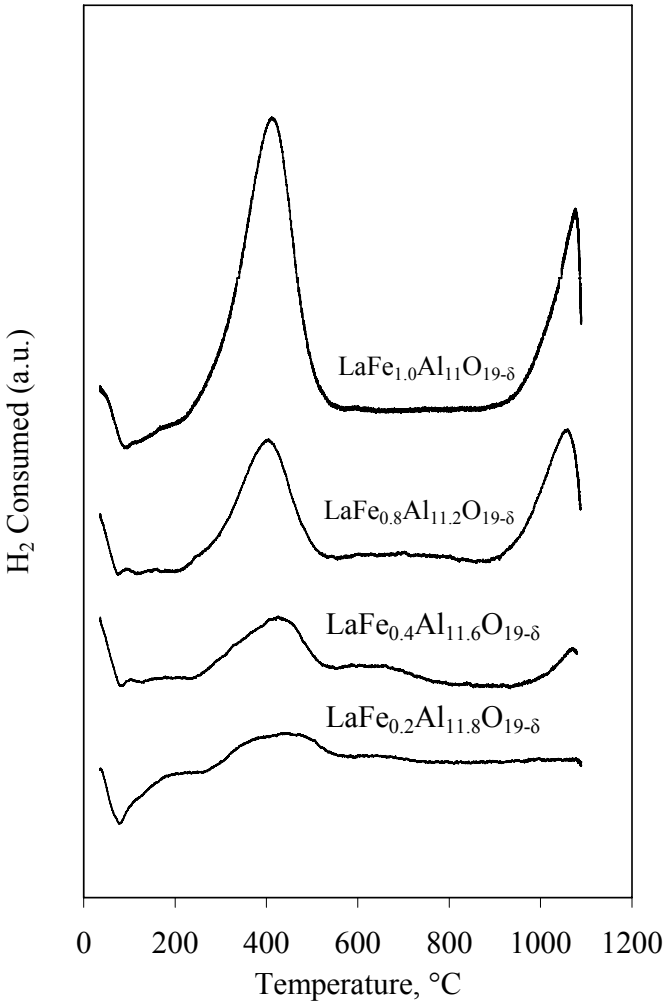

Figure 10. Temperature programmed reduction profile of $LaFe_yAl_{12-y}O_{19-\delta}$. The effect of iron substitution.

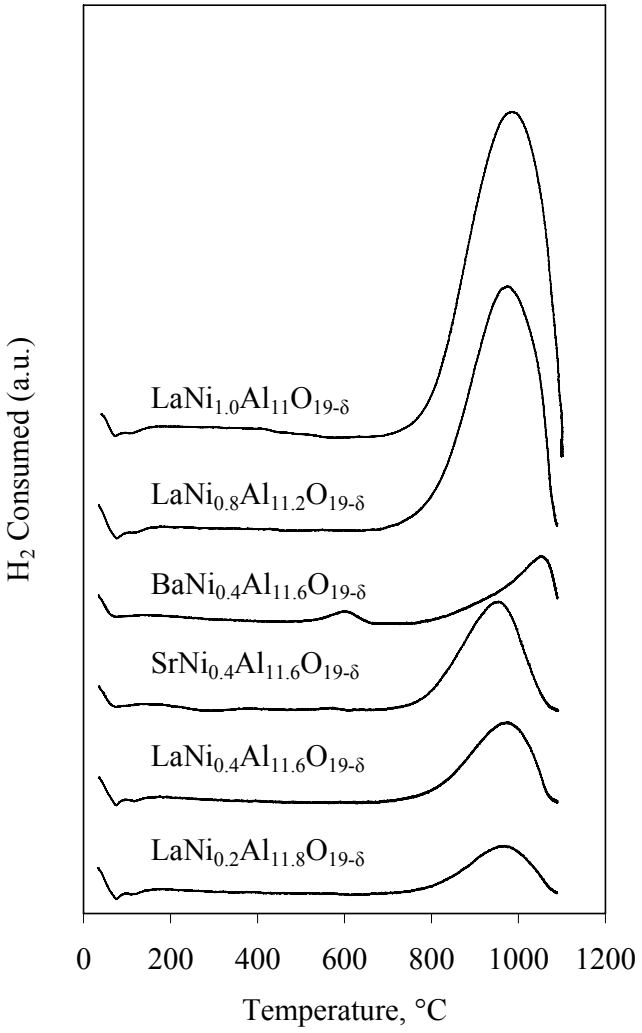

Figure 11. Temperature programmed reduction profile of $LaNi_yAl_{12-y}O_{19-\delta}$ (y = 0.2, 0.4, 0.8 and 1.0) and $M_INi_{0.4}Al_{11.6}O_{19-\delta}$ (M_I = Ba and Sr). The effect of nickel substitution and the mirror cation.

Table 7. Peak temperature assignments and H_2 consumed during the temperature programmed reduction of $M_I(M_{II})_yAl_{12-y}O_{19-\delta}$ catalysts.

Sample	Low Temperature Peak Location (°C)	High Temperature Peak Location (°C)
$LaCo_{1.0}Al_{11.0}O_{19-\delta}$	-	1098
$LaCo_{0.8}Al_{11.2}O_{19-\delta}$	-	1080
$LaCo_{0.4}Al_{11.6}O_{19-\delta}$	-	1088
$LaCo_{0.2}Al_{11.8}O_{19-\delta}$	-	1100
$LaFe_{1.0}Al_{11.0}O_{19-\delta}$	422	1078
$LaFe_{0.8}Al_{11.2}O_{19-\delta}$	415	1064
$LaFe_{0.4}Al_{11.6}O_{19-\delta}$	441	1079
$LaFe_{0.2}Al_{11.8}O_{19-\delta}$	447	-
$LaNi_{1.0}Al_{11.0}O_{19-\delta}$	-	996
$LaNi_{0.8}Al_{11.2}O_{19-\delta}$	-	986
$LaNi_{0.4}Al_{11.6}O_{19-\delta}$	-	982
$LaNi_{0.2}Al_{11.8}O_{19-\delta}$	-	982
$BaNi_{0.4}Al_{11.6}O_{19-\delta}$	611	1064
$SrNi_{0.4}Al_{11.6}O_{19-\delta}$	-	938

The TPR profiles for the $LaCo_yAl_{12-y}O_{19-\delta}$ (y = 0.2, 0.4, 0.8 and1.0) series of catalysts is given in Figure 9. Catalysts within this series exhibited single H_2 consumption peaks located between 1080 and 1100°C. The H_2 consumption peaks located in this region indicated that cobalt had been incorporated into the lattice of the lanthanum hexaaluminate compound. The magnitude of the H_2 consumption peaks correlated with increasing cobalt substitution which indicated that increasing the substitution of cobalt into the lattice increased the number of accessible reduction sites. At a cobalt substitution of y = 0.2, the H_2 consumption peak was shifted to higher temperatures; 1100°C, which indicated that cobalt was more effectively stabilized into the framework lattice at a lower concentration. This behavior suggested an increased next nearest neighbor (-NNN-) interaction between cobalt and aluminum at this concentration.

The TPR profiles for the $LaFe_yAl_{12-y}O_{19-\delta}$ (y = 0.2, 0.4, 0.8 and1.0) series of catalysts are given in Figure 10. Catalysts within this series exhibited two discernable reduction peaks. The low temperature peaks were located between 415 and 447°C and indicated the presence of loosely bound oxygen associated with iron substitution into the lattice as Fe^{3+} (Fe_2O_3). High temperature reduction peaks were located between 1064 and 1069°C for iron substituted into the hexaaluminate lattice at y = 0.4 through 1. The H_2 consumption peak in this region indicated the reduction of Fe^{2+} to Fe^0. It also suggested that iron was more effectively stabilized into the lanthanum hexaaluminate lattice as Fe^{2+} rather than as Fe^{3+}. The magnitude of both the low and high temperature H_2 consumption peaks was found to increase with iron substitution into the framework lattice. This observation indicated that increasing the substitution of iron into the lattice also increased

the number of accessible reduction sites. For iron substituted at y = 0.2, the high temperature peak was not discernable. This characteristic was similar to that observed with the lanthanum cobalt hexaaluminate catalyst substituted at y = 0.2. It is suggested here that an increase in the concentration of more stable Al-O-Fe bonds relative to Fe-O-Fe bonds results in an increased -NNN- interaction.

The TPR profiles for the $LaNi_yAl_{12-y}O_{19-\delta}$ (y = 0.2, 0.4, 0.8 and1.0) series and the $M_INi_{0.4}Al_{11.6}O_{19-\delta}$ (M_I = Ba and Sr) series of catalysts are given in Figure 11. Within the $LaNi_yAl_{12-y}O_{19-\delta}$ (y = 0.2, 0.4, 0.8 and1.0) catalyst series, a single reduction peak was observed for each sample. The H_2 consumption peaks were narrowly distributed between 982 and 996°C indicating that nickel substitution into the lanthanum hexaaluminate framework lattice did stabilize the Ni-O bond toward reduction. The H_2 consumption peaks were observed to increase in magnitude with increasing nickel substitution. This suggests that a greater fraction of the Ni-O sites are reducible with increasing nickel substitution.

Within the $M_INi_{0.4}Al_{11.6}O_{19-\delta}$ (M_I = Ba and Sr) catalyst series, the $LaNi_{0.4}Al_{11.6}O_{19-\delta}$ and the $SrNi_{0.4}Al_{11.6}O_{19-\delta}$ catalysts exhibited single H_2 consumption peaks located at 982 and 938°C, respectively. The TPR profile for $BaNi_{0.4}Al_{11.6}O_{19-\delta}$ catalyst exhibited two H_2 consumption peaks, one located at low temperature, 611°C, and a high temperature peak located at 1064°C. Prior literature has suggested (49) that the low temperature peak was attributed to a $NiAl_2O_4$ spinel phase present in low concentration. However, the presence of the $NiAl_2O_4$ phase is not discernable from the XRD pattern given in Figure 8. The low

temperature H_2 consumption peak, therefore, was attributed to an unidentified minor phase. The H_2 consumption peak for $SrNi_{0.4}Al_{11.6}O_{19-\delta}$ was located at a lower temperature than both the $BaNi_{0.4}Al_{11.6}O_{19-\delta}$ high temperature peak and the $LaNi_{0.4}Al_{11.6}O_{19-\delta}$ peak.

Relative to both lanthanum and strontium, the barium mirror cation produced a stabilizing effect on the Ni-O bond in the hexaaluminate lattice toward reduction. This stabilization behavior suggested that the reduced nickel sites were located in a region near the mirror cation. Likely, the stabilization of Ni-O bonds in this region was influenced by the physico-chemical properties of the mirror cation. As given in Table 2, the larger ionic radius of barium relative to strontium may have produced a structural rearrangement of nickel in the mirror plane region which could have accounted for the reduction of $SrNi_{0.4}Al_{11.6}O_{19-\delta}$ at lower temperatures over that of $BaNi_{0.4}Al_{11.6}O_{19-\delta}$. Other physico-chemical properties such as the electronegativity and the valence state of the mirror cation may also have influenced Ni-O bond stability within the lattice. As indicated in Table 2, lanthanum possessed a smaller ionic radius relative to both barium and strontium; however, the peak H_2 consumption temperature for $LaNi_{0.4}Al_{11.6}O_{19-\delta}$ occurred in a higher temperature region than $SrNi_{0.4}Al_{11.6}O_{19-\delta}$ and a lower region than $BaNi_{0.4}Al_{11.6}O_{19-\delta}$. This result suggests that bond reduction is not controlled simply by the ionic radius of the mirror cation.

5.3.4 Determination of Active Area by H_2 Pulse Chemisorption

The TPR data discussed in Section 5.3.3 suggested that the mirror cation in the nickel series of catalysts produced a stabilization effect toward reduction of the Ni-O bond. It was desired to elucidate the nature of this phenomenon and its impact on catalytic activity and selectivity in greater detail. In this study, the active nickel area of the reduced $BaNi_{0.4}Al_{11.6}O_{19-\delta}$, $LaNi_{0.4}Al_{11.6}O_{19-\delta}$ and $SrNi_{0.4}Al_{11.6}O_{19-\delta}$ oxide catalysts was determined by H_2 pulse chemisorption. The H_2 pulse chemisorption data provided information related to how the mirror cation influenced the concentration of reducible nickel sites on the surface of the catalyst.

For nickel substituted into the hexaaluminate lattice to become catalytically active, the Ni-O bond within the hexaaluminate lattice must first be reduced. The reduced nickel sites within the lattice form either metallic nickel or a nickel ion. If metallic nickel sites form, then the active sites exist as nano-dispersed nickel sites which remain embedded at surface. If the reduced sites are present in sufficiently high concentration, then the formation of larger metallic clusters is likely. Nickel may also remain in a defective state within the lattice as a nickel ion. The properties which are unique to nickel substituted into the hexaaluminate lattice are the number of nickel sites that can be reduced and their coordinative environment.

The number of reduced nickel sites was determined by first subjecting nickel substituted hexaaluminate catalysts with the same nickel content, but with different

mirror cations, $M_INi_{0.4}Al_{11.6}O_{19-\delta}$ (M_I = Ba, La and Sr), to a reducing environment. Secondly, the reduced nickel sites that were formed were then titrated by H_2 pulse chemisorption to determine their number. The nickel dispersion, which was reported as H/Ni, or mole of atomic hydrogen adsorbed per mole of nickel substituted into the lattice, was taken to be proportional to the number of reduced nickel sites that were formed.

Results from the H_2 pulse chemisorption experiments are given in Table 8. The accuracy of the method and equipment was first checked using a $Ru/\gamma\text{-}Al_2O_3$ standard. A replicate run was performed on the $LaNi_{0.4}Al_{11.6}O_{19-\delta}$ catalyst to ensure experimental repeatability. The dispersions obtained were less than 3% for all three catalysts which indicated that after exposure to a reducing environment that greater than 97% of the nickel remained as nickel oxide within the hexaaluminate lattice. This observation indicated that only a fraction of the nickel within the lattice was reduced and was responsible for catalytic reaction. The partial reduction of the nickel sites within the lattice is consistent with a prior observation by Xu et al. (46).

The nickel dispersions obtained correlated with the mirror cation type which suggested that the introduction of different mirror cations into the hexaaluminate lattice was significant in influencing the concentration of reducible Ni-O bonds. The nickel dispersions obtained were determined to increase in the following order: $LaNi_{0.4}Al_{11.6}O_{19-\delta} > SrNi_{0.4}Al_{11.6}O_{19-\delta} > BaNi_{0.4}Al_{11.6}O_{19-\delta}$. The dispersions also correlated with the nickel surface concentrations obtained by XPS that are reported later in Section 5.3.5. This

Table 8. Determination of metal dispersion by H_2 pulse chemisorption onto reduced $M_INi_{0.4}Al_{11.6}O_{19-\delta}$ (M_I = Ba, Sr and La) catalysts. The effect of mirror cation type on the number of reducible nickel sites.

Catalyst	**Surface area (m^2/g)**	**mL H_2 (STP) adsorbed/g cat.**	**Catalyst dispersion (H/M)[†]**
$LaNi_{0.4}Al_{11.6}O_{19-\delta}$	22.6	0.1022	0.025
$LaNi_{0.4}Al_{11.6}O_{19-\delta}$ (Replicate)	22.6	0.0986	0.024
$BaNi_{0.4}Al_{11.6}O_{19-\delta}$	14.3	0.0423	0.0095
$SrNi_{0.4}Al_{11.6}O_{19-\delta}$	16.2	0.0845	0.019
$Ru/\gamma\text{-}Al_2O_3$ (standard – 1/2002)	122	0.1322	0.28
$Ru/\gamma\text{-}Al_2O_3$ (standard – 2/2005)	122	0.1205	0.26

[†]M – metal (Ni or Ru).

result is also in agreement with the findings of Machida et al. (37) who have suggested that oxygen within the mirror plane is more weakly bound than oxygen present in the close packed spinel block. Certainly, weakly held oxygen is more susceptible to reduction, leaving nickel atoms in the mirror plane region in a reduced state. The effect that the mirror cation produced on nickel sites, therefore, was likely structural in nature by defining the concentration of nickel which was at the catalyst surface and the concentration of reducible nickel sites.

5.3.5 Surface Composition by X-ray Photoelectron Spectroscopy

The surface composition of the catalyst is a critical component in determining both the catalytic activity and selectivity of a catalyst system. The formation of carbon onto the surface of a metallic catalyst is reported in the literature as a 'structure sensitive' reaction (50). A reaction is structure sensitive when the turnover frequency depends on the dispersion of the catalyst (51). Perhaps even more important than the dispersion of active metals on the catalyst surface is their coordinative environment. The rate and strength of elemental carbon and hydrocarbon adsorption onto active sites is affected by the coordinative environment (52, 53, 54). It is therefore, desirable to determine the relative surface composition of active metals present on the surface of the hexaaluminate catalysts.

From the TPR data presented in Section 5.3.3, it was observed that the mirror cation produced an influence on the reduction of the Ni-O bond. The H_2 pulse chemisorption data discussed in Section 5.3.4, indicated that catalyst dispersion correlated with the type of mirror cation substituted into the hexaaluminate lattice. To further examine this result, the chemical state of the oxides present in these catalysts as well as the nickel surface concentration was determined by XPS. The catalysts examined were the same nickel mirror cation series studied in the previous two sections: $BaNi_{0.4}Al_{11.6}O_{19-\delta}$, $LaNi_{0.4}Al_{11.6}O_{19-\delta}$ and $SrNi_{0.4}Al_{11.6}O_{19-\delta}$.

Ni(2P) and La(3d) XPS spectra for the $LaNi_{0.4}Al_{11.6}O_{19-\delta}$ catalyst are given in Figure 12. The La(3d) peaks were located at 834.0 and 850.7 eV and were observed with corresponding satellite peaks which were shifted 3 eV higher in binding energy. Satellite peaks known as shake-up lines were observed for La(3d) in the literature (45). Shake-up lines in XPS spectra are known to occur when complex photo-emission processes lead to the formation of ions which are excited a few eV above the ground state. When the excited state is above the ground state, the kinetic energy of the emitted photo-electron is reduced by that energy difference which results in the formation of a satellite peak a few eV higher in binding energy than the main peak. The binding energy values obtained indicate that lanthanum is present in the La^{3+} oxidation state. The Ni($2P_{3/2}$) peak was located at 854.5 eV as a shoulder on the asymmetrically shaped La($3d_{3/2}$) shake-up line. Binding energies obtained for the nickel, given in Table 10, indicate that nickel was present in the Ni^{2+} oxidation state.

The Ni(2p) spectra for the $BaNi_{0.4}Al_{11.6}O_{19-\delta}$ catalyst is given in Figure 13. The Ni(2p) spectra exhibited a shakeup line from the Ni($2p_{1/2}$) line located at 860 eV (45). The binding energies obtained for the nickel, given in Table 11, indicate that nickel was present in the Ni^{2+} oxidation state. The Ba(3d) XPS spectra given in Figure 14 shows two peaks which are located at 779.4 and 794.7 eV indicating that barium is also present in the Ba^{2+} oxidation state.

The Ni(2p) spectra for the $SrNi_{0.4}Al_{11.6}O_{19-\delta}$ catalyst is given in Figure 15. As observed in the Ni(2P) spectra for both the $LaNi_{0.4}Al_{11.6}O_{19-\delta}$ and the $BaNi_{0.4}Al_{11.6}O_{19-\delta}$

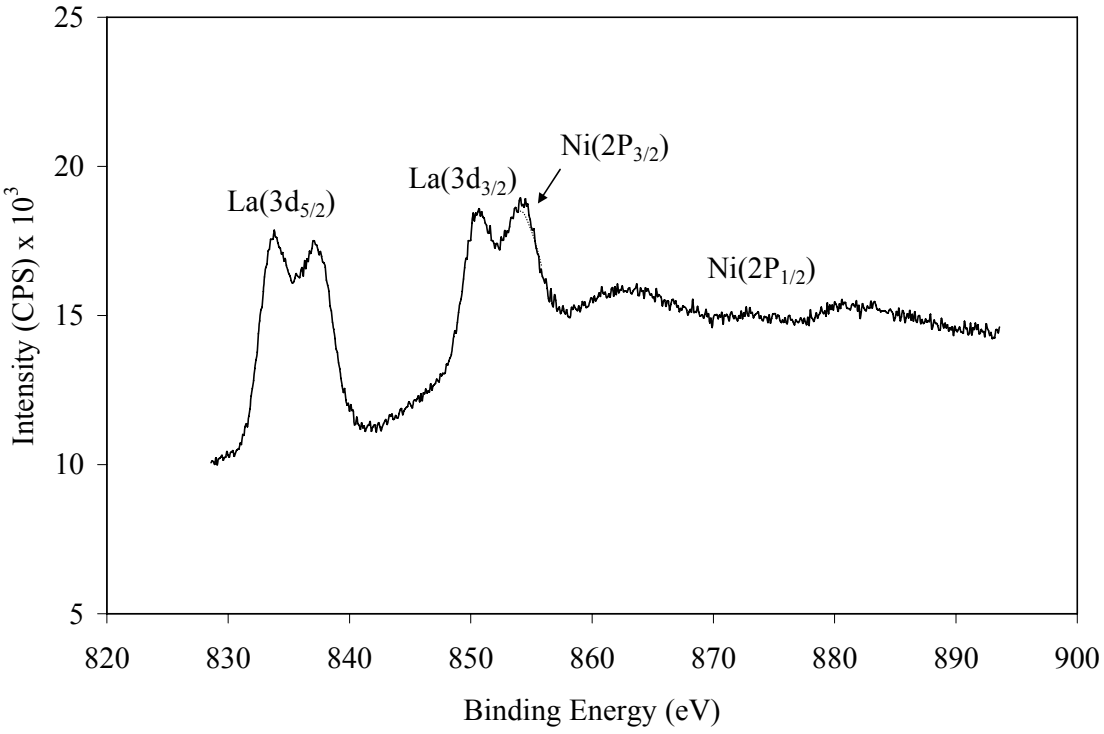

Figure 12. $Ni(2p_{3/2})$, $Ni(2p_{1/2})$ and $La(3d_{5/2})$ spectra of $LaNi_{0.4}Al_{11.6}O_{19-\delta}$.

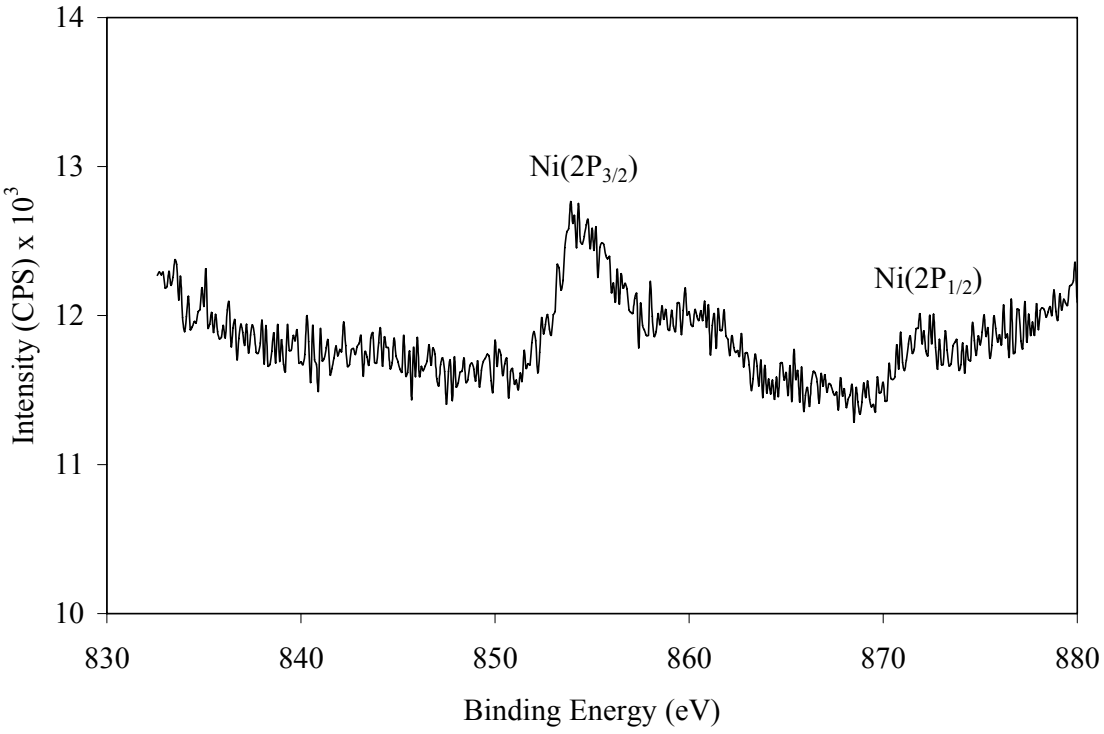

Figure 13. Ni($2p_{1/2}$) and Ni($2p_{3/2}$) spectra of $BaNi_{0.4}Al_{11.6}O_{19-\delta}$.

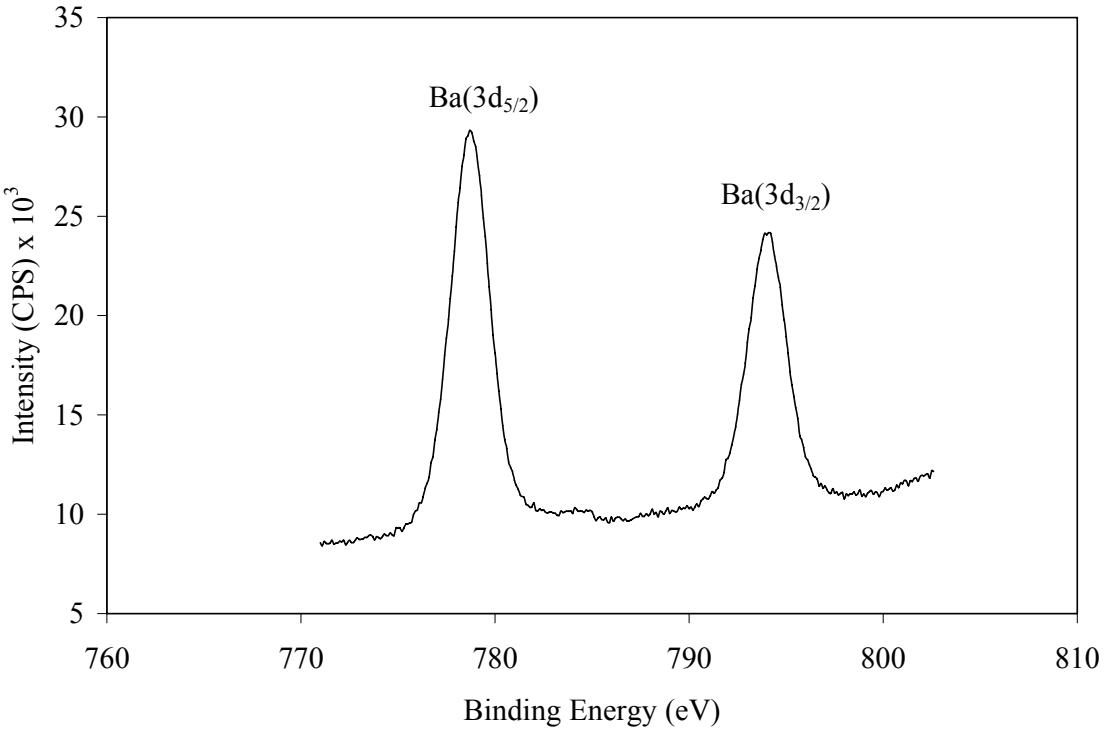

Figure 14. $Ba(3d_{5/2})$ spectra of $BaNi_{0.4}Al_{11.6}O_{19-\delta}$.

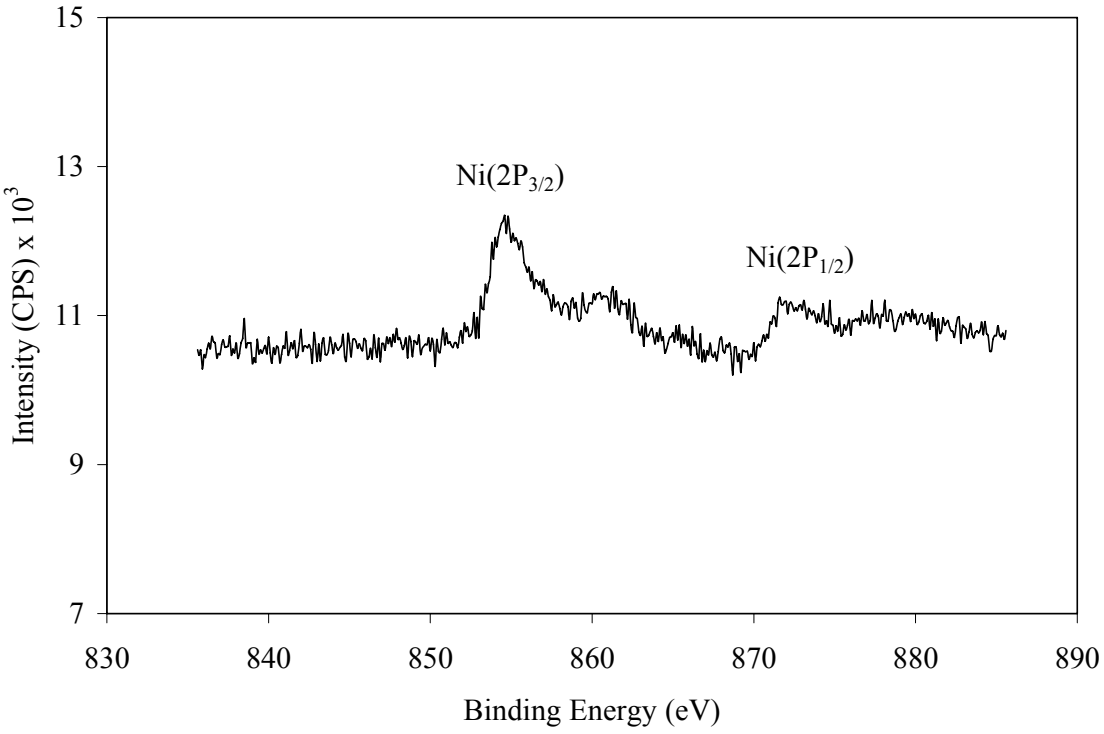

Figure 15. Ni($2p_{1/2}$) and Ni($2p_{3/2}$) spectra of $SrNi_{0.4}Al_{11.6}O_{19-\delta}$.

catalyst, a shakeup line from the Ni($2p_{1/2}$) line was observed for the $SrNi_{0.4}Al_{11.6}O_{19-\delta}$ catalyst located at 860 eV (45). A single peak was observed for the Sr(3d) XPS spectra which is given in Figure 16. Prior literature, however, has suggested that two peaks, Sr($3d_{5/2}$) and Sr($3d_{3/2}$), should be located in this region for Sr^{2+} (45). The width of the observed single peak in the Sr(3d) region spanned the reported binding energies previously reported for both peaks (45). Additionally, the observed single peak was asymmetric which suggested the presence of two overlapping peaks. Resolved peaks are given as a dashed line in Figure 16, their location and intensity at their full width at half the maximum (FWHM) intensity indicated that strontium was present in the Sr^{2+} oxidation state.

A complete listing of the binding energies of the surface elements present in the hexaaluminate catalysts are given in Table 10. The binding energies for the lattice framework oxides: oxygen, barium, lanthanum, strontium and aluminum were consistent with prior reported literature values (45, 46, 47, 55) for O^{2-}, Ba^{2+}, La^{3+}, Sr^{2+} and Al^{3+}, respectively. The similarity between the observed binding energy values and the literature values indicate that the incorporation of nickel into the framework lattice did not affect the binding energies of the surrounding oxides.

The bulk and surface nickel Al/Ni ratios are given in Table 9. The nickel concentrations were obtained from the FWHM data which was taken to be proportional to peak area. The different mirror cations produced nickel concentrations that differed

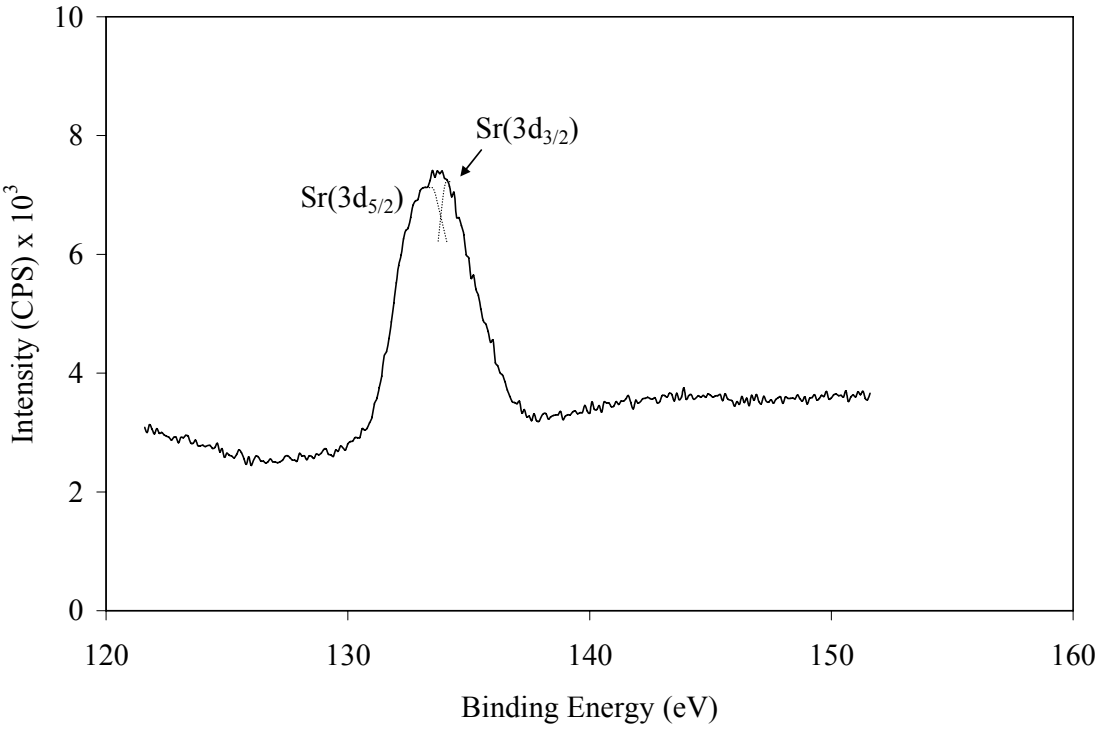

Figure 16. $Sr(3d_{5/2})$ and $Sr(3d_{3/2})$ spectra of $SrNi_{0.4}Al_{11.6}O_{19-\delta}$.

Table 9. Bulk and surface composition of $M_INi_{0.4}Al_{11.6}O_{19-\delta}$ (M_I = Ba, La and Sr) catalysts.

Catalyst	Bulk[†]	Surface
$M_INi_{0.4}Al_{12-y}O_{19-\delta}$	Al/Ni	Al/Ni
$LaNi_{0.4}Al_{11.6}O_{19-\delta}$	31.4	4.4
$BaNi_{0.4}Al_{11.6}O_{19-\delta}$	28.8	~Al[‡]
$SrNi_{0.4}Al_{11.6}O_{19-\delta}$	28.9	32.1

[†]The bulk Ni concentration was obtained by chemical analysis.
[‡]The observed Ni surface concentration was below the quantification limit.

Table 10. Binding energies of $M_INi_{0.4}Al_{11.6}O_{19-\delta}$ (M_I = Ba, La and Sr) catalysts.

Catalyst	Binding Energies (eV)					
			M_I		Ni	
	Al 2p	O 1s	3 $d_{5/2}$	3 $d_{3/2}$	2 $p_{3/2}$	2 $p_{1/2}$
$LaNi_{0.4}Al_{11.6}O_{19-\delta}$	74.0	529.9	834.0	850.7	854.5	872.3
$BaNi_{0.4}Al_{11.6}O_{19-\delta}$	74.0	530.3	779.4	794.7	854.6	872.4
$SrNi_{0.4}Al_{11.6}O_{19-\delta}$	74.0	530.5	133.2	134.1	854.9	872.1

from their respective bulk phase concentrations. Surface nickel enrichment beyond that of the bulk phase was observed with the $LaNi_{0.4}Al_{11.6}O_{19-\delta}$ catalyst. In contrast, the $SrNi_{0.4}Al_{11.6}O_{19-\delta}$ and $BaNi_{0.4}Al_{11.6}O_{19-\delta}$ catalysts exhibited less nickel present on the surface than in the bulk phase. The concentration of nickel at the surface of the catalyst was determined to follow the order: $LaNi_{0.4}Al_{11.6}O_{19-\delta} > SrNi_{0.4}Al_{11.6}O_{19-\delta} > BaNi_{0.4}Al_{11.6}O_{19-\delta}$. The effect that the mirror cation produced on the surface nickel concentration, obtained by XPS, was in agreement with the dispersions obtained from H_2 pulse chemisorption.

The segregation of nickel from the bulk phase to the surface was driven by a difference in binding energies between the respective elements (56). Xu et al. (46) have suggested that the surface nickel concentration of hexaaluminate catalysts correlated with both the size and valence of the mirror cation. This observation indicated that the chemical bonding of nickel in the mirror plane region was influenced by the mirror cation. Xu et al. (46) have found that nickel surface enrichment occured in the following order: $LaNi_{0.4}Al_{11.6}O_{19-\delta} > BaNi_{0.4}Al_{11.6}O_{19-\delta} > SrNi_{0.4}Al_{11.6}O_{19-\delta}$. The disparity between the results obtained in this investigation and the results obtained by Xu et al. were not resolved since they did not provide a bulk sample analysis. Notwithstanding, the observation that nickel surface concentration was influenced by both the mirror cation valence and its ionic radius was consistent with the data developed in this investigation.

5.4 Conclusions

Based on the aforementioned catalyst characterization experiments, the following relationships have been observed. The co-precipitation method utilized to prepare the hexaaluminate catalysts produced sufficient variance in surface area between catalyst samples such that it was not possible to discern an effect with metal substitution into the hexaaluminate lattice.

Cobalt, iron and nickel substituted lanthanum hexaaluminates all exhibited $P6_3/mmc$ crystal symmetry indicative of the $LaAl_{11}O_{18}$ compound. Similar to the $LaAl_{11}O_{18}$ compound, the $BaAl_{12}O_{19}$ and $SrAl_{12}O_{19}$ compounds also exhibited $P6_3/mmc$ crystal symmetry. The effect of increasing the active metal substitution into the lattice produced an increase in sample crystallinity. The observed change in the rate of sample crystallization suggested that the microstructure of the lanthanum hexaaluminate catalysts were altered by active metal addition. Minor phase impurities were also observed to be present in relatively low concentration. Oxides of cobalt, iron and nickel were not observed.

TPR experiments on the catalysts indicated that the substitution of cobalt, iron and nickel cations into the lattice stabilized their reducibility. The reduction temperature for the nickel series correlated with the type of mirror cation. The number of reducible active metal sites correlated with the concentration of metal substituted into the lattice. H_2 pulse chemisorption performed on the reduced nickel hexaaluminate catalysts

confirmed that the number of substituted nickel sites that were reduced was a function of the type of mirror cation type. This influence suggested that the reduction of lattice bound nickel sites had occurred in a region near the mirror plane. The concentration of reducible nickel sites per gram of nickel present in the catalyst was observed as follows: $LaNi_{0.4}Al_{11.6}O_{19-\delta} > SrNi_{0.4}Al_{11.6}O_{19-\delta} > BaNi_{0.4}Al_{11.6}O_{19-\delta}$.

XPS analysis of $LaNi_{0.4}Al_{11.6}O_{19-\delta}$, $SrNi_{0.4}Al_{11.6}O_{19-\delta}$ and $BaNi_{0.4}Al_{11.6}O_{19-\delta}$ catalysts indicated that variation in the nickel surface concentration correlated with the type of mirror cation substituted into the lattice. The concentration of nickel observed on the surface of the catalyst was as follows: $LaNi_{0.4}Al_{11.6}O_{19-\delta} > SrNi_{0.4}Al_{11.6}O_{19-\delta} > BaNi_{0.4}Al_{11.6}O_{19-\delta}$. These results were in qualitative agreement with the number of reduced sites observed with H_2 pulse chemisorption.

6.0 TEMPERATURE PROGRAMMED REACTION OF n-TETRADECANE OVER $M_I(M_{II})_yAl_{12-y}O_{19-\delta}$ CATALYSTS

6.1 Introduction

One of the most important properties of a middle distillate reforming catalyst is its performance over a wide range of operating temperatures. Since the start-up of fuel cell power units occur from ambient temperature conditions, the development of a catalyst which possess reforming activity and carbon deposition resistance at lower than normal operating temperature conditions are particularly important. Therefore, catalyst light-off temperature, catalyst activity and selectivity over a variety of temperatures are important to the APU application and require detailed study.

When catalytically active metals are substituted into the lattice of the hexaaluminate compound the result is a composite oxide. The catalytic properties of the composite oxide are derived when the material is exposed to a reducing environment and oxygen adjacent to the active metal is stripped from the lattice. Reduced transition metal sites within the lattice are 'defect' sites. These defect sites become the catalytically active sites on the surface of the catalyst. The activity of the catalyst is a function of the concentration of active sites on the catalyst surface; however, carbon deposition as well as catalyst selectivity has been shown to be closely related to catalyst structure (10, 57). If the coordinative environment of active metal substituted into the hexaaluminate lattice is high, as would occur when the surface concentration of the metal is high, then when reduction occurs the propensity for active metals to aggregate and form large metallic

clusters is high. When the coordination of active metals in the lattice is low then the reduced metal sites will have a tendency to remain isolated. Therefore, the role that the hexaaluminate structure serves in the development of a catalyst is both as a support and as a template to disperse the active metal in a manner that will inhibit aggregation and the formation of large metallic clusters which are more prone to carbon deposition.

Three distributions of active sites result from the substitution of active metal cations into the lattice of the hexaaluminate lattice. The distributions are defined by the number of metal cations (M_{II}) that are substituted as next nearest neighbors (NNNs) relative to the reference metal cation (M_{II}`). When the concentration of substituted active metal cations is high, then the concentration of $M_{II}$` cations with two adjacent metal cation NNNs (M_{II}-O-M_{II}`-O-$M_{II}$), is also high. Similarly, active metal cations may also substitute into the lattice in a lower coordination pattern to yield one adjacent NNN as $M_{II}$-O-$M_{II}$`-O-Al or with no adjacent NNNs as Al-O-M_{II}`-O-Al. Sites substituted with one or more active metal NNNs, rather than Al-NNNs, are more likely to form large metallic clusters when reduced. XRD studies on post reacted $LaNiAl_{11}O_{19-\delta}$ have suggested that a metallic nickel phase can separate from the bulk hexaaluminate phase to form small metallic clusters (47).

It is anticipated that if the substituted active metal cations are distributed in low coordination within the hexaaluminate lattice that hydrocarbons will not be as effectively stabilized onto the catalyst surface resulting in a catalyst with a relatively low activity (50, 58, 59). Conversely, if the active transition metal cations are distributed in relatively

high coordination then hydrocarbons and their intermediates will have a tendency to form excessively strong chemical bonds with the surface of the catalyst. Hydrocarbons that have longer residence times on the surface of the catalyst are more prone to undergo dehydrogenation and form coke (54). The oxidative and thermal dehydrogenation of large chain hydrocarbons into elemental carbon and coke is thermodynamically favorable at high temperatures (60).

The temperature programmed reaction experiments discussed in this chapter examine the effect of cobalt, iron and nickel substitution into the hexaaluminate lattice and its effect on catalytic performance. The purpose of this study was to relate the observed properties of these composite oxide catalysts to catalytic performance. n-Tetradecane was used as a middle distillate fuel model compound. Catalyst activity and selectivity were assessed through H_2, CO, CO_2 and CH_4 yields which were compared and contrasted to equilibrium and thermal partial oxidation results. For comparative purposes the results for each catalyst series were plotted as overlays of yield for each product species formed.

6.2 Experimental

6.2.1 Temperature Programmed Reaction

H_2, CO, CO_2 and CH_4 yields for the partial oxidation of n-tetradecane over $M_I(M_{II})_yAl_{12-y}O_{19-\delta}$ catalysts were examined over the temperature range of 750 to 900°C. Catalysts were first pre-reduced at 900°C for 1 hour in 15 vol% H_2/N_2 to expose the

active metal sites. The reactant pre-heat temperature was set at 350°C to ensure proper vaporization of the fuel and to avoid pre-ignition and coking of the catalyst and feed lines. The O/C was set at 1.2 to avoid excessive coking on the catalyst. Catalyst GHSV was kept constant for all runs at 50,000 $cm^3g^{-1}h^{-1}$. The total inlet feed flow rate was set at 450 sccm, the inlet N_2 flow rate was set at 50 sccm and the air flow rate was 390 sccm. The pressure was kept constant at 197.9 kPa. Once the catalyst samples had been pre-reduced for 1 hour, the temperature in the reactor was lowered to 750°C under N_2 purge. When the reactor temperature reached 750°C, the fuel, air and nitrogen reactants were introduced into the reactor and the temperature programmed reaction was initiated with a ramp rate of 1°C/min. Due to the transient nature associated with temperature programmed reactions at these process conditions, product gas composition was analyzed continuously by mass spectrometry.

The H_2, CO, CO_2 and CH_4 yields were calculated from gas phase exit N_2, H_2, CO, CO_2 and CH_4 concentrations. N_2 was assumed to pass through the system unreacted. The expressions given in equations (6) though (12) were used to calculate the product yields:

$$F_{N_2,i} = F_{N_2,o} \tag{6}$$

$$x_{N_2,i}F_{T,i} = x_{N_2,o}F_{T,o} \tag{7}$$

$$Y_{H_2}(\%) = \frac{\text{mol H}}{\text{mol hydrogen fed}} \cdot 100 = \frac{2x_{H_2} \cdot F_{T,o}}{30x_{n\text{-}C_{14}H_{30}} \cdot F_{T,i}} \cdot 100 \tag{9}$$

$$Y_{CO}(\%) = \frac{\text{mol CO}}{\text{mol carbon fed}} \cdot 100 = \frac{x_{CO} \cdot F_{T,o}}{14x_{n\text{-}C_{14}H_{30}} \cdot F_{T,i}} \cdot 100 \tag{10}$$

$$Y_{CO_2}(\%) = \frac{\text{mol } CO_2}{\text{mol carbon fed}} \cdot 100 = \frac{x_{CO_2} \cdot F_{T,o}}{14x_{n\text{-}C_{14}H_{30}} \cdot F_{T,i}} \cdot 100 \quad (11)$$

$$Y_{CH_4}(\%) = \frac{\text{mol } CH_4}{\text{mol carbon fed}} \cdot 100 = \frac{x_{CH_4} \cdot F_{T,o}}{14x_{n\text{-}C_{14}H_{30}} \cdot F_{T,i}} \cdot 100 \quad (12)$$

Where $F_{N_2,i}$ is the inlet molar flow rate of N_2, $F_{N_2,o}$ is the exit molar flow rate of N_2, $F_{T,i}$ is the total inlet molar flow rate, $F_{T,o}$ is the total exit molar flow rate, $x_{N_{2,i}}$ is the inlet mole fraction of N_2, $x_{N_{2,o}}$ is the exit mole fraction of N_2, x_{H_2} is the H_2 mole fraction in the product stream, x_{CO} is the CO mole fraction in the product stream, x_{CO_2} is the CO_2 mole fraction in the product stream and $x_{n\text{-}C_{14}H_{30}}$ is the n-tetradecane mole fraction in the feed. Experimentally, n-tetradecane was not observed in the product stream at the conditions tested indicating that conversion was nearly 100% in all cases.

Since the accumulation of carbon onto a catalytic surface at a given temperature is a central point in the design of a catalyst, assessing catalytic performance from this viewpoint provides an important perspective and measure of performance. The effectiveness of a catalyst at converting carbon present in the n-tetradecane feed into useful gas phase products rather than carbon can be assessed through the total gas phase carbon exiting the reaction system. Here, an instantaneous measure of the condensable carbon within the reactor may be determined as the difference between the total carbon entering the reactor and the gas phase carbon exiting the reactor. The condensable carbon yield is defined as:

$$Y_{Carbon} = \frac{\text{mol carbon produced}}{\text{mol carbon fed}} = 100 - (Y_{CO} + Y_{CO_2} + Y_{CH_4}) \quad (13)$$

When the observed $Y_{Carbon} > 0$, then carbon is prone to accumulate within the reactor and most likely is depositing onto the catalyst surface.

6.3 Results and Discussion

H_2, CO, CO_2 and CH_4 yields for the partial oxidation of n-tetradecane over cobalt, iron and nickel substituted hexaaluminate catalysts were examined over the temperature range between 750 to 900°C to assess their activity and selectivity as a function of metal type, substitutional concentration and mirror cation type. The equilibrium H_2, CO, CO_2 and CH_4 yields for n-tetradecane partial oxidation were carried out using HCS chemistry software (23). The calculated yields over this temperature range are given in Table 11. Equilibrium H_2 yields range narrowly between 89.2% and 90.1% and CH_4 yields are less than 1%. Equilibrium CO yields exhibit a weak functionality with temperature by increasing from 88.0% at 750°C to 91.5% at 900°C; correspondingly, CO_2 yields decrease from 11.2% to 8.5%.

The gas phase thermal partial oxidation (TPOx) of n-tetradecane was carried out over quartz chips which filled the entire volume of the reactor. Results from n-tetradecane TPOx are given in Figure 17. Relative to equilibrium, the TPOx yields of both H_2 and

Table 11. Equilibrium H_2, CO, CO_2 and CH_4 yields for n-tetradecane partial oxidation.

Temp (°C)	H_2 Yield (%)	CO Yield (%)	CO_2 Yield (%)	CH_4 Yield (%)
750	89.6	88.0	11.2	0.81
775	90.0	89.0	10.6	0.43
800	90.1	89.7	10.0	0.23
825	90.0	90.3	9.6	0.13
850	89.7	90.8	9.2	0.07
875	89.5	91.1	8.8	0.04
900	89.2	91.5	8.5	0.02

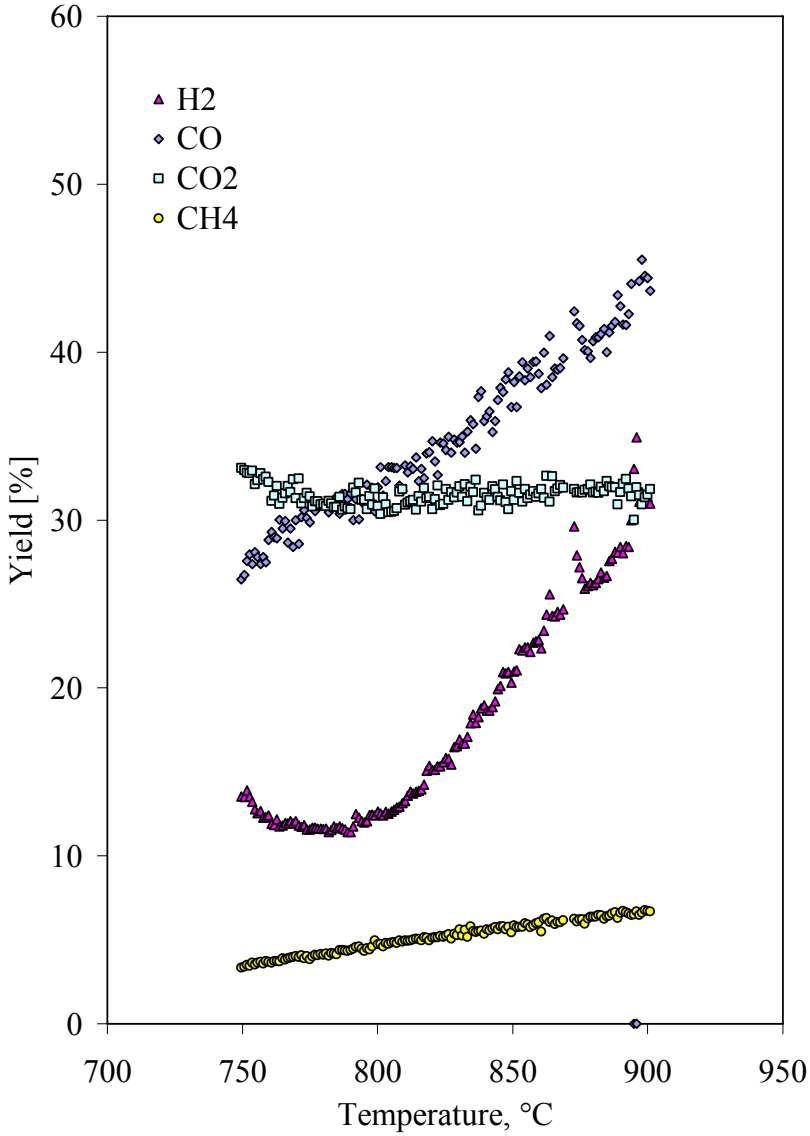

Figure 17. H_2, CO, CO_2 and CH_4 yields for the temperature programmed TPOx of n-tetradecane over quartz chips: blank run.

CO were relatively low at 750°C producing yields of 13 and 26%, respectively. At 750°C, the CO_2 yield obtained from TPOx was 32% suggesting a high selectivity toward combustion. At 900°C, H_2 and CO yields increase to 31% and 44.5%, respectively. It was apparent from the TPOx data that over the entire temperature range, the selectivity of a purely gas phase reaction toward CO production was greater than that for H_2 production. At temperatures between 750 and 800°C an observable shift in the rate of CO and CO_2 production occurred as indicted by a change in the slope of the their yields. Within this temperature range an increase in CO yield, a corresponding decrease in CO_2 yield and approximately no change in the H_2 yield were observed. At 800°C, the rate of H_2 production increased as indicted by a change in the slope of the yield. Between 800 and 900°C both yield and selectivity improved with temperature for CO and H_2. By comparing the TPOx yields to the equilibrium yields it was apparent that the residence time employed was insufficient to achieve near equilibrium yields.

6.3.1 Temperature Programmed Reaction over $LaCo_yAl_{12-y}O_{19-\delta}$ Series Catalysts

The H_2, CO, CO_2 and CH_4 yields produced from the temperature programmed reaction of n-tetradecane over the $LaCo_yAl_{12-y}O_{19-\delta}$ series of catalysts are given in Figures 18, 19, 20 and 21, respectively. In this series of experiments the effect of varying the concentration of cobalt substituted into the hexaaluminate lattice with y = 0.2, 0.4, 0.8 and 1.0 was examined. The respective yields were compared over the temperature range between 750 to 900°C.

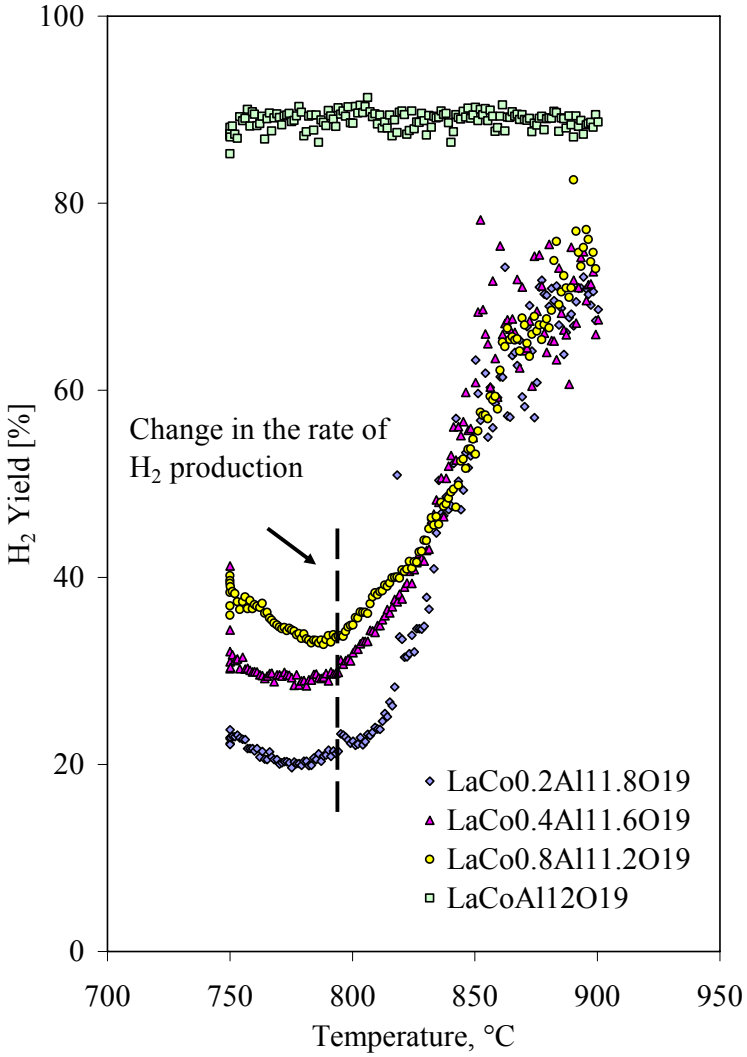

Figure 18. H_2 yields for the temperature programmed reaction of n-tetradecane over $LaCo_yAl_{12-y}O_{19-\delta}$ with y = 0.2, 0.4, 0.8 and 1.0.

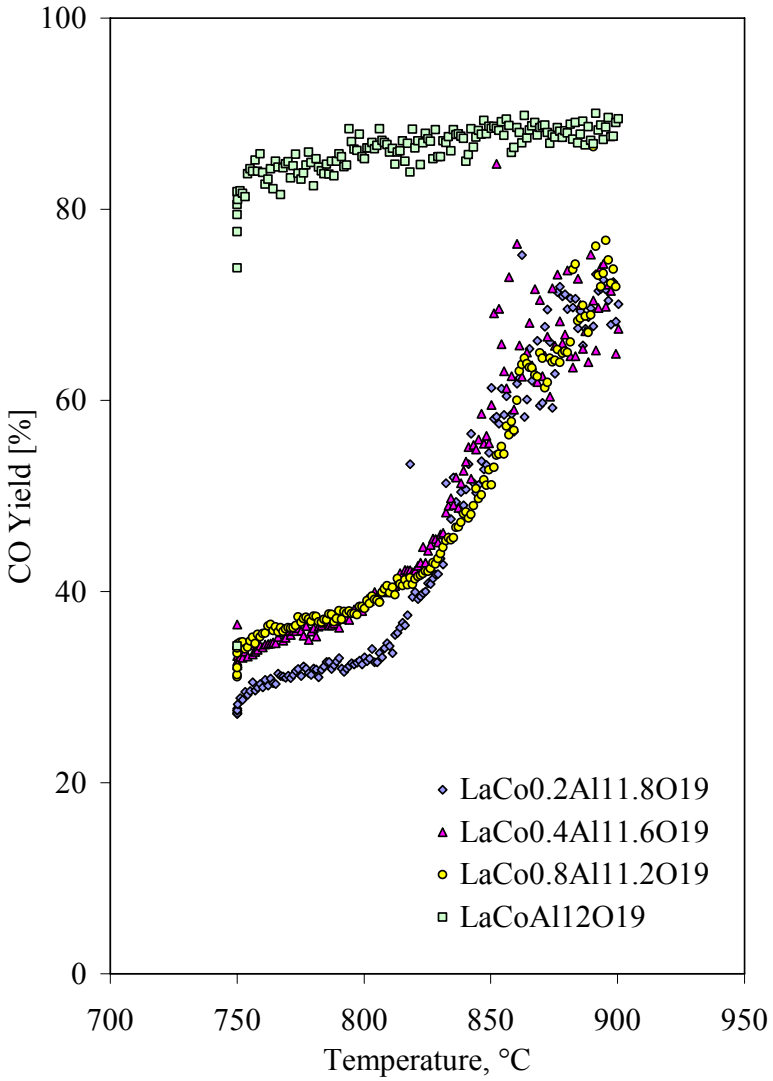

Figure 19. CO yield for the temperature programmed reaction of n-tetradecane over $LaCo_yAl_{12-y}O_{19-\delta}$ with y = 0.2, 0.4, 0.8 and 1.0.

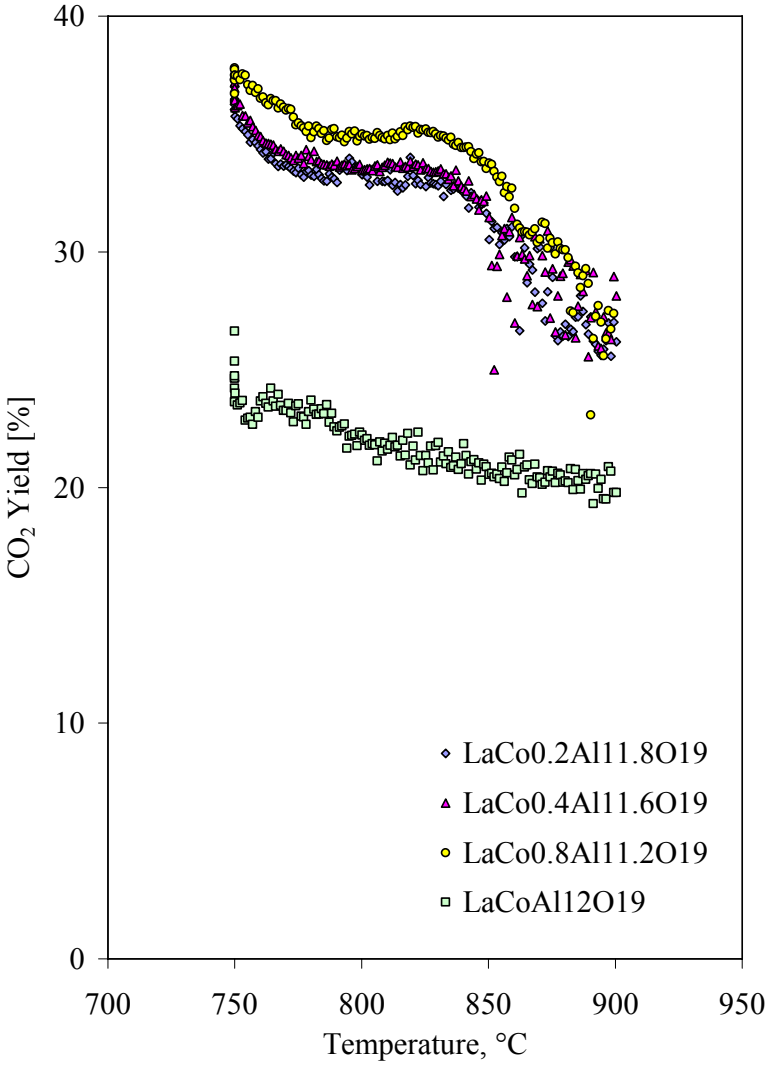

Figure 20. CO_2 yield for the temperature programmed reaction of n-tetradecane over $LaCo_yAl_{12-y}O_{19-\delta}$ with y = 0.2, 0.4, 0.8 and 1.0.

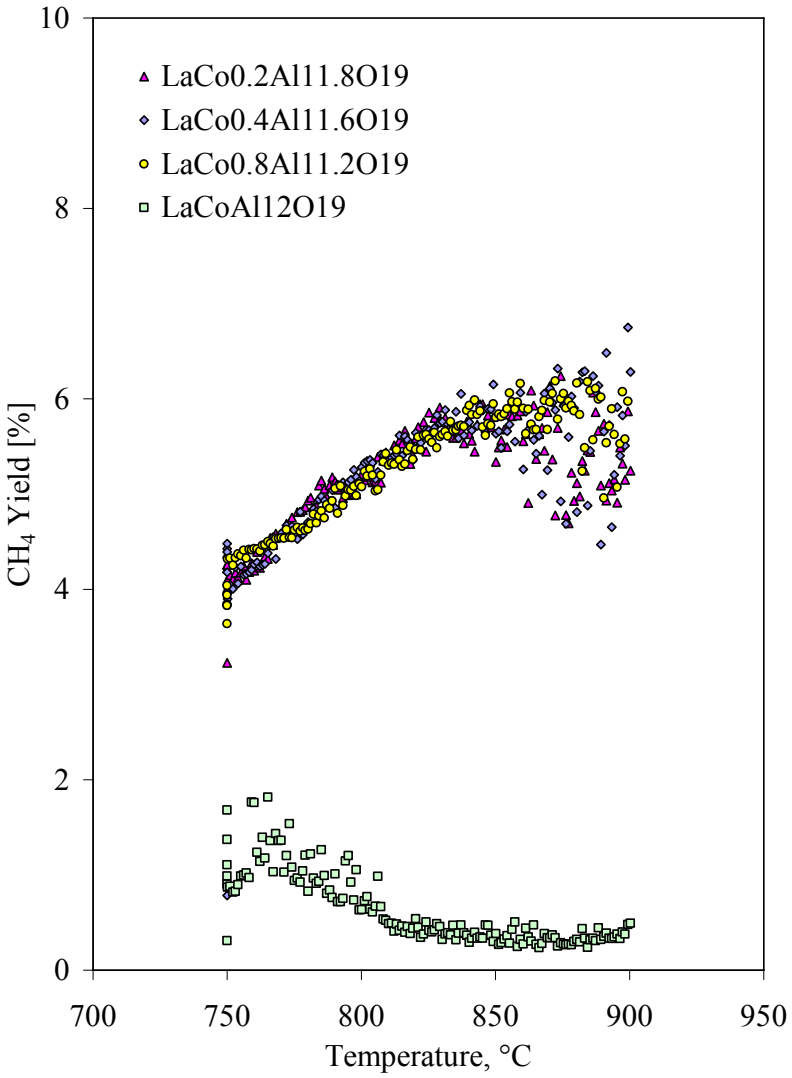

Figure 21. CH_4 yield for the temperature programmed reaction of n-tetradecane over $LaCo_yAl_{12-y}O_{19-\delta}$ with y = 0.2, 0.4, 0.8 and 1.0.

The H_2 yields produced during the temperature programmed reaction of n-tetradecane over the $LaCo_yAl_{12-y}O_{19-\delta}$ (y = 0.2, 0.4, 0.8 and 1.0) series of catalysts are given in Figure 18. For the entire catalyst series, the observed yields were well above those observed for TPOx. Below 850°C, the H_2 yields were observed to correlate with the concentration of cobalt substituted into the hexaaluminate lattice. Above 850°C, for catalysts substituted at $y \leq 0.8$, the dependence of H_2 yield on the concentration of cobalt substitution produced a tightly grouped set of yields which increased toward equilibrium with increasing temperature. For these catalysts, H_2 yields between catalysts were comparable and increased toward equilibrium with increasing temperature. The H_2 yield for the catalyst with cobalt substituted into the lattice at a concentration of y = 1.0 produced equilibrium yields over the entire temperature range. The disparity between H_2 yields from the catalyst substituted at y = 1.0 compared to the catalysts with cobalt substitution at $y \leq 0.8$ suggested that the surface concentration of cobalt in this catalyst was more effective at trapping and catalyzing hydrocarbons into H_2.

The CO yields produced during the temperature programmed reaction of n-tetradecane over the $LaCo_yAl_{12-y}O_{19-\delta}$ (y = 0.2, 0.4, 0.8 and 1.0) series of catalysts are given in Figure 19. Similar to the trend with H_2 yield, for cobalt substituted at y = 1.0 the CO yield was observed at equilibrium. However, in contrast to the observed H_2 yields, the CO yields for the catalysts with cobalt substituted at $y \leq 0.8$ were observed as comparable over the entire temperature range. The CO yields for the entire series of catalysts were greater than those obtained with TPOx.

The CO_2 yields produced during the temperature programmed reaction of n-tetradecane over the $LaCo_yAl_{12-y}O_{19-\delta}$ (y = 0.2, 0.4, 0.8 and 1.0) series of catalysts are given in Figure 20. At temperatures below 850°C, the CO_2 yields for catalysts with cobalt substitutions of $y \leq 0.8$ were greater than those observed from TPOx. However, as the temperature was increased to 900°C, the CO_2 yields become smaller than those observed with the TPOx reaction. At a cobalt substitution of y = 1.0, the observed CO_2 yield was significantly smaller than those observed with lower cobalt substitution into the hexaaluminate lattice. For all catalysts within the series, the CO_2 yields produced decreased with temperature. This was in contrast to the CO_2 yields observed for the TPOx reaction which remain relatively constant over the entire temperature range. The differentiation in behavior between the TPOx reaction and the catalytic reactions suggested that the $LaCo_yAl_{12-y}O_{19-\delta}$ series of catalysts exhibited a relatively high selectivity toward combustion.

The CH_4 yields produced during the temperature programmed reaction of n-tetradecane over the $LaCo_yAl_{12-y}O_{19-\delta}$ (y = 0.2, 0.4, 0.8 and 1.0) series of catalysts are given in Figure 21. For catalysts with cobalt substitutions of $y \leq 0.8$ the CH_4 yields exhibited a 2% increase over the entire temperature range. The magnitude of the CH_4 yields and the observed increasing yield trend was consistent with that observed in the TPOx reaction. For the catalyst with cobalt substituted at a concentration of y = 1.0, the magnitude and decreasing trend observed was consistent with equilibrium. This catalytic behavior suggested that a minimum active site density was necessary to effectively adsorb and catalyze CH_4 into synthesis gas.

Figure 22 gives the yield data from a replicate temperature programmed reaction experiment performed over the $LaCo_yAl_{12-y}O_{19-\delta}$ (y = 1.0) catalyst. The replicate experiment was performed due to the observed disparity in catalytic performance of this catalyst over catalysts with cobalt substitutions of $y \leq 0.8$. The results of the replicate were similar to those observed from the first experiment with the exception that the observed CO_2 yields were slightly lower in the replicate. The disparity observed in the catalytic performance between the catalysts with lower cobalt substitution and higher cobalt substitution suggested that the observed catalytic activity was a strong function of the cobalt active site density in the range $y \leq 0.8$.

The CO, CO_2 and CH_4 yield data was examined to determine the extent with which carbon was accumulating within the reactor. For catalyst samples with cobalt substituted into the lattice at $y \leq 0.8$, the carbon yield at 750°C was between 24 and 31% which suggested that at lower temperatures carbon was prone to accumulate within the reactor. The condensable carbon within the reactor for the catalyst with y = 1 was 0%. At 900°C, the condensable carbon yield was 0% for all catalysts in the series which suggested that operation at higher temperatures was more conducive to avoiding carbon deposition.

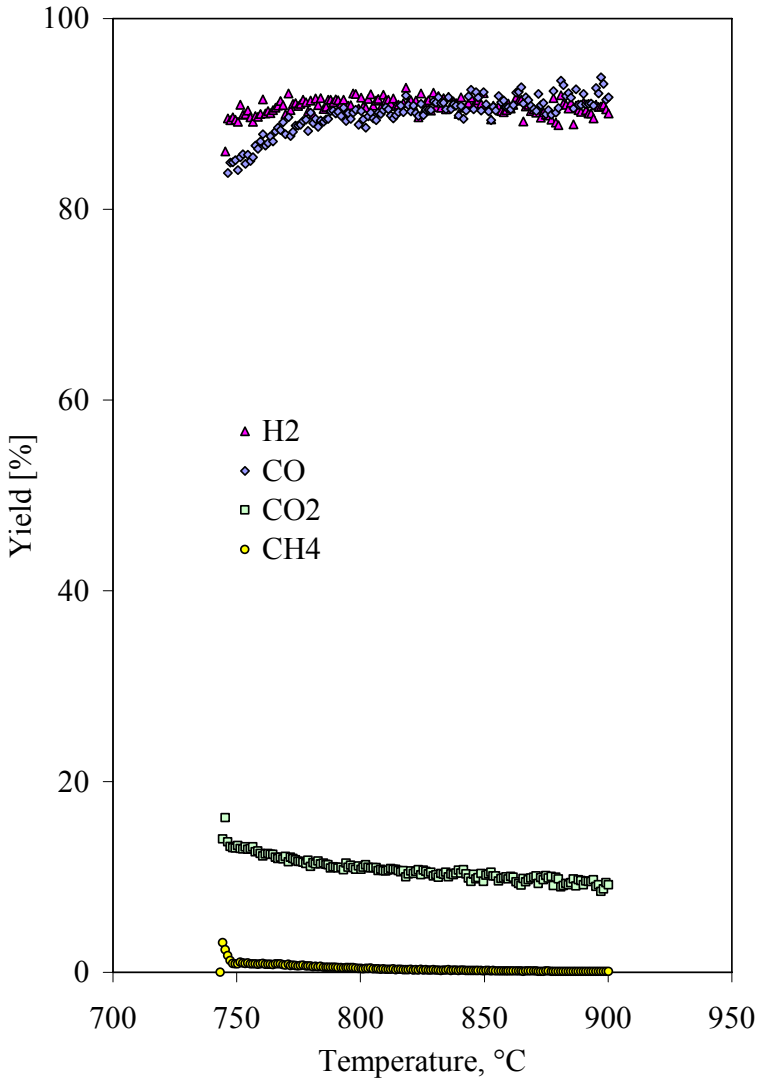

Figure 22. Product gas yields for the temperature programmed reaction of n-tetradecane over $LaCoAl_{11}O_{19-\delta}$. Replicate run.

6.3.2 Temperature Programmed Reaction over $LaFe_yAl_{12-y}O_{19-\delta}$ Series Catalysts

The H_2, CO, CO_2 and CH_4 yields for the temperature programmed reaction of n-tetradecane over $LaFe_yAl_{12-y}O_{19-\delta}$ with y = 0.2, 0.4, 0.8 and 1.0 are given in Figures 23, 24, 25 and 26, respectively. In this series of experiments the effect of varying the concentration of iron substituted into the hexaaluminate lattice with y = 0.2, 0.4, 0.8 and 1.0 was examined. The respective yields were compared over the temperature range between 750 to 900°C.

The H_2 yields that were produced during the temperature programmed reaction of n-tetradecane over the $LaFe_yAl_{12-y}O_{19-\delta}$ (y = 0.2, 0.4, 0.8 and 1.0) series of catalysts are given in Figure 23. For the entire catalyst series, the observed yields are well above those observed for TPOx. All catalysts in this series initially produced high H_2 yields that declined with increasing temperature in the low temperature region between 750 and 780°C. The H_2 yields in this region correlated with the concentration of iron substituted into the hexaaluminate lattice. This correlation did suggest that catalysts with higher iron concentrations were more effective at producing H_2 at low temperatures. The H_2 yields in this region were observed to decline with increasing temperature, which suggested that as the temperature programmed reaction progressed, hydrocarbons in the feed had accumulated onto the catalyst surface due to rapid adsorption kinetics relative to a slower surface reaction rate. As the temperature was increased from 780 to 900°C, the H_2 yield profile was observed to increase with increasing temperature. Yields in this region were observed to be tightly grouped which indicated that the entire series of iron

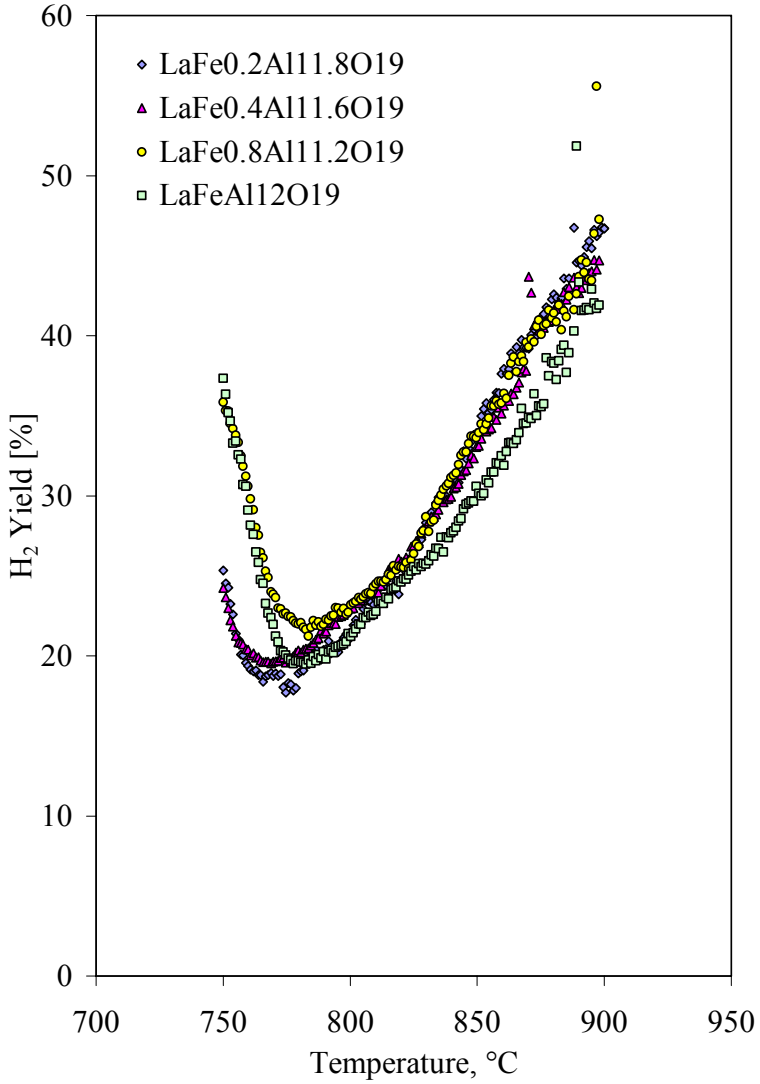

Figure 23. H_2 yields for the temperature programmed reaction of n-tetradecane over $LaFe_yAl_{12-y}O_{19-\delta}$ with y = 0.2, 0.4, 0.8 and 1.0.

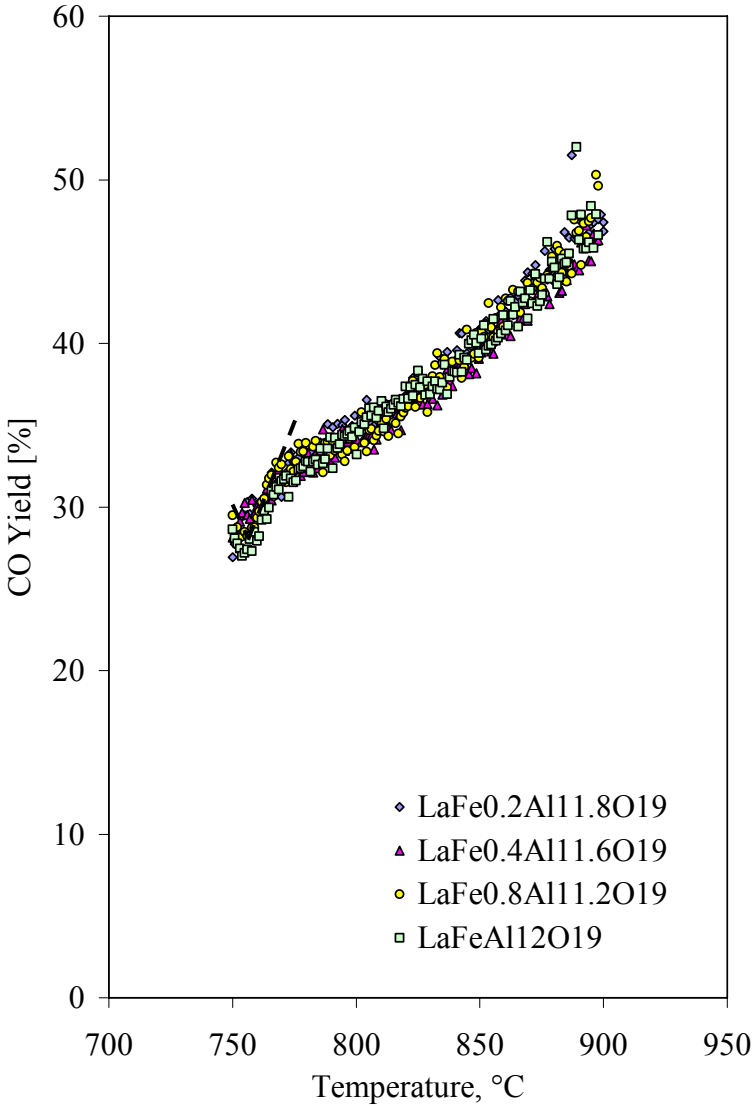

Figure 24. CO yield for the temperature programmed reaction of n-tetradecane over $LaFe_yAl_{12-y}O_{19-\delta}$ with y = 0.2, 0.4, 0.8 and 1.0.

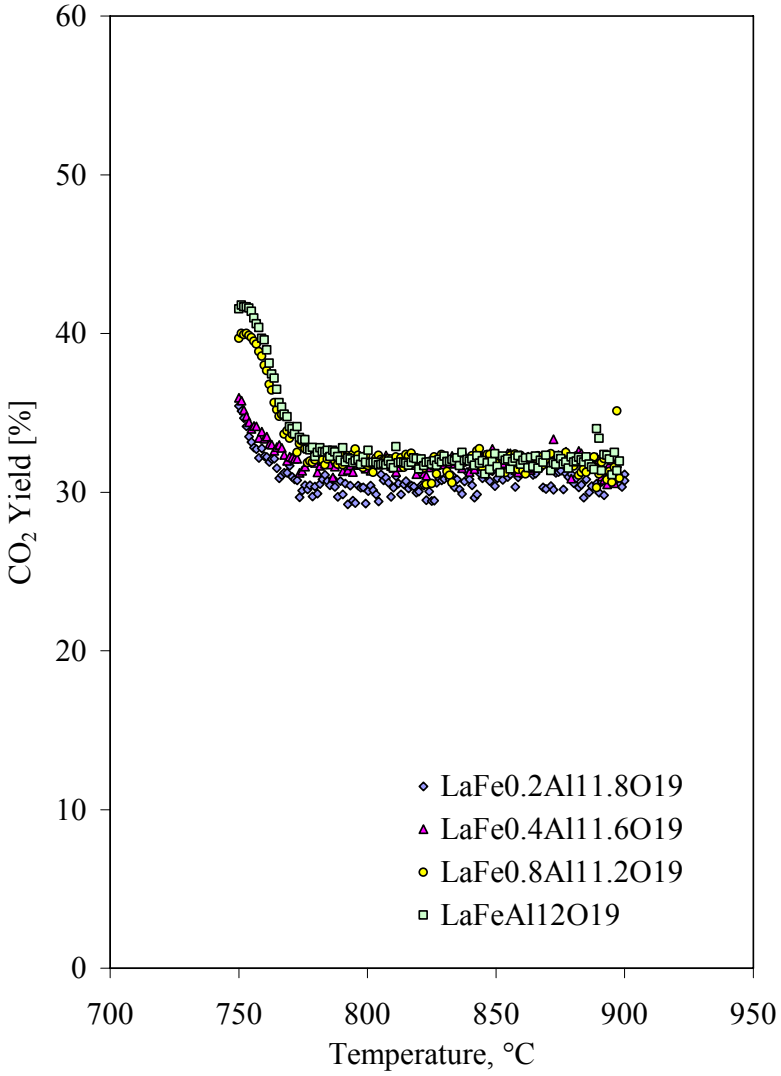

Figure 25. CO_2 yield for the temperature programmed reaction of n-tetradecane over $LaFe_yAl_{12-y}O_{19-\delta}$ with y = 0.2, 0.4, 0.8 and 1.0.

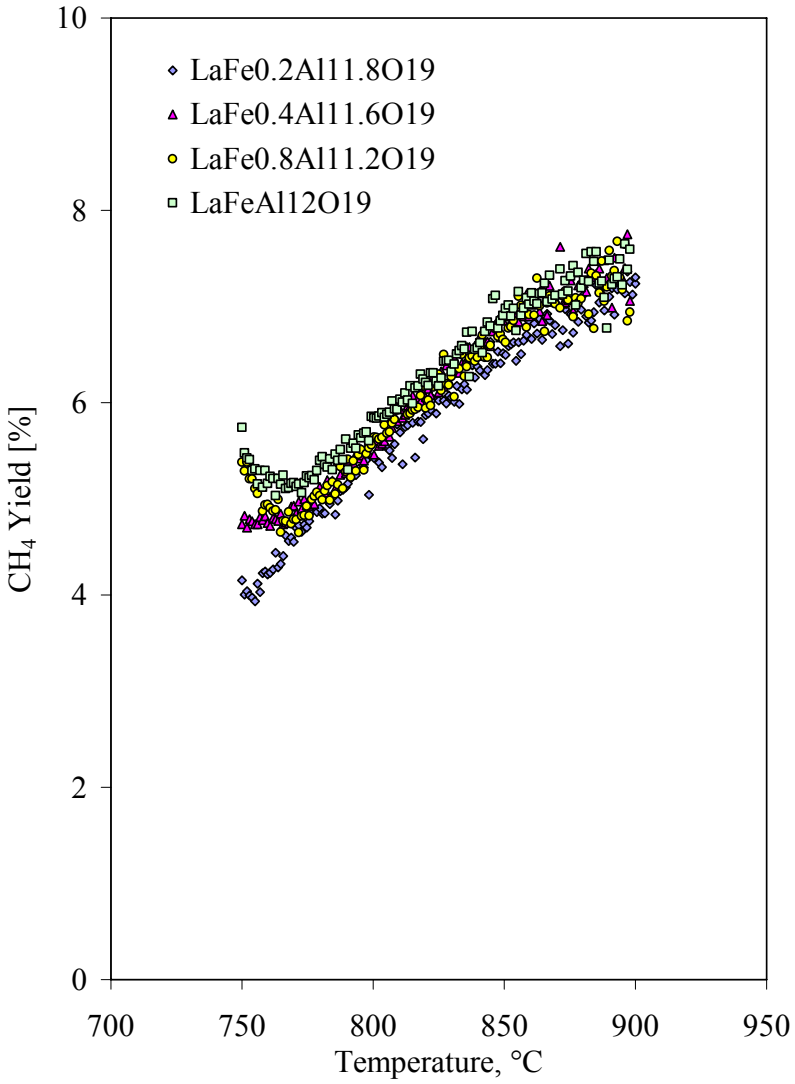

Figure 26. CH_4 yield for the temperature programmed reaction of n-tetradecane over $LaFe_yAl_{12-y}O_{19-\delta}$ with y = 0.2, 0.4, 0.8 and 1.0.

substituted hexaaluminate catalysts possessed relatively low activities.

The CO yields produced during the temperature programmed reaction of n-tetradecane over the $LaFe_yAl_{12-y}O_{19-\delta}$ (y = 0.2, 0.4, 0.8 and 1.0) series of catalysts are given in Figure 24. At the initiation of the temperature programmed reaction, all catalysts in the series produced an initially high CO yield which declined between 750 and 760°C. CO yields in this region were observed to be marginally higher than those observed by TPOx. At temperatures above 760°C, the CO yields dropped approximately to those observed with TPOx. This observation suggested that at lower temperatures, CO production had occurred through both catalytic and gas phase chemistry routes and at higher temperatures, the observed CO production was dominated by gas phase chemistry.

The CO_2 yields produced during the temperature programmed reaction of n-tetradecane over the $LaFe_yAl_{12-y}O_{19-\delta}$ (y = 0.2, 0.4, 0.8 and 1.0) series of catalysts are given in Figure 25. Catalysts with iron substitution at a concentration of y = 0.2 and 0.4 produced CO_2 yields which were equivalent to those produced from the TPOx reaction. Over the temperature range between 750 to 780°C, catalysts with iron substituted at concentrations of y = 0.8 and 1.0 produced CO_2 yields that were greater than those observed during the TPOx reaction. Above 780°C, the CO_2 yields declined and produced yields equivalent to those observed from the TPOx reaction. The differentiation in catalytic behavior between catalysts suggested that catalysts with higher concentrations of iron substituted into the lattice produced greater selectivity toward CO_2 and combustion at temperatures below 780°C. At temperatures above 780°C, sufficient

carbon or coke had deposited onto the catalytic surface to reduce the activity of the catalysts.

CH_4 yields were also observed to be affected by the concentration of iron substituted into the hexaaluminate lattice. From Figure 26 it was observed that in the temperature range between 750 and 780°C, the CH_4 yields were greater for catalysts with higher iron concentrations. Above 780°C, the CH_4 yields produced from all $LaFe_yAl_{12-y}O_{19-\delta}$ catalysts in the series were tightly grouped and were consistent with the TPOx yields. This behavior suggested that iron substituted into the hexaaluminate lattice was a relatively low activity catalyst and that gas phase chemistry dominated at temperatures above 780°C.

The CO, CO_2 and CH_4 yield data was examined to determine the extent with which condensable carbon was formed. For all catalyst samples, the condensable carbon yield observed at 750°C was between 25 and 33% which suggested that at the lower temperatures condensable carbon was prone to occur within the reactor. At 900°C, the condensable carbon yield was between 11 and 17% for all catalysts. For the iron substituted hexaaluminate catalyst series, it was not possible to identify an operating temperature where condensable carbon would form.

6.3.3 Temperature Programmed Reaction over $LaNi_yAl_{12-y}O_{19-\delta}$ Series Catalysts

The H_2, CO, CO_2 and CH_4 yields for the temperature programmed reaction of n-tetradecane over $LaNi_yAl_{12-y}O_{19-\delta}$ with y = 0.2, 0.4, 0.8 and 1.0 are given in Figures 27, 28, 29 and 30, respectively. In this series of experiments the effect of varying the concentration of nickel substituted into the hexaaluminate lattice with y = 0.2, 0.4, 0.8 and 1.0 was examined. The respective yields were compared over the temperature range between 750 to 900°C.

The H_2 yields produced during the temperature programmed reaction of n-tetradecane over the $LaNi_yAl_{12-y}O_{19-\delta}$ (y = 0.2, 0.4, 0.8 and 1.0) series of catalysts are given in Figure 27. All nickel substituted lanthanum hexaaluminate catalysts within the series were observed to produce H_2 yields that were greater than those observed with the TPOx reaction. Overall, the H_2 yields were found to correlate with the concentration of nickel substituted into the lanthanum hexaaluminate lattice, where the magnitude of the H_2 yields increased with increasing nickel substitution. The low temperature activity of catalysts in this series produced an initial decline in H_2 yield with increasing temperature. This behavior was previously observed with both the cobalt and iron substituted lanthanum hexaalumiante catalysts. However; with the nickel catalysts, the temperature range and the decay rate with which the H_2 yield declined correlated with the concentration of nickel substituted into the lattice. The order of H_2 yield decay occurred as follows: $y = 0.2 > 0.4 > 0.8 > 1.0$.

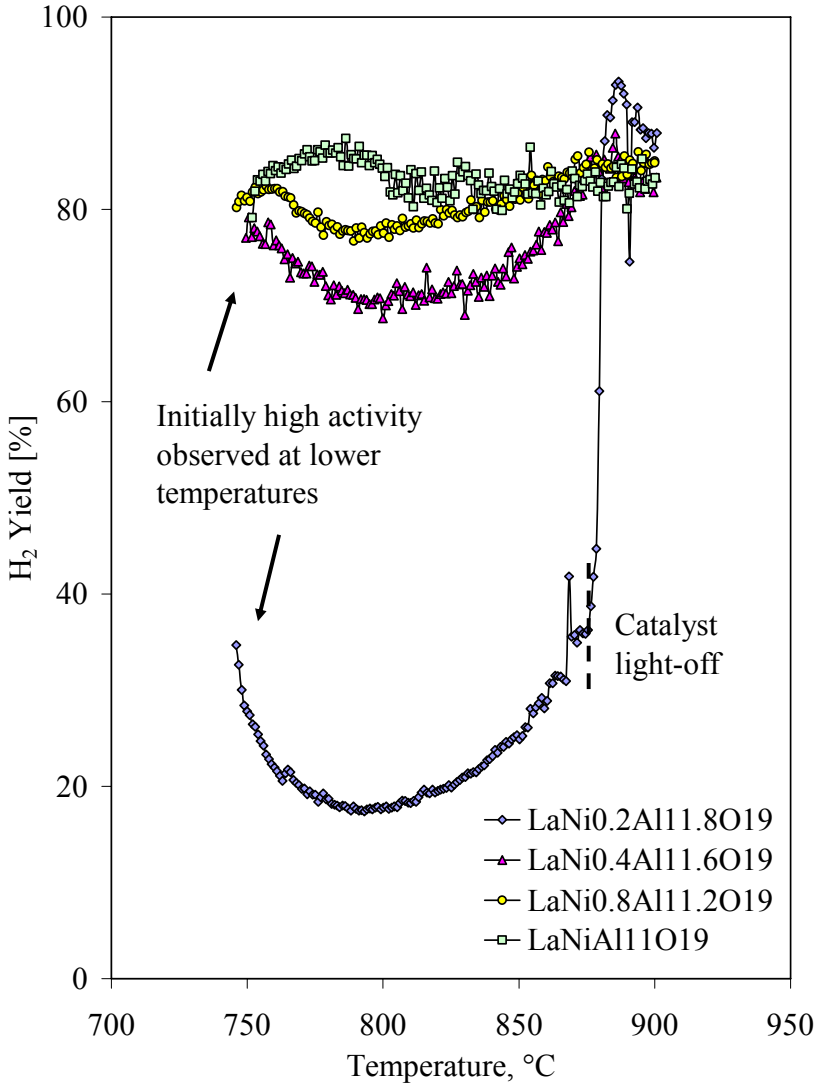

Figure 27. H_2 yields for the temperature programmed reaction of n-tetradecane over $LaNi_yAl_{12-y}O_{19-\delta}$ with y = 0.2, 0.4, 0.8 and 1.0.

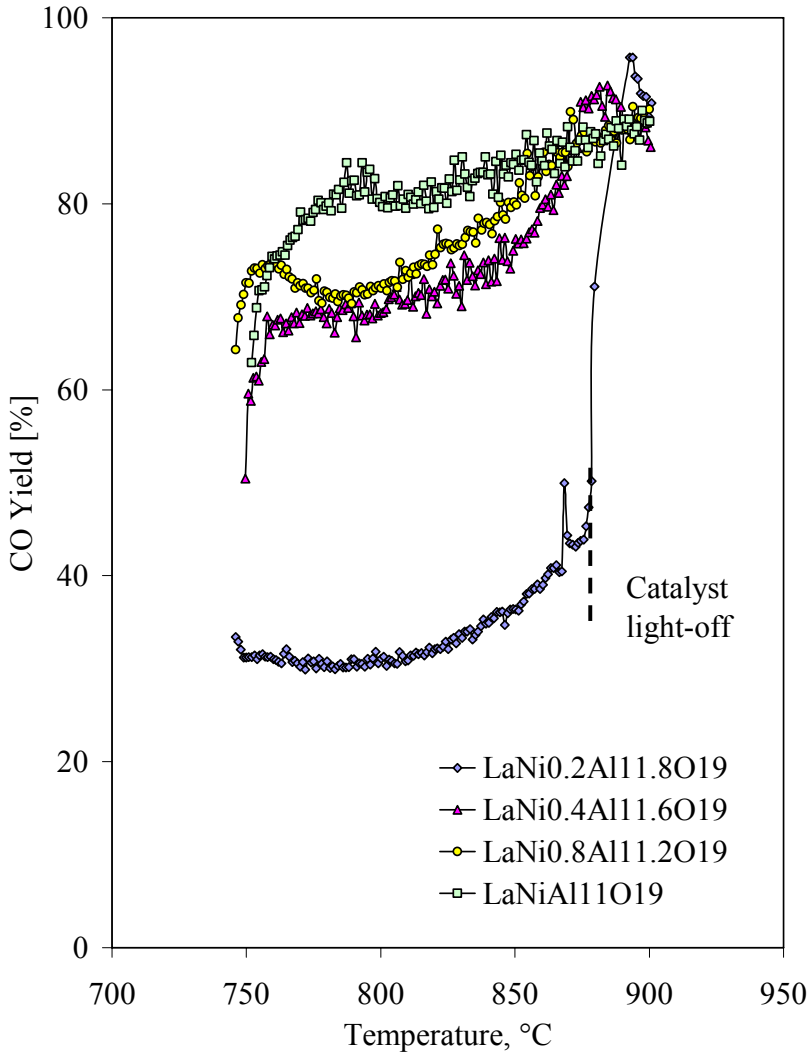

Figure 28. CO yield for the temperature programmed reaction of n-tetradecane over $LaNi_yAl_{12-y}O_{19-\delta}$ with y = 0.2, 0.4, 0.8 and 1.0.

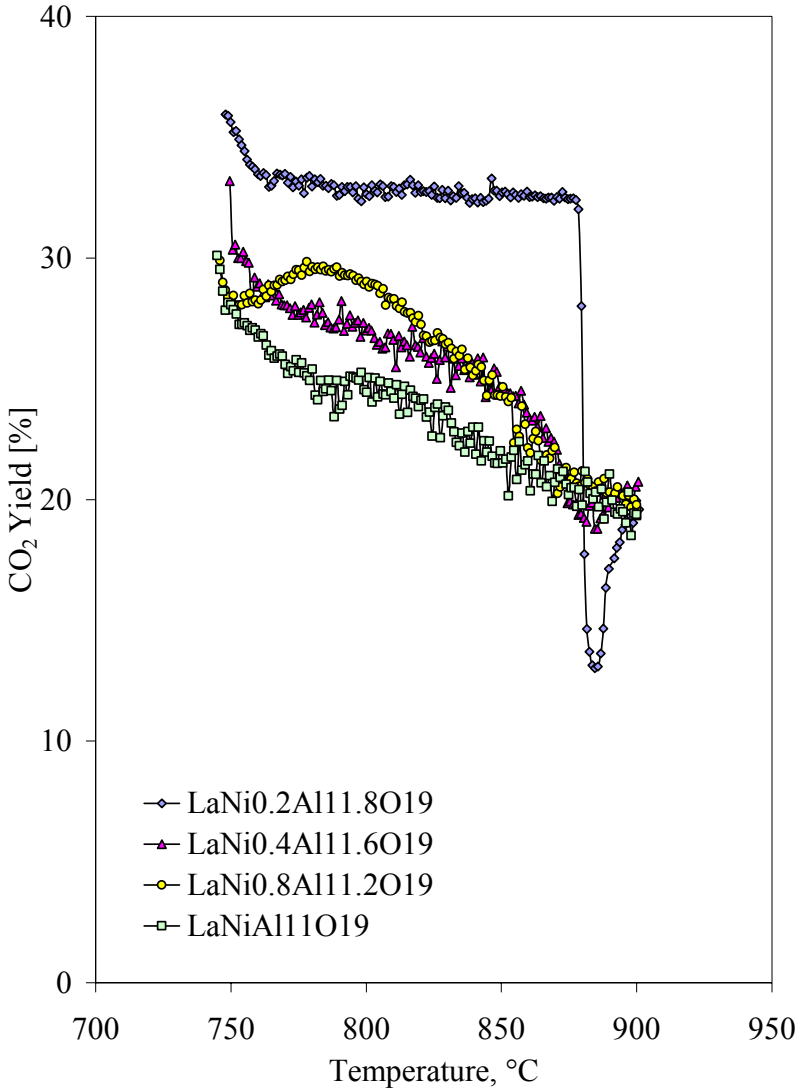

Figure 29. CO_2 yield for the temperature programmed reaction of n-tetradecane over $LaNi_yAl_{12-y}O_{19-\delta}$ with y = 0.2, 0.4, 0.8 and 1.0.

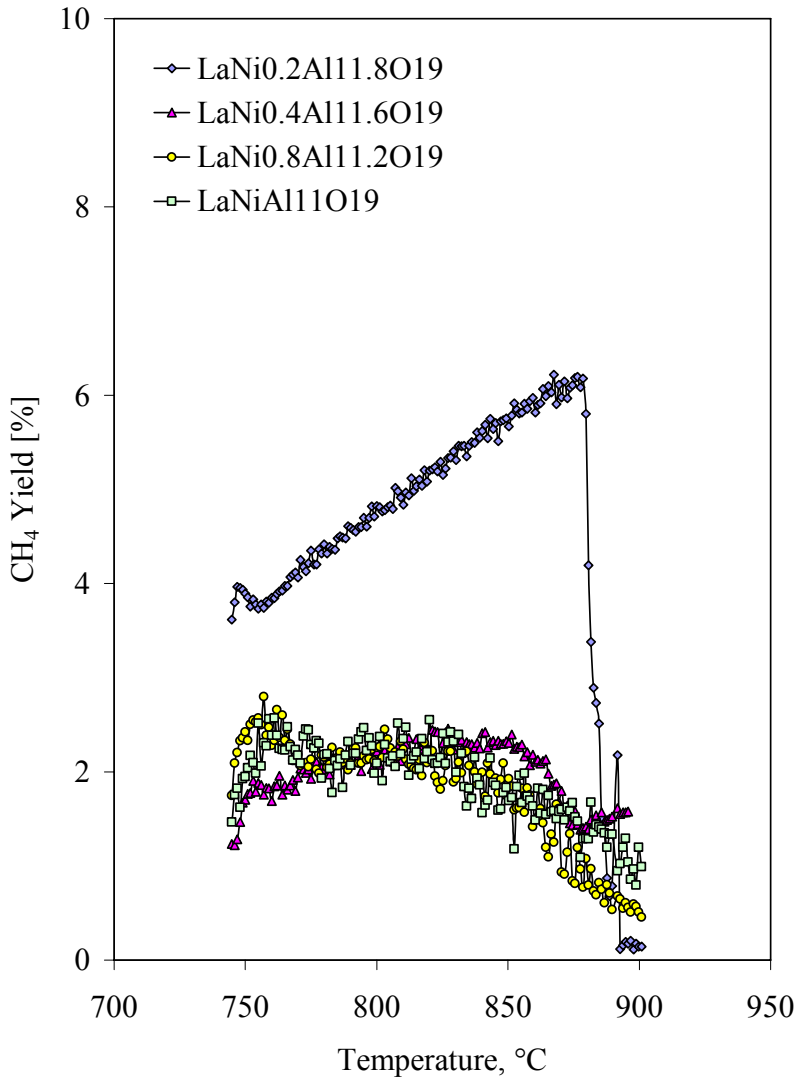

Figure 30. CH_4 yield for the temperature programmed reaction of n-tetradecane over $LaNi_yAl_{12-y}O_{19-\delta}$ with y = 0.2, 0.4, 0.8 and 1.0.

The initial loss of catalytic activity which occurred at low temperatures appeared to be related to the strong adsorption tendency of hydrocarbons in the feed relative to the activity of the catalytic. Where catalysts with less active ensemble of nickel sites were initially less active and exhibited a more rapid decay in yield due to carbon deposition onto the catalyst surface. Probabilistically, catalysts with a greater concentration of nickel substituted into the lattice had more active area and a greater concentration of Ni-NNN sites. The correlation between increasing catalytic activity and nickel substitution into the hexaaluminate lattice was consistent with prior literature which suggested that activity correlated with nickel concentration in the hexaaluminate lattice for the partial oxidation of methane (47, 55). The $LaNi_yAl_{12-y}O_{19-\delta}$ catalyst with a nickel substitution of $y = 0.2$ exhibited a significant departure in catalytic performance over the other catalysts with higher concentrations of nickel in the lattice. This catalyst exhibited a sharp increase in H_2 yield at 875°C and correspondingly a sharp decrease in CH_4 yield which indicated that the additional H_2 was derived from CH_4 reforming. This catalytic behavior suggested that the product CH_4 was not as effectively adsorbed and dissociated onto this catalytic surface relative to the other catalysts in the series at temperatures less than 875°C. Since a low concentration of nickel sites was associated with low coordination sites, this effect was likely related to the catalyst surface structure. Above 875°C, equilibrium H_2 yields were observed with all catalysts in the series.

The CO yields produced from the temperature programmed reaction are given in Figure 28. The trends observed with the CO yields differed from the H_2 yields by exhibiting an initially steep increase in yield with temperature between 750 to 760°C.

This behavior suggested that the catalyst was undergoing an induction period within this region. Above this temperature range, the CO yield profiles were similar to the H_2 yield, where the CO yield dropped followed by an increase as temperature was increased. Catalysts with nickel substituted into the lattice with y = 0.4, 0.8 and 1.0 produced a decay rate which increased with increasing nickel substitution into the lattice. The trend with CO yield was similar to that found in the H_2 yield where the yields correlated with the nickel substitution in the following order: y = 1 > 0.8 > 0.4 > 0.2. Light-off was observed to occur at 875°C which was the same location that H_2 was observed to light-off.

The CO_2 yields produced from the temperature programmed reaction are given in Figure 29. The observed yields suggested a high selectivity toward combustion and that some gas phase chemistry had occurred with all catalyst samples. All catalysts in the series undergo an induction period between 750 to 760°C similar to that observed with CO yields. However, in contrast to the CO and H_2 yields, the CO_2 yields were initially high and declined with increasing temperature between 750 and 760°C. For the nickel catalysts substituted at y = 0.2, the CO_2 yields were observed to be equivalent to those observed with the TPOx experiment which indicated that the gas phase chemistry route to synthesis gas production was more dominant in this catalyst than with other higher nickel content catalysts in the series. Consistent with the prior observations for H_2 and CO yields, the CO_2 yield rapidly dropped at 875°C when the catalyst exhibited light-off. At the light-off temperature, the CO_2 yields exceeded the yields observed with the other catalysts in this series followed by recovery to produce yields which were consistent with

the other catalysts in the series. For catalysts with y = 0.4, 0.8 and 1.0 the CO_2 yields were tightly grouped and decreased with increasing temperature. In general, the differentiation in catalytic behavior between nickel catalysts suggested that a minimum active site density of nickel substituted into the lattice was necessary to improve catalyst selectivity toward synthesis gas production at lower temperatures.

The CH_4 yields produced from the temperature programmed reaction over n-tetradecane are given in Figure 30. Catalysts with nickel substituted into the lattice with concentrations greater than $y \geq 0.4$ produced tightly grouped CH_4 yields that decreased with increasing temperature and produced yields which were consistent with equilibrium. Similar to the TPOx reaction, the catalyst with a nickel substitution of y = 0.2 produced a CH_4 yield that increased with increasing temperature until 875°C was reached. At 875°C, catalyst light-off was observed and the CH_4 yields rapidly drop approaching those of the other catalysts in the series.

The CO, CO_2 and CH_4 yield data was examined to determine the extent with which condensable carbon was formed within the reactor. The condensable carbon yield observed at 750°C is 24, 9, 7 and 5% for catalysts with nickel substitutions of y = 0.2, 0.4, 0.8 and 1.0, respectively. The amount of condensable carbon formed within the reactor decreased with the increasing concentration of nickel substituted into hexaaluminate lattice. However, at the low temperature condition, condensable carbon was still prone to occur with all catalysts. At 900°C the condensable carbon yield was

0% for all catalysts in the series which suggested that operation at higher temperatures was more conducive to avoiding carbon deposition.

6.3.4 Temperature Programmed Reaction over $M_INi_{0.4}Al_{11.6}O_{19-\delta}$ Series Catalysts

The purpose of this study was to examine the effect of introducing different mirror cations into the nickel substituted hexaaluminate lattice and to relate the observed physico-chemical properties to catalytic performance. H_2, CO, CO_2 and CH_4 yields for the partial oxidation of n-tetradecane over $M_INi_{0.4}Al_{11.6}O_{19-\delta}$ with M_I = Ba, La and Sr are given in Figures 31, 32, 33 and 34. The catalyst performance was normalized between the three samples by fixing the nickel composition substituted into the hexaaluminate lattice at y = 0.4.

The H_2 yields produced from the temperature programmed reaction are given in Figure 31. At the initiation of the reaction, the H_2 yields observed for all three catalysts were 80%. As the temperature was increased to 800°C, the H_2 yields for these catalysts steadily dropped. The magnitude of the H_2 yield and its departure from its value at 750 to its value at 800°C correlated with the surface nickel concentration observed by XPS in Section 5.3.5 and the concentration of reduced nickel sites observed by H_2 pulse chemisorption in Section 5.3.4. Above 800°C, the H_2 yields for the three catalysts increased until near equilibrium yields were achieved at 900°C. The $BaNi_{0.4}Al_{11.6}O_{19-\delta}$ catalyst exhibited similar catalytic behavior to that previously observed with the $LaNi_{0.2}Al_{11.6}O_{19-\delta}$ catalyst where the CH_4 present in the reformate was spontaneously

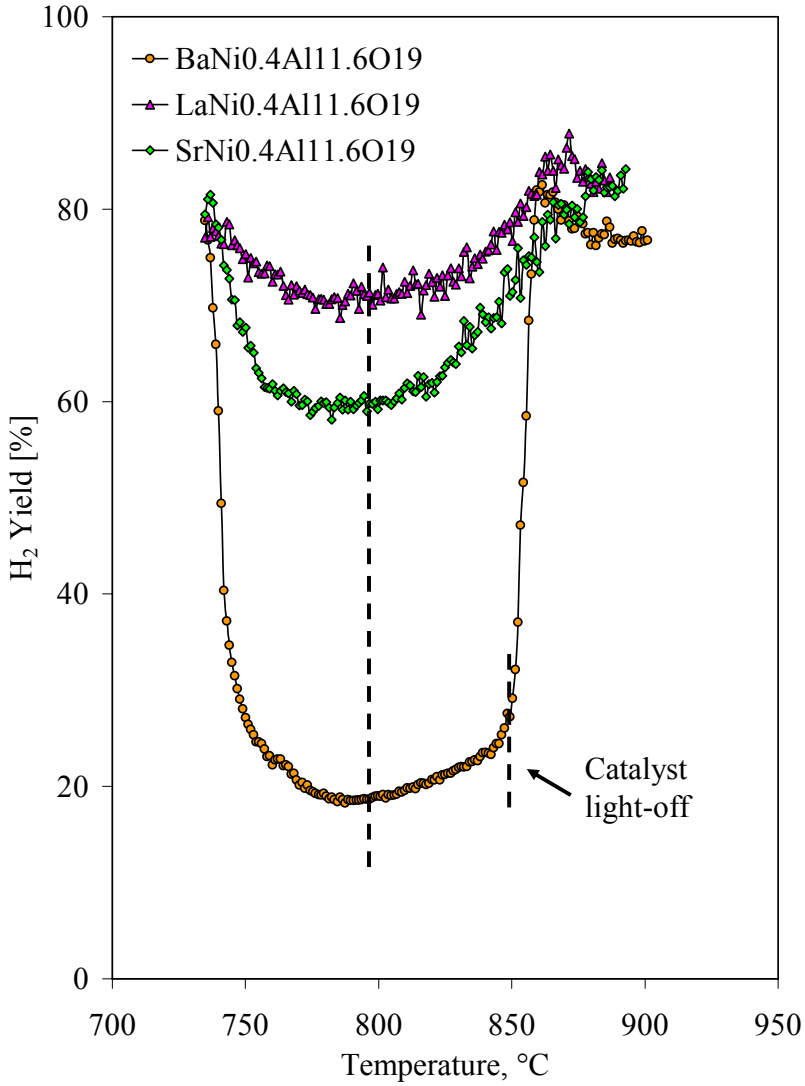

Figure 31. H_2 yield for the temperature programmed reaction of n-tetradecane over $M_INi_{0.4}Al_{11.6}O_{19-\delta}$ with M_I = Ba, La and Sr.

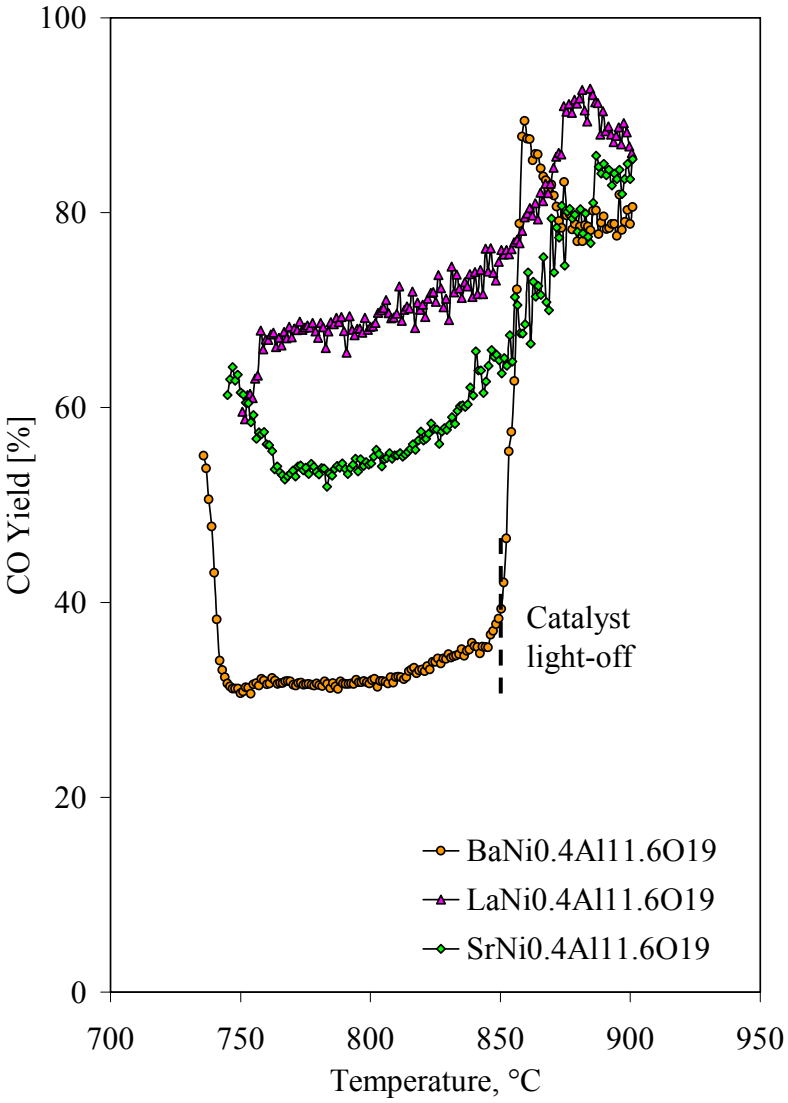

Figure 32. CO yield for the temperature programmed reaction of n-tetradecane over $M_INi_{0.4}Al_{11.6}O_{19-\delta}$ with M_I = Ba, La and Sr.

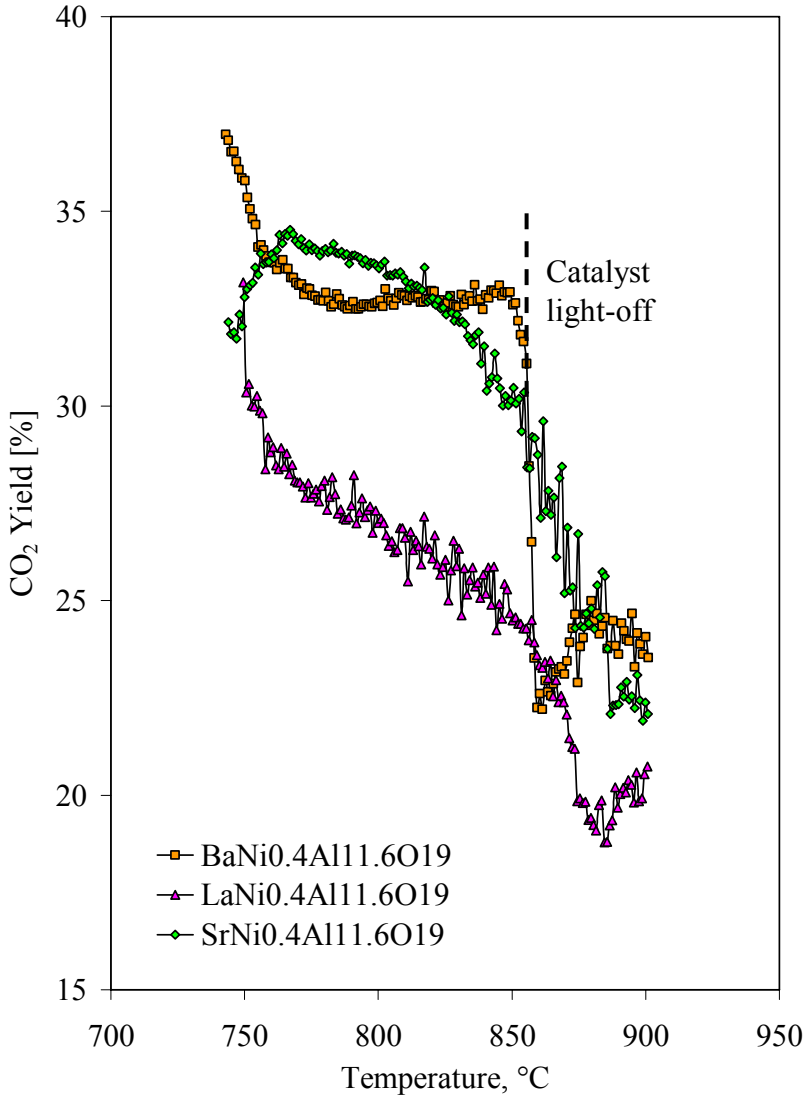

Figure 33. CO_2 yield for the temperature programmed reaction of n-tetradecane over $M_INi_{0.4}Al_{11.6}O_{19-\delta}$ with M_I = Ba, La and Sr.

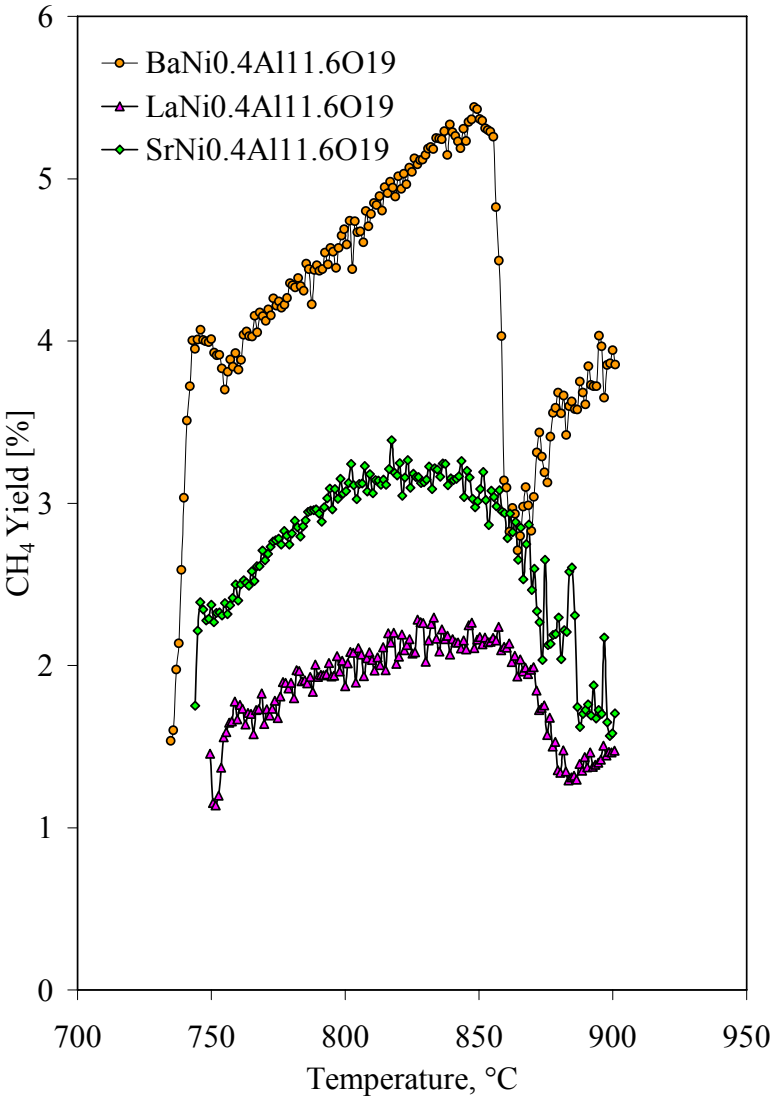

Figure 34. CH_4 yield for the temperature programmed reaction of n-tetradecane over $M_INi_{0.4}Al_{11.6}O_{19-\delta}$ with M_I = Ba, La and Sr.

activated at high temperatures to produce increased H_2 yields. However; with the $BaNi_{0.4}Al_{11.6}O_{19-\delta}$ catalyst, light-off was observed at 850°C, rather than 875°C. The similarity in the catalytic behavior between the $BaNi_{0.4}Al_{11.6}O_{19-\delta}$ and the $LaNi_{0.2}Al_{11.6}O_{19-\delta}$ catalyst suggested that the CH_4 light-off was related to the surface concentration of nickel on the surface of the catalyst. The delayed activation of CH_4 onto the surface of these two catalysts was likely related to the formation of low coordination sites which influence CH_4 adsorption and dissociation onto nickel surfaces (52).

The CO yields produced from the temperature programmed reaction are given in Figure 32. At the initiation of the reaction, the $LaNi_{0.4}Al_{11.6}O_{19-\delta}$ catalyst exhibited an initial increase in the CO yield between 750 and 760°C, while the $BaNi_{0.4}Al_{11.6}O_{19-\delta}$ and $SrNi_{0.4}Al_{11.6}O_{19-\delta}$ catalysts exhibited an initially steep decrease in yield. The catalytic behaviors observed between the slopes of the CO yields in this region were attributed to differences in the surface nickel concentration between the catalysts where the catalyst with increasing activity exhibited the greatest nickel surface concentration. As the reaction temperature was increased to 900°C, the CO yields correspondingly increased to equilibrium which indicated that the reaction rate which increased with temperature. In this temperature region, the CO yields produced correlated with the concentration of surface nickel on the catalysts. With the $BaNi_{0.4}Al_{11.6}O_{19-\delta}$ catalyst, light-off was observed as a sharp increase in the CO yields at 850°C.

The CO_2 yields produced from the temperature programmed reaction are given in Figure 33. The CO_2 yields for the $BaNi_{0.4}Al_{11.6}O_{19-\delta}$ and $SrNi_{0.4}Al_{11.6}O_{19-\delta}$ catalysts were

greater than those observed with the $LaNi_{0.4}Al_{11.6}O_{19-\delta}$ catalyst. The CO_2 yield and profile in the region between 750 and 850°C over the $BaNi_{0.4}Al_{11.6}O_{19-\delta}$ catalyst were similar to the thermal partial oxidation yields. All catalysts in the series experienced an induction period similar to that observed with CO yields. Consistent with the prior observations for H_2 and CO yields, the CO_2 yield rapidly dropped at 850°C when the CH_4 partial oxidation reaction lit-off. At the light-off temperature, the CO_2 yields exceeded the yields observed with the other catalysts in this series followed by recovery to produce yields consistent with the other catalysts. The CO_2 yields were comparable between catalysts at temperatures above 850°C.

The CH_4 yields produced from the temperature programmed reaction are given in Figure 34. The magnitude of the CH_4 yields correlated with the concentration of nickel on the surface of the catalysts. This relationship suggested that the ability for this catalyst to activate CH_4 was influenced by the nickel surface concentration. The $BaNi_{0.4}Al_{11.6}O_{19-\delta}$ catalyst produced a CH_4 yield that increased with increasing temperature until 850°C was reached. At 850°C, catalyst light-off was observed and the CH_4 yield rapidly approached those of the other catalysts in the series. The decrease in CH_4 yield approximately correlated with the additional H_2 produced which suggested that CH_4 was the source of the increase in H_2 yield. The differentiation in catalytic behavior between the catalysts with different mirror cations suggested that a minimum active site density of nickel was necessary to improve catalyst selectivity toward synthesis gas production at the lower temperatures.

The CO, CO_2 and CH_4 yield data was examined to determine the extent with which condensable carbon was formed within the reactor. The observed condensable carbon yields at 750°C are 11, 5 and 9% for $BaNi_{0.4}Al_{11.6}O_{19-\delta}$, $SrNi_{0.4}Al_{11.6}O_{19-\delta}$, $LaNi_{0.4}Al_{11.6}O_{19-\delta}$, respectively. At the low temperature condition, condensable carbon products were prone to form within the reactor. At 900°C, the condensable carbon yield was 0% for all catalysts in the series which suggested that operation at higher temperatures was more conducive to avoiding carbon deposition.

6.4 Conclusions

Hexaaluminate catalyst activity toward the partial oxidation of n-tetradecane was examined as a function of transition metal type (e.g., Co, Fe and Ni), temperature, the concentration of active metal substituted into the lattice and the mirror cation type. Catalyst selectivity was assessed through H_2, CO, CO_2 and CH_4 yields and compared to equilibrium and thermal partial oxidation results.

Iron substituted into the lanthanum hexaaluminate lattice was shown to exhibit poor catalytic activity and selectivity at all concentrations during the temperature programmed reaction with n-tetradecane. Cobalt substituted into the lanthanum hexaaluminate lattice at concentrations of $y \leq 0.8$ exhibited equally poor catalytic activity and selectivity. However, the $LaCoAl_{11}O_{19-\delta}$ catalyst exhibited equilibrium CO and H_2 yields.

The $LaNi_yAl_{12-y}O_{19-\delta}$ series and the $M_INi_{0.4}Al_{11.6}O_{19-\delta}$ series of catalysts possessed the greatest H_2 and CO activity and selectivity over the temperature region examined. Both the $LaNi_{0.2}Al_{11.8}O_{19-\delta}$ and the $BaNi_{0.4}Al_{11.6}O_{19-\delta}$ catalysts exhibited a sharp increase in H_2 yield at 850 and 875°C, respectively. The increase in H_2 yield in this region corresponded to a decrease in CH_4 yield which indicated that the additional H_2 was derived from CH_4. This catalytic behavior suggested that CH_4 in the reformate was not as effectively adsorbed and dissociated onto the nickel sites present in these catalysts and that a complex kinetic balance existed between the adsorption of hydrocarbons onto the hexaaluminate catalyst surface and their rate of reaction.

From the temperature programmed reaction data examined, the differentiation in catalytic performance between catalysts was shown to be closely related not only to the active metal substituted into the hexaaluminate lattice, but also to its concentration in the lattice. The metal concentration, therefore, affected the catalytic surface structure which was evolved and was available for reaction. The surface reaction rate and the dehydrogenation activity were functions of the choice of metal introduced into the lattice. The catalytic properties that were related to performance, therefore, were active metal type and area and the coordination of active sites which were achieved.

The mirror cation was also shown to affect catalytic performance. The differentiation in catalytic behavior observed between catalysts with different mirror cations suggested that the surface nickel concentration, not the bulk nickel concentration, controls catalyst activity and selectivity.

7.0 n-TETRADECANE PARTIAL OXIDATION OVER $M_INi_{0.4}Al_{11.6}O_{19-\delta}$ CATALYSTS

7.1 Introduction

Reforming of middle distillate fuels for distributed fuel cell power is a very attractive source of H_2 and CO. However, these fuels contain heavy hydrocarbons that are prone to coking. The simplest reforming technology is passive, where a catalyst is employed to reform the middle distillate into H_2 and CO and to convert the organo-sulfur compounds into more easily removed H_2S. This approach necessitates the development of a catalyst which does not deactivate under these conditions.

The use of hexaaluminate-type materials are of growing importance in catalysis due to their refractory nature. Its thermal stability is attributed to its structure, which has proven useful in retaining the large surface area necessary for catalytic reaction. In a series of studies on CO_2–CH_4 and the partial oxidation of methane (46, 47, 62, 49), nickel doped hexaaluminate catalysts have demonstrated useful activity, selectivity and long term stability. The activity and selectivity for these catalysts has been suggested to originate from metallic nickel sites (47, 62, 68).

It is expected that oxygen within the mirror plane of nickel doped hexaaluminate will preferentially reduce over oxygen in the spinel block, exposing metallic nickel sites in this region. Therefore, the excellent stability toward coking exhibited by nickel

substituted hexaaluminate catalysts may well be due to reduced nickel sites that have been atomically dispersed within the lattice.

One of the most challenging problems to reforming middle distillate fuels is achieving stable long term performance. The catalyst characterization results indicate the likelihood that the mirror cation influences the coordinative environment of the active sites. Therefore, the effectiveness at controlling coke formation by dispersing nickel within the hexaaluminate lattice with different mirror cations is evaluated by assessing catalytic stability during the isothermal partial oxidation of n-tetradecane. In this study, the structural effect that the mirror cation provided to stability is evaluated over $LaNi_{0.4}Al_{11.6}O_{19-\delta}$, $SrNi_{0.4}Al_{11.6}O_{19-\delta}$ and $BaNi_{0.4}Al_{11.6}O_{19-\delta}$ catalysts.

7.2 Experimental

7.2.1 Steady-State Reactions

The stability of hexaaluminate catalysts was examined by isothermal partial oxidation of n-tetradecane over $M_INi_{0.4}Al_{11.6}O_{19-\delta}$ (M_I = Ba, Sr and La). Catalysts were first pre-reduced at 850°C for 1 hour in 10 vol% H_2/N_2 to expose the active nickel sites. The reactant pre-heat temperature was set at 350°C to ensure proper vaporization of the fuel and to avoid pre-ignition and coking of the catalyst and feed lines. Catalyst GHSV was kept constant for all runs at 50,000 $cm^3g^{-1}h^{-1}$. The O/C was set at 1.2 to avoid excessive coking on the catalyst. The total inlet feed flow rate was set at 450 sccm with the inlet N_2

flow rate set at 50 sccm and the air flow rate set at 390 sccm. The pressure was kept constant at 197.9 kPa. Catalysts were run for approximately 5.5 hours. Product gas compositions were monitored continuously by mass spectrometer.

H_2, CO, CO_2 and CH_4 yields were calculated from gas phase exit N_2, H_2, CO, CO_2 and CH_4 concentrations. The H_2, CO, CO_2 and CH_4 yields were calculated from equations (6) though (12) defined in Section 6.2.1. Experimentally, n-tetradecane was not observed in the product stream at the conditions tested indicating that conversion was nearly 100% in all cases.

7.3 Results and Discussion

The effectiveness at controlling coke formation by atomically dispersing nickel into the lattice of hexaalumina was evaluated by assessing each catalyst's stability during the partial oxidation of n-tetradecane. This reaction was carried out by introducing n-tetradecane over the $LaNi_{0.4}Al_{11.6}O_{19-\delta}$, $SrNi_{0.4}Al_{11.6}O_{19-\delta}$ and $BaNi_{0.4}Al_{11.6}O_{19-\delta}$ catalysts. The H_2, CO, CO_2 and CH_4 yields were examined as function of time.

The product composition from the partial oxidation of n-tetradecane over $LaNi_{0.4}Al_{11.6}O_{19-\delta}$ is shown in Figure 35. For the first 30 minutes of reaction time, H_2 and CO concentrations continued to increase steadily until a stable activity level was achieved. This increase was the result of feed lag time introduced by the dead volume of

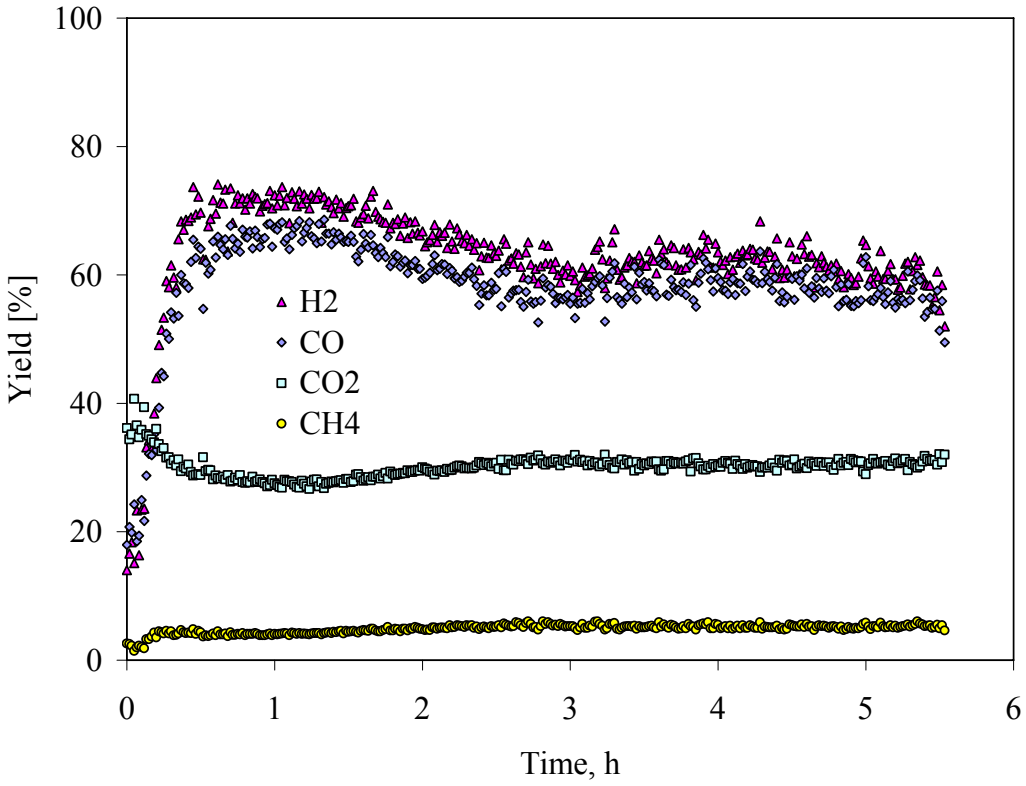

Figure 35. Partial oxidation of n-tetradecane over $LaNi_{0.4}Al_{11.6}O_{19-\delta}$ catalyst.

the reactor system. The scatter observed in the data was the result of pressure fluctuations induced by the vaporization of the n-tetradecane. The catalytic activity for $LaNi_{0.4}Al_{11.6}O_{19-\delta}$ peaked after 45 minutes producing average H_2 and CO yields of 77.2 and 66.0%, respectively.

After 1 hour, H_2 and CO concentrations began to decline indicating that carbon deposition onto the catalyst surface was occluding active sites. For hydrocarbons to form carbon deposits on the surface of the catalyst suggested that the coordinative environment of active nickel sites stabilized hydrocarbon adsorption onto the surface of the catalyst such that dehydrogenation and carbon deposition resulted. After 3 hours of reaction time, a carbon overlayer likely passivated the ensemble of nickel sites which were more active toward carbon deposition and a more stationary level of activity was observed. Though the activity of the catalyst changed over the course of the experiment, the selectivity, $H_2/CO = 1.18$, remained constant. These results suggested that the $LaNi_{0.4}Al_{11.6}O_{19-\delta}$ catalyst likely possessed two types of active sites, those that were more active toward carbon deposition and those that were less active. The total carbon deposited onto the $LaNi_{0.4}Al_{11.6}O_{19-\delta}$ catalyst surface was determined by TPO to be 29.1 wt%.

The partial oxidation performance of n-tetradecane over the $BaNi_{0.4}Al_{11.6}O_{19-\delta}$ and $SrNi_{0.4}Al_{11.6}O_{19-\delta}$ catalysts is shown in Figures 36 and 37, respectively. Both catalysts achieved a steady state activity after approximately 30 minutes with average H_2 and CO yields of 72 and 71.9 % observed for $BaNi_{0.4}Al_{11.6}O_{19-\delta}$ and 75 and 75 % observed for

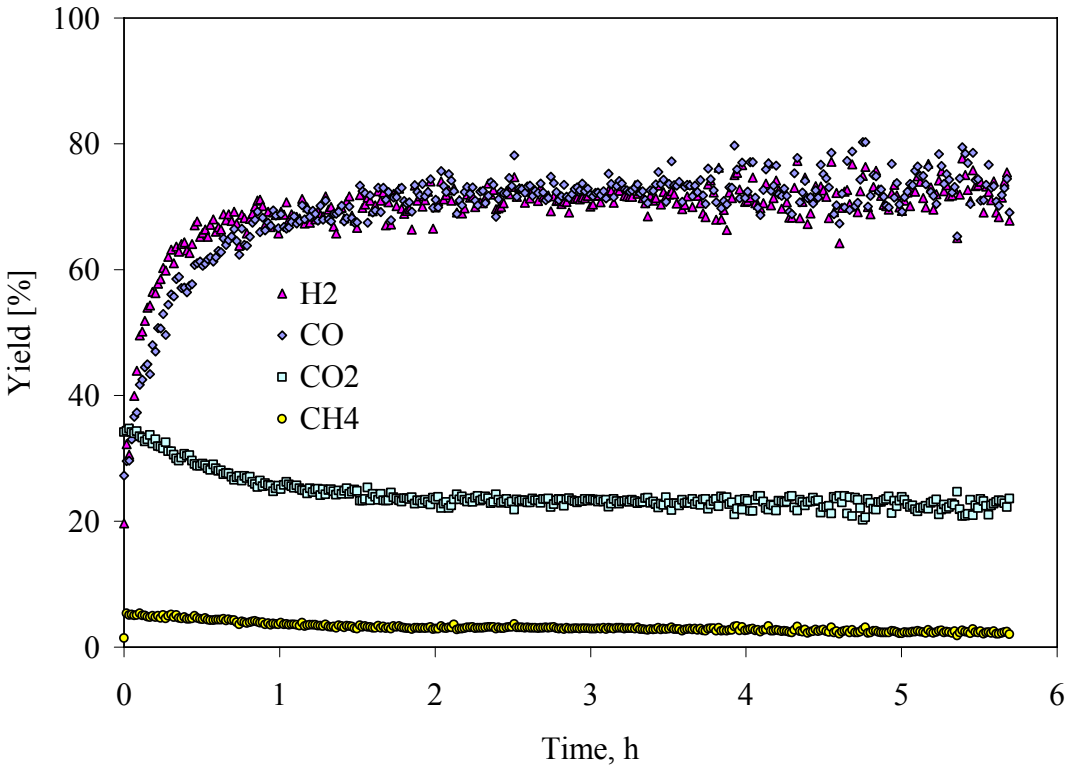

Figure 36. Partial oxidation of n-tetradecane over $BaNi_{0.4}Al_{11.6}O_{19-\delta}$ catalyst.

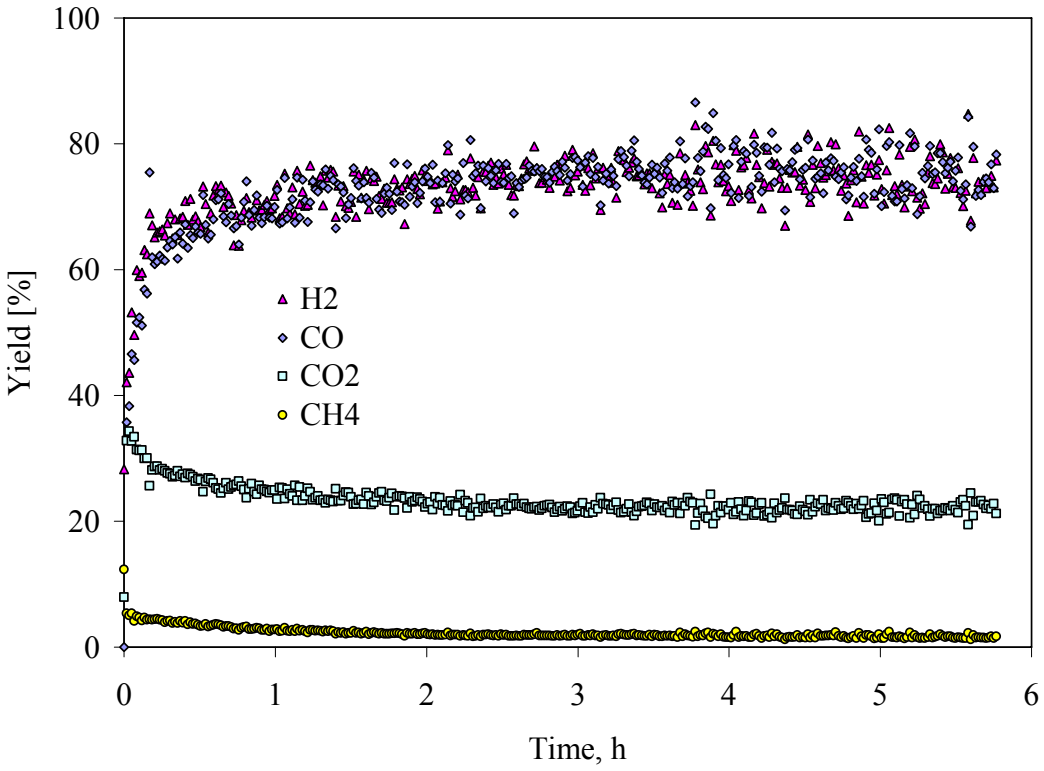

Figure 37. Partial oxidation of n-tetradecane over $SrNi_{0.4}Al_{11.6}O_{19-\delta}$ catalyst.

$SrNi_{0.4}Al_{11.6}O_{19-\delta}$. In contrast to the $LaNi_{0.4}Al_{11.6}O_{19-\delta}$ catalyst, there was no decline in activity observed over the 5.5 hours online with $BaNi_{0.4}Al_{11.6}O_{19-\delta}$ and $SrNi_{0.4}Al_{11.6}O_{19-\delta}$.

In addition, their selectivity remained constant over the course of these runs with $H_2/CO = 1.05$ for $BaNi_{0.4}Al_{11.6}O_{19-\delta}$ and $H_2/CO = 1.07$ for $SrNi_{0.4}Al_{11.6}O_{19-\delta}$. The total carbon deposited onto the $BaNi_{0.4}Al_{11.6}O_{19-\delta}$ and $SrNi_{0.4}Al_{11.6}O_{19-\delta}$ catalyst surfaces were determined by TPO to be 11.8 and 10.0 wt%, respectively.

Highly coordinated active sites have been shown to be more effective at stabilizing hydrocarbons onto the surface of a catalyst which adsorb through multi-point mechanisms (54). Hydrocarbons that are more effectively stabilized to the surface of a catalyst are more prone to undergo dehydrogenation reactions that lead to carbon deposition (54). Certainly, in an atomically dispersed catalyst system once the concentration of active sites changes, so to will the number of active site neighbors.

Since the nickel concentration on the hexaaluminate catalyst surface varies with the mirror cation, it is suggested here that $BaNi_{0.4}Al_{11.6}O_{19-\delta}$ and $SrNi_{0.4}Al_{11.6}O_{19-\delta}$ catalysts, which exhibit lower nickel dispersions than $LaNi_{0.4}Al_{11.6}O_{19-\delta}$, exhibit greater stability and are less prone to form carbon deposits due to a reduction in highly coordinated nickel sites relative to those present in $LaNi_{0.4}Al_{11.6}O_{19-\delta}$. The apparent activity loss in $LaNi_{0.4}Al_{11.6}O_{19-\delta}$ was consistent with the presence of two types of active sites, those that

exist in high coordination and are more active toward carbon formation and those that are present in a lower state of coordination and are less active toward carbon formation.

The long term stability of the $BaNi_{0.4}Al_{11.6}O_{19-\delta}$ was examined over 100 hours of n-tetradecane partial oxidation. The process conditions were the same as the shorter 5.5 hour tests. The H_2, CO, CO_2 and CH_4 yields over 100 hours are given in Figure 38. The catalyst exhibited excellent activity, selectivity and stability over this time period. This suggests that nickel substituted into the barium hexaaluminate compound is an effective method to control carbon deposition onto the catalyst surface.

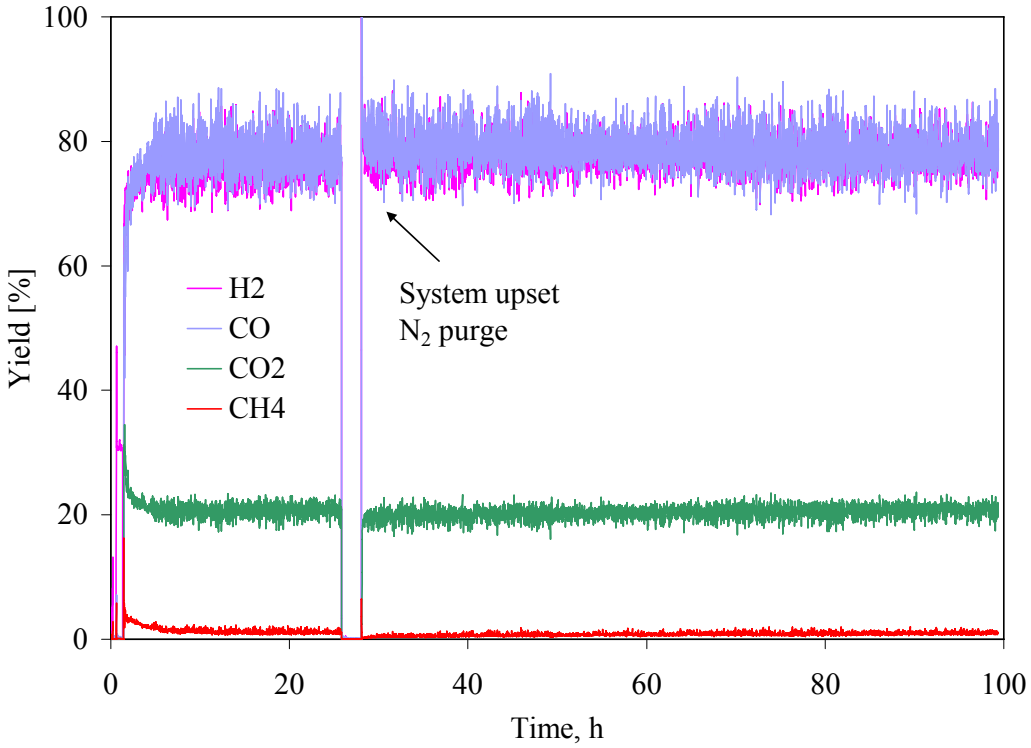

Figure 38. 100 hour catalyst stability assessment: partial oxidation of n-tetradecane over $BaNi_{0.4}Al_{11.6}O_{19-\delta}$.

7.4 Conclusions

The role that the mirror cation produced on nickel substituted hexaaluminate stability during n-tetradecane partial oxidation with n-tetradecane was examined. Nickel substituted hexaaluminate catalysts with divalent, Ba^{2+} and Sr^{2+}, mirror cations exhibited greater stability during n-tetradecane partial oxidation than did the trivalent mirror cation, La^{3+}, containing nickel substituted hexaaluminate. The unstable activity exhibited by $LaNi_{0.4}Al_{11.6}O_{19-\delta}$ indicated that carbon rapidly deposits onto the surface of the catalyst. The initial loss in activity of $LaNi_{0.4}Al_{11.6}O_{19-\delta}$ followed by the stationary level of activity suggested the presence of two different types of active nickel sites: those that were more active toward carbon deposition and those that were less active. The catalytic behavior induced by the mirror cation suggested that its influence on controlling carbon deposition was structural. Likely, the more active carbon forming sites were present as higher coordination nickel sites and the less active carbon forming nickel sites were present in a lower state of coordination.

8.0 CHARACTERISTICS OF CARBON FORMATION ON $M_INi_{0.4}Al_{11.6}O_{19-\delta}$ CATALYSTS

8.1 Introduction

One of the most challenging problems to reforming middle distillate fuels is the prevention of carbon on the catalyst. Carbon deposition onto the surface of a catalyst can occur through two routes, both of which lead to deactivation. The first route occurs when elemental carbon is formed directly by reactions involving either the decomposition of hydrocarbons in the feed stream, or reactions from CO formed during the reforming reaction (60). The second route involves the formation of unsaturated hydrocarbons known as "coke" (60).

Carbon deposition onto the catalyst surface results in the blocking of catalytically active sites. This causes the reforming reaction rate to decline over time as the carbon accumulates. The catalytic factors that affect the selectivity toward carbon formation include the intrinsic reaction rate of the metal, its dehydrogenation activity and the surface structure of the catalyst including both the dispersion and the coordinative environment of the active sites. The adsorption and desorption of hydrocarbons onto the catalyst surface is greatly influenced by their electronic environment (63, 64, 65). The interaction of catalytic metal atoms on the surface of a catalyst imparts electron deficient character to the metal due to the presence of strong metal-support interactions (12, 50). Therefore, by increasing the metal dispersion on the surface of the catalyst, electron

deficiency may be increased resulting in both a reduced rate of adsorption as well as a less strongly bonded adsorbate (50).

Carbon deposition onto the surface of a catalyst is also affected by the respective rate of bond dissociation which has been shown to be affected by the coordinative environment of active sites (53, 54). As mentioned earlier, the formation of carbon is influenced by a kinetic balance between the surface reaction of the hydrocarbon with oxygen species and the further disassociation of the hydrocarbon into adsorbed carbon atoms. Elemental carbon has been shown to adsorb more strongly onto five-fold coordinated sites at the step edges of crystallite faces (52). Over time, elemental carbon will reorganize to form the more ordered graphitic carbon which is not as easily gasified (52).

The deposition of carbon onto the surface of the catalyst is, therefore, kinetically driven. The catalytic technology that can be incorporated into a catalyst to decrease the activity toward carbon deposition includes: enhanced adsorption of steam and CO_2, faster surface reaction rates and decreasing the rate and strength of hydrocarbon adsorption onto the surface of the catalyst.

Few investigations of carbon deposition onto hexaaluminate catalysts have been reported in the literature (49, 62). Lui et al. have studied carbon deposition during the CO_2-CH_4 reforming over $LaNiAl_{11}O_{19}$ (49) and $La_{0.8}Pr_{0.2}NiAl_{11}O_{19}$ (62) catalysts. The $La_{0.8}Pr_{0.2}NiAl_{11}O_{19}$ catalyst exhibited excellent long term stability over 300 hours of

operation. These studies have suggested that the predominant cause of carbon deposition at the reaction conditions studied is CH_4 pyrolysis. Graphite is suggested as the more dominant form of carbon deposited onto the catalyst surface with whisker carbon and metal carbides also being formed. Carbon deposition could be suppressed under suitable reaction conditions that include high CO_2/CH_4 ratios. Post characterization of the catalysts was performed by XRD to identify nickel phases. From the XRD pattern, catalysts with short reaction times exhibited a peak located at 44.5°, consistent with metallic nickel formation, while the authors claim that catalysts which were exposed for longer reaction times produce a peak shift to a lower angle of 44.4° suggesting NiC formation.

For liquid hydrocarbon feedstocks, a survey of the literature indicated that studies on carbon deposition onto hexaaluminate catalysts has not yet been reported. In this work, the study of carbon deposition onto hexaaluminate catalysts is extended to include a liquid hydrocarbon feed and to include the effect that the mirror cation produced on carbon deposition. The partial oxidation of n-tetradecane was used as a probe reaction to access the carbon deposition characteristics on the surface of $M_INi_{0.4}Al_{11.6}O_{19-\delta}$ with M_I = Ba, La and Sr catalysts. Temperature programmed oxidation (TPO) was performed to identify the location and quantify the amount of carbon deposited onto each catalyst. Post characterization of reacted catalysts by XRD was performed to examine the catalysts for the formation of nickel phases.

8.2 Experimental

8.2.1 Temperature Programmed Oxidation

TPO was performed by first exposing the catalysts to isothermal n-tetradecane partial oxidation for 5.5 hours. The reaction was carried out by first introducing n-tetradecane over the catalysts at an O/C = 1.2, GHSV = 50,000 $cm^3g^{-1}h^{-1}$, a temperature of 850°C and a pressure of 197.9 kPa. Prior to performing the TPO experiment, the reactor was cooled and the catalyst samples were separated from the quartz chips. The reacted catalyst was reloaded into the reactor for TPO. The reactor was then heated to 200°C while under N_2 purge. Air and nitrogen were then introduced into the reactor at a GHSV of 15,333 $cm^3g^{-1}h^{-1}$, a flow rate of 108 sccm N_2 and 30 sccm air. The ramp rate was set at 1°C/min from 200 to 900°C. The reactor was held at 900°C overnight until all carbon was oxidized off the catalyst surface. CO_2 evolution was monitored continuously by mass spectrometer.

The carbon ($C_{accumulated}$) that had been deposited onto the catalyst surface was calculated by integration of the instantaneous mass flow rate of CO_2 exiting the reactor:

$$C_{accumulated} = \frac{12\frac{g\,C}{mol\,C}}{44\frac{g\,CO_2}{mol\,CO_2}}\int \dot{m}_{CO_2}\,dt \qquad (12)$$

Where $\dot{m}_{CO_2}$ is the instantaneous mass flow rate of CO_2 exiting the reactor. The separation of catalyst from the quartz chips was utilized to more carefully identify burn-

off regions specific to the catalyst; however, it is recognized that more carbon may be present within the reactor bed.

8.3 Results and Discussion

8.3.1 Temperature Programmed Oxidation

The TPO of catalysts deactivated by carbon deposition provided direct information regarding the oxidation rate of the carbon. Carbon oxidation kinetics was related to such useful information as carbon deposit location and morphology. In this study, it was desired to determine the location and quantity of carbon deposited onto the nickel hexaaluminate catalyst surfaces. Active nickel sites present in the nickel hexaaluminate lattice have a catalytic burning effect, which result in the presence of two main peaks. The low temperature peak corresponds to carbon deposits residing on the metal surface, or in its vicinity (67). The high temperature peak corresponds to carbon deposited onto the support (67). Using this methodology, it is possible to study the effect of catalyst formulation on the deposition of carbon onto the surface of the catalyst.

The burn-off profiles for the $M_INi_{0.4}Al_{11.6}O_{19-\delta}$ (M_I = Ba, La and Sr) series of catalysts are given in Figure 39 and the total carbon burned-off the catalysts and its location on the catalyst are given in Table 12. From Figure 39, all three hexaaluminate catalysts showed evidence of metal burn-off in the region between 250 to 275°C. The amount of carbon residing in this region was much less than that observed at higher

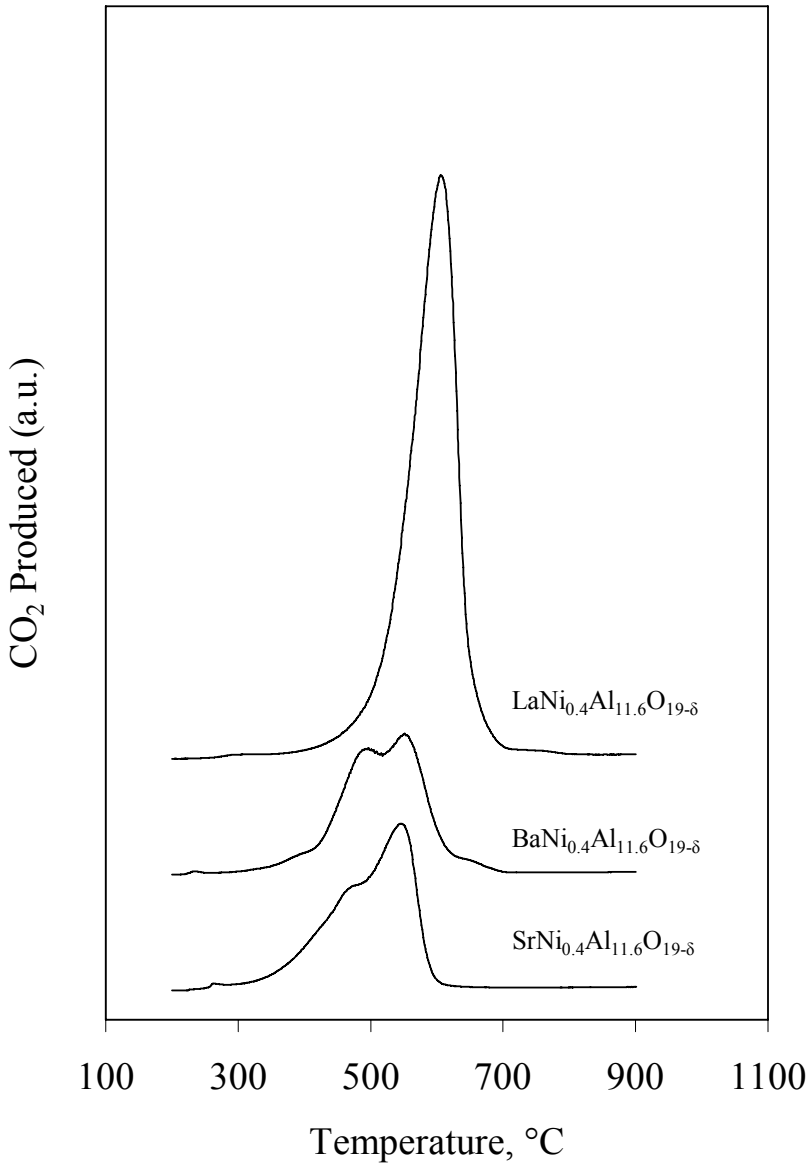

Figure 39. Temperature programmed oxidation profile of $M_INi_{0.4}Al_{11.6}O_{19-\delta}$ (M_I = Ba, La and Sr) catalysts: the effect that the mirror cation has on carbon formation.

Table 12. Peak temperature assignments and total carbon burn-off during the TPO of $M_INi_{0.4}Al_{11.6}O_{19-\delta}$ (M_I = Ba, La and Sr) catalysts.

Sample	**Peak Temperature (°C)**	**Carbon burn-off (wt%)**
$BaNi_{0.4}Al_{11.6}O_{19-\delta}$	250, 500, 555	11.8
$LaNi_{0.4}Al_{11.6}O_{19-\delta}$	275, 609	29.1
$SrNi_{0.4}Al_{11.6}O_{19-\delta}$	250, 478, 553	10.0

temperatures for all three catalysts. The $LaNi_{0.4}Al_{11.6}O_{19-\delta}$ catalyst exhibited a single high temperature CO_2 burn-off peak located at 609°C, where the $BaNi_{0.4}Al_{11.6}O_{19-\delta}$ and the $SrNi_{0.4}Al_{11.6}O_{19-\delta}$ catalysts exhibited two high temperature peaks located at 500, 555°C and 478, 553°C, respectively.

The presence of two high temperature burn-off peaks in the $BaNi_{0.4}Al_{11.6}O_{19-\delta}$ and the $SrNi_{0.4}Al_{11.6}O_{19-\delta}$ catalysts suggested that the carbon deposits are located inter-facially, near, but not on the metal surface as well as on the support (69, 70). Carbon that was located inter-facially to an active site will burn-off at temperatures somewhere in between the metal and the support burn-off temperature region (69, 70). Therefore, the inter-facial burn-off region for these two catalysts was located at 500 and 478°C, respectively. The support burn-off region was located at 555 and 553°C, respectively. In contrast, the $LaNi_{0.4}Al_{11.6}O_{19-\delta}$ catalyst exhibited a single high temperature burn-off peak located at 609°C. The shift in the support burn-off peak to a temperature region higher than that observed with the other two catalysts suggested that the carbon that had deposited onto the surface of the catalyst may have possessed a more ordered structure which was less rapidly oxidized (67).

The total carbon deposited onto these catalysts increased with increasing surface nickel concentration. As shown in Table 12, the concentration of carbon deposited onto the hexaaluminate catalysts was 11.8 and 10.0 wt% for the $BaNi_{0.4}Al_{11.6}O_{19-\delta}$ and the $SrNi_{0.4}Al_{11.6}O_{19-\delta}$ catalysts; respectively, while the $LaNi_{0.4}Al_{11.6}O_{19-\delta}$ catalyst exhibited almost three times the carbon deposited onto the catalyst surface with 29.1 wt%.

The $LaNi_{0.4}Al_{11.6}O_{19-\delta}$ catalyst was observed to possess a surface nickel concentration that was over five times that of the $BaNi_{0.4}Al_{11.6}O_{19-\delta}$ and $SrNi_{0.4}Al_{11.6}O_{19-\delta}$ catalysts. The observed trend of increasing carbon deposition with increasing nickel dopant concentration was consistent with increasing nickel site coordination within the catalysts. When nickel substitution was increased, likely a sufficient number of highly coordinated sites, or sufficiently large metallic clusters, were formed that stabilized hydrocarbons onto the catalyst surface which lead to carbon formation.

Figure 40 is the burn-off profile of $BaNi_{0.4}Al_{11.6}O_{19-\delta}$. This figure also includes the O_2 profile which clearly indicates that there was no discernable uptake of O_2 that was not accounted for by CO_2 formation. This behavior indicated that there was little or no O_2 uptake observed from the hexaaluminate catalyst during burn-off. These results suggested that the excellent stability toward coking exhibited by nickel substituted hexaaluminate was primarily due to electronic and geometric effects induced by small active clusters.

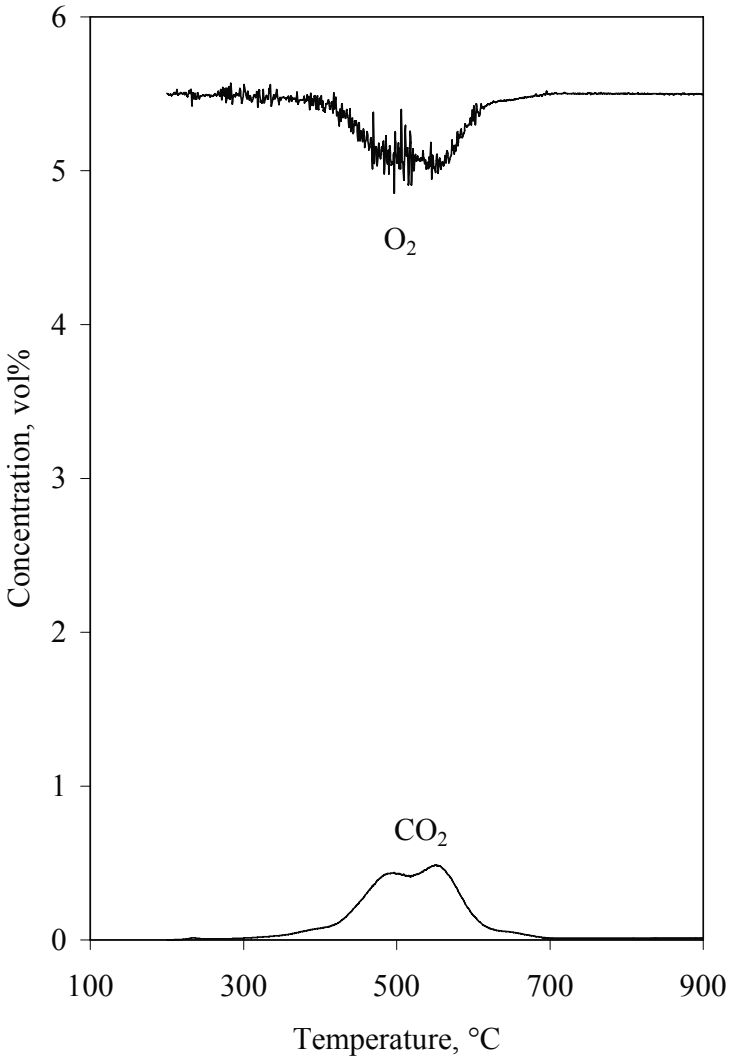

Figure 40. O_2 and CO_2 concentrations during the temperature programmed oxidation of $BaNi_{0.4}Al_{11.6}O_{19-\delta}$.

8.3.2 Post Characterization by XRD

After exposure to n-tetradecane partial oxidation for 5.5 hours, the catalysts were examined for the formation of metallic nickel and nickel carbide formation. Figure 41 is an XRD scan of the post reacted catalysts over the range 43.5 to 45.5°. The formation of a peak located at 44.5° was observed in both the $SrNi_{0.4}Al_{11.6}O_{19-\delta}$ and $LaNi_{0.4}Al_{11.6}O_{19-\delta}$ catalysts. The location of this peak was consistent with the high intensity line for metallic nickel [JCPDS: 00-004-0850]. The formation of metallic nickel indicated that some of the nickel initially present within the hexaaluminate lattice was reduced and separated to form an individual metallic phase. Metallic nickel formation was not discernable in the $BaNi_{0.4}Al_{11.6}O_{19-\delta}$ catalyst due to peak overlap between the barium hexaaluminate phase and the metallic nickel phase. The metallic nickel peaks for the $SrNi_{0.4}Al_{11.6}O_{19-\delta}$ and $LaNi_{0.4}Al_{11.6}O_{19-\delta}$ catalysts were sufficiently broad such that it was not possible to discern if NiC was present in the samples.

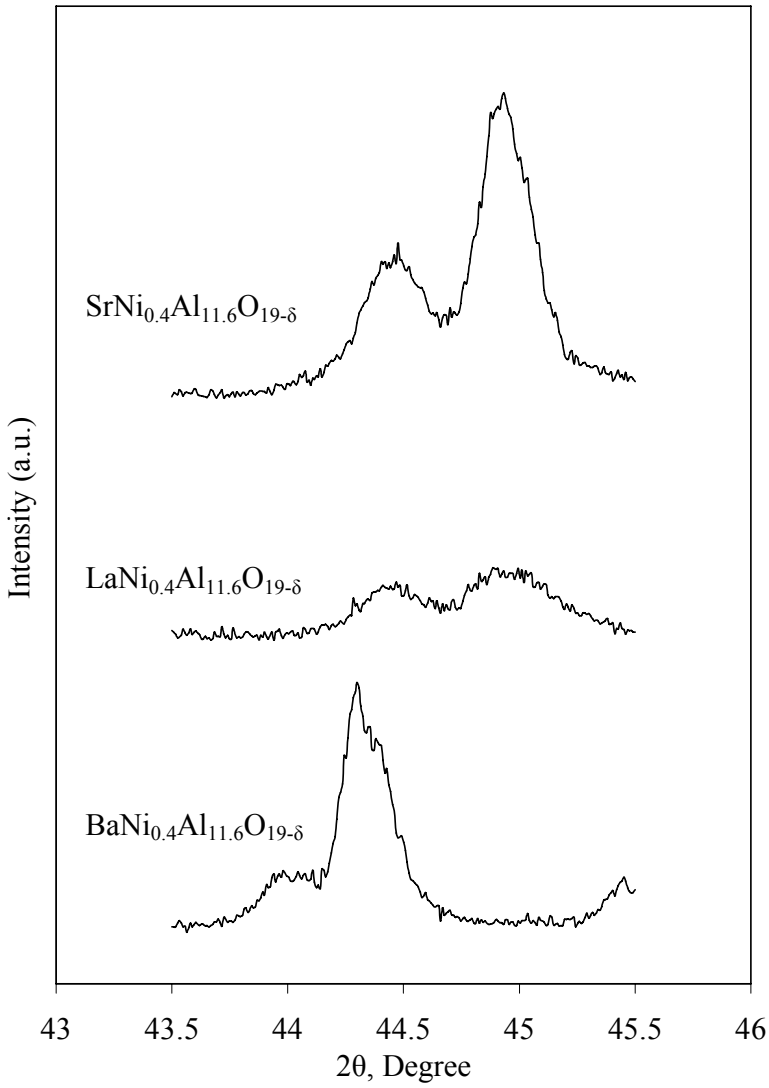

Figure 41. XRD scans of post reacted $M_INi_{0.4}Al_{11.6}O_{19-\delta}$ (M_I = Ba, La and Sr) catalysts.

8.4 Conclusions

TPO was performed on $M_INi_{0.4}Al_{11.6}O_{19-\delta}$ (M_I = Ba, La and Sr) catalysts. All catalysts exhibited a low temperature burn-off peak located on the nickel site. The $BaNi_{0.4}Al_{11.6}O_{19-\delta}$ and $SrNi_{0.4}Al_{11.6}O_{19-\delta}$ catalysts exhibited two high temperature burn-off peaks. The lower of the two high temperature peaks was attributed to carbon located at inter-facial sites while the higher temperature peak was attributed to carbon located on the support. The magnitude of the carbon formed on the surface of the catalysts correlated with the observed surface nickel concentration with the $LaNi_{0.4}Al_{11.6}O_{19-\delta}$ catalyst exhibiting three times the carbon deposited onto the $BaNi_{0.4}Al_{11.6}O_{19-\delta}$ and $SrNi_{0.4}Al_{11.6}O_{19-\delta}$ catalysts.

Post characterization by XRD of the catalyst samples revealed that a metallic nickel phase had separated from the hexaaluminate lattice in the $LaNi_{0.4}Al_{11.6}O_{19-\delta}$ and $SrNi_{0.4}Al_{11.6}O_{19-\delta}$ catalysts. These results suggested that the excellent stability toward coking exhibited by nickel substituted hexaaluminate catalysts was primarily due to electronic and geometric effects induced by small active metallic clusters.

9.0 CONCLUSIONS AND RECOMMENDATIONS

The objective of this research was to investigate the catalytic properties of hexaaluminate catalysts for the partial oxidation of middle distillate fuels using n-tetradecane as a model fuel compound. The goals for this effort were to develop catalysts with useful activities and stability at high temperatures and to achieve a fundamental understanding of catalyst structure and surface properties and how they related to the activity, selectivity and carbon deposition resistance.

A series of hexaaluminate catalysts were developed based on cobalt, iron and nickel transition metals which were substituted into the lattice. These catalysts were characterized by a series of techniques including: N_2 BET surface area, powder XRD, TPR, H_2 pulse chemisorption, bulk elemental analysis by ICP, and surface analysis by XPS.

The preparation method utilized was based on the co-precipitation of metal nitrate precursors with an ammonia carbonate base. The co-precipitation method utilized to prepare the hexaaluminate catalysts produced sufficient variance in surface area between catalyst samples such that it was not possible to discern an effect with metal substitution into the hexaaluminate lattice. The resulting catalysts produced have N_2 BET surface areas that narrowly ranged between 9.9 to 26.3 m^2/g.

The synthesized cobalt, iron and nickel substituted lanthanum hexaaluminate catalysts all exhibited $P6_3/mmc$ crystal symmetry indicative of the $LaAl_{11}O_{18}$ compound. Similar to the $LaAl_{11}O_{18}$ compound, the $BaAl_{12}O_{19}$ and $SrAl_{12}O_{19}$ compounds also exhibited $P6_3/mmc$ crystal symmetry. The effect of increasing the active metal substitution into the lattice produced an increase in sample crystallinity. The observed change in the rate of sample crystallization suggested that the microstructure of the lanthanum hexaaluminate catalysts was altered by the addition of transition metals. Minor phase impurities were also observed to be present in the catalysts, but in relatively low concentration. Oxides of cobalt, iron and nickel were not observed.

TPR experiments on the catalysts indicated that the substitution of cobalt, iron and nickel cations into the lattice stabilized their reducibility. The reduction temperature for the nickel series correlated with the mirror cation type. The number of reducible transition metal sites was observed to correlate with the concentration of transition metal substituted into the lattice. H_2 pulse chemisorption performed on reduced nickel hexaaluminate catalysts confirmed that the number of active sites that were reduced was a function of the mirror cation type. The influence that the mirror cation produced on nickel reducibility suggested that the reduction of lattice bound nickel sites had occurred in a region near the mirror plane. The concentration of reducible nickel sites per gram of nickel present in the catalyst was as follows: $LaNi_{0.4}Al_{11.6}O_{19-\delta} > SrNi_{0.4}Al_{11.6}O_{19-\delta} > BaNi_{0.4}Al_{11.6}O_{19-\delta}$.

XPS analysis of $LaNi_{0.4}Al_{11.6}O_{19-\delta}$, $SrNi_{0.4}Al_{11.6}O_{19-\delta}$ and $BaNi_{0.4}Al_{11.6}O_{19-\delta}$ catalysts indicated that the variation in the nickel surface concentration correlated with the mirror cation type. The concentration of nickel observed on the surface of the catalyst surface was as follows: $LaNi_{0.4}Al_{11.6}O_{19-\delta} > SrNi_{0.4}Al_{11.6}O_{19-\delta} > BaNi_{0.4}Al_{11.6}O_{19-\delta}$. These results were in qualitative agreement with the number of reduced sites observed with H_2 pulse chemisorption.

The activity of these catalysts toward the partial oxidation of n-tetradecane was examined as a function of transition metal type (e.g., Co, Fe and Ni), temperature, the concentration of active metal substituted into the lattice and the mirror cation type. Iron substituted into the lanthanum hexaaluminate lattice exhibited poor catalytic activity and selectivity at all concentrations during the temperature programmed reaction with n-tetradecane. Cobalt substituted into the lanthanum hexaaluminate lattice at concentrations of $y \leq 0.8$ exhibited equally poor catalytic activity and selectivity. However, the $LaCoAl_{11}O_{19-\delta}$ catalyst exhibited equilibrium CO and H_2 yields.

The $LaNi_yAl_{12-y}O_{19-\delta}$ series and the $M_INi_{0.4}Al_{11.6}O_{19-\delta}$ series of catalysts possessed the greatest H_2 and CO activity and selectivity over the temperature region examined. Both the $LaNi_{0.2}Al_{11.8}O_{19-\delta}$ and the $BaNi_{0.4}Al_{11.6}O_{19-\delta}$ catalysts exhibited sharp increases in H_2 yield at 850 and 875°C, respectively. The increase in H_2 yield in this region corresponded to a decrease in CH_4 yield indicating that the additional H_2 was derived from CH_4. This catalytic behavior suggested that CH_4 in the reformate was not as effectively adsorbed and dissociated onto the nickel sites present in these catalysts and

that a complex kinetic balance existed between the adsorption of hydrocarbons onto the hexaaluminate catalyst surface and their rate of reaction.

From the temperature programmed reaction data examined, the differentiation in catalytic performance between catalysts was closely related not only to the active metal substituted into the hexaaluminate lattice, but also to its concentration in the lattice. The metal concentration, therefore, affected the catalytic surface structure which was evolved and was available for reaction. The surface reaction rate and the dehydrogenation activity were functions of the choice of metal introduced into the lattice. The catalytic properties that were related to performance, therefore, were the active metal type, the active area and the coordination of active sites achieved.

The mirror cation was also shown to affect catalytic performance. The differentiation in catalytic behavior observed between catalysts with different mirror cations suggested that the surface nickel concentration, not the bulk nickel concentration, controlled catalyst activity and selectivity.

The role that the mirror cation produced on nickel substituted hexaaluminate isothermal stability during n-tetradecane partial oxidation was examined. Hexaaluminate catalysts with divalent, Ba^{2+} and Sr^{2+}, mirror cations exhibited greater stability during n-tetradecane partial oxidation than did the trivalent mirror cation, La^{3+}, containing nickel substituted hexaaluminate. The unstable activity exhibited by $LaNi_{0.4}Al_{11.6}O_{19-\delta}$ indicated that carbon had deposited onto the surface of the catalyst. The initial loss in activity of

$LaNi_{0.4}Al_{11.6}O_{19-\delta}$ followed by the stationary level of activity suggested the presence of two different types of active nickel sites: those that were more active toward carbon deposition and those that were less active. The catalytic behavior induced by the mirror cation suggested that its influence on controlling carbon deposition was structural. Likely, the more active carbon forming sites were present as higher coordination nickel sites and the less active carbon forming nickel sites were present in a lower state of coordination.

TPO was performed on spent catalysts to determine the amount and location of the carbon formed. All catalysts exhibited a low temperature burn-off peak located on the nickel site. The $BaNi_{0.4}Al_{11.6}O_{19-\delta}$ and $SrNi_{0.4}Al_{11.6}O_{19-\delta}$ catalysts exhibited two high temperature burn-off peaks. The lower of the two high temperature peaks was attributed to carbon located at inter-facial sites, while the higher temperature peak was attributed to carbon located on the support. The magnitude of the carbon formed on the surface of the catalysts correlated with the observed surface nickel concentration with the $LaNi_{0.4}Al_{11.6}O_{19-\delta}$ catalyst that exhibited three times the amount of carbon that was observed on the $BaNi_{0.4}Al_{11.6}O_{19-\delta}$ and $SrNi_{0.4}Al_{11.6}O_{19-\delta}$ catalysts.

Post characterization by XRD of the catalyst samples revealed that a metallic nickel phase had separated from the hexaaluminate lattice in the $LaNi_{0.4}Al_{11.6}O_{19-\delta}$ and $SrNi_{0.4}Al_{11.6}O_{19-\delta}$ catalysts. These results suggested that the excellent stability toward coking exhibited by nickel substituted hexaaluminate was primarily due to electronic and geometric effects induced by small metallic clusters.

In order to optimize catalysts for this application, the detailed interactions of the reactant species with the catalyst surface and the type and distribution of the active sites must be better understood. In this work, some of these answers were given. It was found that the type of mirror cation strongly influenced the stability and carbon deposition resistance of the catalyst. The finding that site coordination and metal dispersion were significant factors that had affected carbon deposition onto the surface of the catalyst provided insight into the continued improvement of these catalysts and the development of future middle distillate catalyst systems.

Based on the observations in this investigation, the coordinative environment and dispersion of nickel present within the hexaalumina lattice should be studied in greater detail. Long term aging studies should be performed to determine the extent to which metallic clusters had changed, as well as sintering and active metal vaporization. The effect of different reforming feeds on carbon formation should be examined including the addition of steam and CO_2 addition, autothermal reforming and fuel cell anode recycle. Since diesel fuel contains several different classes of organic compounds, there is a need to study carbon deposition as a function of hydrocarbon type. Finally, the use of alternate synthesis methods, the development of structured catalytic hexaaluminate foams and the combination of O_2-ionic conducting compounds (e.g., CeO_2) with hexaaluminate catalysts to further mitigate carbon deposition are recommended.

LITERATURE CITED

1. www.epa.gov/SmartwayLogistics/idle-questions.htm

2. www.epa.gov/smartway/idling.htm

3. Cabrera, A. L., Heinemann, H., Somorjai, G. A., "Potassium Catalyzed Methane Production from Graphite at Low Temperatures (473–673 K)," Chemical Physics Letters, Vol. 81 (1981) P. 402-405.

4. Otto, K. and Shelf, M., Proceedings 6th International Catalysis London, 1976 (Bond, G. C., Wells, P. B., and Tompkins, F. C. eds.) The Chemical Society, London (1977) p. 1082.

5. Guczi, L., "Mechanisms of Reactions on Multimetallic Catalysts," Journal of Molecular Catalysis, Vol. 25 (1984) p. 13-29.

6. Frennet, A., Kienard, G., Crucq, A. and Degols, L., "Effect of Multiple Sites and Competition in Adsorption on the Kinetics of Reactions Catalyzed by Metals," Journal of Catalysis, Vol. 53 (1978) p. 150.

7. Salazar, M., Berry, D. A., Gardner, T. H., Shekhawat, D., Floyd, D., "Catalytic Partial Oxidation of Methane Over Pt/Ceria Doped Catalysts: Effect of Ion Conductivity," Applied Catalysis A: General, Vol. 310 (2006) pp. 54-60.

8. Salazar, M., Berry, D. A., Gardner, T. H., Shekhawat, D. and Celik, I., "Synthesis Gas by Catalytic Partial Oxidation and the Role of Oxygen-Conducting Supports: A Review," Proceedings of the 2nd ASME Fuel Cell Science Engineering and Technology Conference (2004) pp. 681-690.

9. Rostrup-Nielsen, J. R., "Carbon Formation on Steam Reforming Catalysts," Catalytic Steam Reforming. Haldor-Topsøe A/S (1984) pp. 90-91.

10. Barbier, J., Corro, G., Zhang, Y., Bournonville, J. P. and Franck, J. P., "Coke Formation on Platinum-Alumina Catalyst of Wide Varying Dispersion," Applied Catalysis, Vol. 13 (1985) pp. 245-255.

11. Biswas, J., Bickle, G. M., Gray, P. G., Do, D. D. and Barbier, "The Role of Deposited Poisons and Crystallite Surface Structure in the Activity and Selectivity of Reforming Catalysts," Catal. Rev. Sci. Eng., Vol. 30 (1988) p. 161-247.

12. Barbier, J. and Marecot, P., "Effect of Presulfurization on the Formation of Coke on Supported Metal Catalysts," Journal of Catalysis, Vol. 102 (1986) pp. 21-28.

13. Besten, I. E. D. and Selwood, P. W. J., "The Chemisorption of Hydrogen Sulfide, Methyl Sulfide, and Cyclohexene on Supported Nickel Catalysts," Journal of Catalysis, Vol. 1 (1962) pp. 93-102.

14. Arai, H. and Machida, M., Applied Catalysis A: General, "Thermal Stabilization of Catalyst Supports and their Application to High-Temperature Catalytic Combustion," Vol. 138 (1996) pp. 161-176.

15. Sidwell, R. W., Zhu, H., Kibler, B. A., Kee, R. J., Wickham, D. T., "Experimental Investigation of the Activity and Thermal Stability of Hexaaluminate Catalysts for Lean Methane–Air Combustion," Applied Catalysis A: General, Vol. 255 (2003) pp. 279-288.

16. Thevenin, P. O., Ersson, A. G., Kusar, H. M. J., Menon P. G., Jaras, S. G., "Deactivation of High Temperature Combustion Catalysts," Applied Catalysis A: General, Vol. 212 (2001) pp. 189-197.

17. Machida, M., Eguchi, K. and Arai, H., "Effect of Additives on the Surface Area of Oxide Supports for Catalytic Combustion," Journal of Catalysis, Vol. 103 (1987) pp. 385-393.

18. Janzen, C. M. and Neurgaonkar, R. R., Material Research Bulletin, "Solid State Reactions in the System Al_2O_3-Nd_2O_3-CaO: A System Pertinent to Radioactive Waste Disposal," Vol. 16 (1981) pp. 519-524.

19. Kahn, A., Lejus, A. M., Madsac, M., Thery, J., Viven, D. and Bernier, J. C., "Preparation, Structure, Optical, and Magnetic Properties of Lanthanide Aluminate Single Crystals ($LnMAl_{11}O_{19}$)," Journal of Applied Physics, Vol. 52 (1981) p. 6864-6869.

20. Groppi, G., Bellotto, M., Cristiani, C., Forzatti, P. and Villa, P. L., "Preparation and Characterization of Hexaaluminate-Based Materials for Catalytic Combustion," Journal of Catalysis, Vol. 104 (1993) pp. 101-108.

21. Majocchi, L., Groppi, G., Cristiani, C., Foratti, P. and Guarinoni, A., "Partial Oxiation of Methane to Synthesis gas Over Rh-Hexaaluminate-Based Catalysts," Catalysis Letters, Vol. 65 (2000) pp. 49-56.

22. Gunardson, H., "Synthesis Gas Manufacture," Industrial Gases in Petrochemical Processing. (H. Gunardson, eds.) Marcel Dekker, Inc., New York (1998) p. 69.

23. Roine, A., HSC Chemistry Version 5.1, Outokumpu Research Oy, Pori, Finland (2002).

24. Ran, R., Xiong, G., Sheng, S., Yang, W., Stroh, N. and Brunner, H., "Catalytic Partial Oxidation of n-Heptane for Hydrogen Production," Catalysis Letters, Vol. 88 (2003) pp. 55-59.

25. Zhu, W., Han, W., Xiong, G., and Yang, N., "Mixed Reforming of Simulated Gasoline to Hydrogen in a BSCFO Membrane Reactor," Catalysis Today, Vol. 118 (2004) pp. 39-43.

26. Fujitani Y. and Muraki, H., Kabushiki Kaisha Toyota Chuo Kenkyusho, Japan, U.S. Patent 4087259 (1978).

27. Tanaka, M., Takemura, M. and Ito, N., Nippon Soken, Inc., Japan, U.S. Patent 4088608 (1979).

28. O'Connor, R. P., Klein, E. J. and Schmidt, L. D., "High Yields of Synthesis Gas by Millisecond Partial Oxidation of Higher Hydrocarbons," Catalysis Letters, Vol. 70 (2000) p. 99-107.

29. Schmidt, L. D., Klein, E.J., Leclerc, C. A., Krummenacher, J. J. and West, K. N., "Syngas in Millisecond Reactors: Higher Alkanes and Fast Lightoff," Chemical Engineering Science, Vol. 58 (2003) p. 1037-1041.

30. O'Connor, R.P., Klein, E.J., Henning, D., and Schmidt, L.D., "Tuning Millisecond Chemical Reactors for the Catalytic Partial Oxidation of Cyclohexane," Applied Catalysis A: General, Vol. 238 (2003) p. 29-40.

31. Subramanian, R., Panuccio, G. J., Krummenacher, J. J., Lee, I. C. and Schmidt, L. D., "Catalytic Partial Oxidation of Higher Hydrocarbons: Reactivities and Selectivities of Mixtures," Chemical Engineering Science, Vol. 59 (2004) p. 5501-5507.

32. Krummenacher, J. J., West, K. N. and Schmidt, L. D., "Catalytic Partial Oxidation of Higher Hydrocarbons at Millisecond Contact Times: Decane, Hexadecane, and Diesel Fuel," Journal of Catalysis, Vol. 215 (2003) pp. 332-343.

33. Collongues, R., Thery, J., Boilot, J. P., Solid Electrolytes. (P. Hagenmuller and W. Van Gool, eds.) Academic Press, New York (1979) p. 253.

34. Machida, M., Eguchi, K. and Arai, H., "Effect of Structural Modification on the Catalytic Property of Mn-Substituted Hexaaluminates," Journal of Catalysis, Vol. 123 (1990) pp. 447-485.

35. Machida, M., Eguchi, K. and Arai, H., "Catalytic Properties of $BaMAl_{11}O_{19-\alpha}$, (M = Cr, Mn, Fe, Co and Ni) for High-Temperature Catalytic Combustion," Journal of Catalysis, Vol. 120 (1989) pp. 377-386.

36. Artizzu-Duart, P., Millet, J. M., Guilhaume, N., Garbowski, E., Primet, M., "Catalytic Combustion of Methane on Substituted Barium Hexaaluminates," Catalysis Today, Vol. 59 (2000) pp. 163-177.

37. Machida, M., Shiomitsu, T., Eguchi, K., Arai, H. and Shiomitsu, T., "Observation of Anisotropic Oxygen Diffusion in Hexaaluminate," Journal of Solid State Chemistry, Vol. 95 (1991) pp. 220-223.

38. Arai, H., Eguchi, K., Machida, M., Shiomitsu, T., "Heat Resistance of Hexaaluminate Catalyst for High-Temperature Catalytic Combustion," Catalytic Science and Technology Vol. 1. (1991) pp. 195-199.

39. Groppi, G., Cristiani, C. and Forzatti, P., "$BaFe_xAl_{12-x}O_{19}$ System for High-Temperature Catalytic Combustion: Physico-Chemical Characterization and Catalytic Activity," Journal of Catalysis, Vol. 168 (1997) pp. 95-103.

40. Weast, R. C., CRC Handbook of Chemistry and Physics. 64^{th} Ed. (1983) p. C-530.

41. Groppi, G., Cristiani, C., Forzatti, P., Bellotto, M., "Phase Composition and Mechanism of Formation of Ba-β-alumina-Type Systems for Catalytic Combustion Prepared by Precipitation," Journal of Material Science, Vol. 29 (1994) pp. 3441-3450.

42. Sohn, J. M., Kang, S. K., Woo, S. I., "Catalytic Properties and Characterization of Pd Supported on Hexaaluminate in High Temperature Combustion," Journal of Molecular Catalysis A: Chemical, Vol. 186 (2002) pp. 135-144.

43. Machida, M., Eguchi, K. and Arai, H., "Preparation and Characterization of Large Surface Area BaO $6Al_2O_3$," Bull. Chem. Soc. Japan, Vol. 61 (1988) pp. 3659-3665.

44. Lietti, L., Cristiani, C., Groppi, G. and Forzatti, P., "Mathematical Modelling of Catalytic Combustors Fuelled by Gasified Biomasses," Catalysis Today, Vol. 59 (2000) p. 191.

45. Moulder, J. F., Stickle, W. F., Sohol, P. E., Bomber, K. D., Handbook of X-ray Photoelectron Spectroscopy. Physical Electronics, Inc., Eden Prairie, Minnesota.

46. Xu, Z., Zhen, M., Bi, Y., Zhen, K., "Carbon Dioxide Reforming of Methane to Synthesis Gas Over Hexaaluminate $ANiAl_{11}O_{19-\delta}$ (A = Ca, Sr, Ba and La)," Catalysis Letters, Vol. 64 (2000) p. 157-161.

47. Xu, Z., Zhen, M., Bi, Y., Zhen, K., "Catalytic Properties of Ni Modified Hexaaluminates $LaNi_yAl_{12-y}O_{19-\delta}$ for CO_2 Reforming of Methane to Synthesis Gas," Applied Catalysis A: General, Vol. 198 (2000) pp. 267-273.

48. Inoue, H., Sekizawa, Eguchi, K. and Arai, H., "Changes of Crystalline Phase and Catalytic Properties by Cation Substitution in Mirror Plane of Hexaaluminate Compounds," Journal of Solid State Chemistry, Vol. 121 (1996) pp 190-196.

49. Liu, Y., Xu, Z., Li, D., Cheng, T., Zhou, G., Li, W., Bi, Y., Zhen, K., "Studies on Carbon Deposition on Hexaaluminate $LaNiAl_{11}O_{19}$ Catalysts During CO_2 Reforming of Methane," Kinetics and Catalysis, Vol. 43 (2002) pp. 522-527.

50. Murthy, K. R. Sharma, N. George, N., "Structure and Performance of Reforming Catalysts," Catalytic Naphtha Reforming Science and Technology. (G. J. Antos, A. M. Aitani, J. M. Parera, eds.) Marcel Dekker, New York, (1995) pp. 207-255.

51. Boudart, M., Aldag, A., Benson, J. E., Dougharty, N. A., Harkins, C. G., "On the Specific Activity of Platinum Catalysts," Journal of Catalysis, Vol. 6 (1966) p. 92-99.

52. Bengaard, H. S., Norskov, J. K., Sehested, J., Clausen, B. S., Nielsen, L. P. Molenbroek, A. M., Rostrup-Nielsen, J. R., "Steam Reforming and Graphite Formation on Ni Surfaces," Journal of Catalysis, Vol. 209 (2002) pp. 365-384.

53. Somorjai, G. A., "Active Sites in Heterogeneous Catalysis," Advances in Catalysis. (D. D. Eley, H. Pines, P. B. Weisz, eds.) Academic Press London, Vol. 26 (1977) pp. 1-68.

54. Biswas, J., Bickle, G. M., Gray, P. G., Do, D. D., "The Role of Crystalline Structure on Mechanisms of Coke and Sulfur Poisoning in Catalytic Reforming," Catalyst Deactivation. (B. Delmon, G. F. Froment, eds.) Elsevier, Amsterdam, The Netherlands, (1987) pp. 553-565.

55. Chu, W., Yang, W. and Lin, L., "Selective Oxidation of Methane to Syngas over NiO/Barium Hexaaluminate," Catalysis Letters, Vol. 74 (2001) pp. 139-144.

56. Somorjai, G. A., "Thermodynamics of Surfaces," Introduction to Surface Chemistry and Catalysis, John Wiley and Sons, Inc. (1994) p. 285.

57. Marecot, P., Churin, E. and Barbier, J., "Coke Deposits on Pt/Al_2O_3 Catalysts of Varying Dispersities," Reaction Kinetics Catalysis Letters," Vol. 37 (1988) pp. 233-237.

58. Blakely, D.W. and Somorjai, G.A., "The Dehydrogenation and Hydrogenolysis of Cyclohexane and Cyclohexene on Stepped (High Miller Index) Platinum Surfaces," Journal of Catalysis, Vol. 42 (1976) pp. 181-196.

59. Barbier, J., Morales, A., Marecot, P., Maurel, R., "Influence of the Dispersion of Platinum and Effect of Poisons on its Activity and Selectivity for Various Test Reactions," Bull. Soc. Chim. Belg., Vol. 78 (1979) pp. 569-576.

60. Shekhawat, D., Berry, D., Gardner, T., Spivey, J. J., "Catalytic Reforming of Liquid Hydrocarbon Fuels for Fuel Cell Applications," Catalysis Vol. 19. (J. J. Spivey and K. M. Dooley, eds.) RSC Publishing (2006) pp. 184-244.

61. Chu, W., Yang, W. and Lin, L., "The Partial Oxidation of Methane to Syngas Over the Nickel Modified Hexaaluminate Catalysts $BaNi_yAl_{12-y}O_{19-\delta}$," Applied Catalysis A: General, Vol. 235 (2002) pp. 39-45.

62. Liu, Y., Cheng, T., Li, D., Jiang, P., Wang, J., Li, W., Bi, Y. and Zhen, K., "Studies on the Stability of a $La_{0.8}Pr_{0.2}NiAl_{11}O_{19}$ Catalyst for Syngas Production by CO_2 Reforming of Methane," Catalysis Letters, Vol. 85 (2003) pp. 101-108.

63. Salazar, M., Berry, D. A., Gardner, T. H., Shekhawat, D., Floyd, D., "Catalytic Partial Oxidation of Methane Over Pt/Ceria Doped Catalysts: Effect of Ion Conductivity," Applied Catalysis A: General, Vol. 310 (2006) pp. 54-60.

64. Li, X., Zhang, Y. and Smith, K. J., "Metal–Support Interaction Effects on the Growth of Filamentous Carbon Over Co/SiO_2 Catalysts," Applied Catalysis A: General, Vol. 264 (2004) pp. 81-91.

65. Bradford, M. C. J. and Vannice, M. A., "The Role of Metal–Support Interactions in CO_2 Reforming of CH_4," Catalysis Today, Vol. 50 (1999) pp. 87-96.

66. Querini, C. A., "Coke Characterization," Catalysis Vol. 17. (J. J. Spivey, ed.) RSC Publishing (2004) pp. 166-209.

67. Zhu, T. and Flytzani-Stephanopoulos, M., "Catalytic Partial Oxidation of Methane to Synthesis Gas Over Ni-CeO_2," Applied Catalysis A: General, Vol. 208 (2001) pp. 403-417.

68. Gardner, T. H., Shekhawat, D., Berry, D. A., Smith M. W. and Kugler, E. L. "Effect of Nickel Hexaaluminate Mirror Cation on Structure Sensitive Reactions During n-Tetradecane Partial Oxidation," Applied Catalysis A: General, Vol. 323 (2007) pp. 1-8

69. Shekhawat, D., Gardner, T. H., Berry, D. A., Salazar, M., Haynes, D. J., Spivey, J. J., "Catalytic Partial Oxidation of n-Tetradecane in the Presence of Sulfur or Polynuclear Aromatics: Effects of Support and Metal," Applied Catalysis A: General, Vol. 311 (2006) p. 8.

70. Shamsi, A., Baltrus, J. P., Spivey, J. J., "Characterization of Coke Deposited on Pt/alumina Catalyst During Reforming of Liquid Hydrocarbons," Applied Catalysis A: General, Vol. 293 (2005) p. 145.

APPENDIX

A.1 Material Balances

The carbon that had been deposited onto the catalyst was calculated by integration of the instantaneous mass flow rate of CO_2 exiting the reactor:

$$C_{accumulation} = \frac{12\frac{g\,C}{mol\,C}}{44\frac{g\,CO_2}{mol\,CO_2}} \int \dot{m}_{CO_2}\,dt \qquad (12)$$

Where $\dot{m}_{CO_2}$ is the instantaneous mass flow rate of CO_2 exiting the reactor. This data was developed in Section 8.3.1. From the carbon mass balance, carbon accumulation is defined as:

$$C_{accumulation} = C_{in} - C_{out} \qquad (A1)$$

The carbon entering the reactor is calculated by the following equation:

$$C_{in} = \frac{14\frac{mol\,C}{mol\,C_{14}H_{30}} \cdot 12\frac{g\,C}{mol\,C}}{198.4\frac{g\,C_{14}H_{30}}{mol\,C_{14}H_{30}}} \dot{m}_{C_{14}H_{30}}\,t \qquad (A2)$$

The carbon exiting the reactor is calculated by the taking the integral average of the gas phase yield data:

$$C_{out} = \frac{C_{in}}{t} \int (Y_{CO} + Y_{CO_2} + Y_{CH_4})\,dt \qquad (A3)$$

where t is the time on stream. The mass balance is defined by the difference between carbon entering the reactor and the carbon which is exiting and has accumulated onto the catalyst surface by the following equation:

$$\text{Difference}\,(\%) = \frac{C_{in} - \left(C_{out} + C_{accumulation}\right)}{C_{in}} \cdot 100 \qquad \text{(A4)}$$

Table A1. Material balances from the isothermal reaction experiments in Section 7.3.

Catalyst	Run Duration (h)	Carbon Accumulation‡ (g)	Carbon In (g)	Gas Phase Carbon Out (g)	Difference (%)
$BaNi_{0.4}Al_{11.6}O_{19-\delta}$	5.7	0.059	25.0	24.3	2.7
$LaNi_{0.4}Al_{11.6}O_{19-\delta}$	5.5	0.141	24.3	22.7	5.9
$SrNi_{0.4}Al_{11.6}O_{19-\delta}$	5.8	0.062	25.3	24.9	1.3
$BaNi_{0.4}Al_{11.6}O_{19-\delta}$	99.4	-	436.4	419.9	3.8

‡Residual carbon present only on the surface of the catalyst.

A.2 Y_{Carbon} Residual Plots

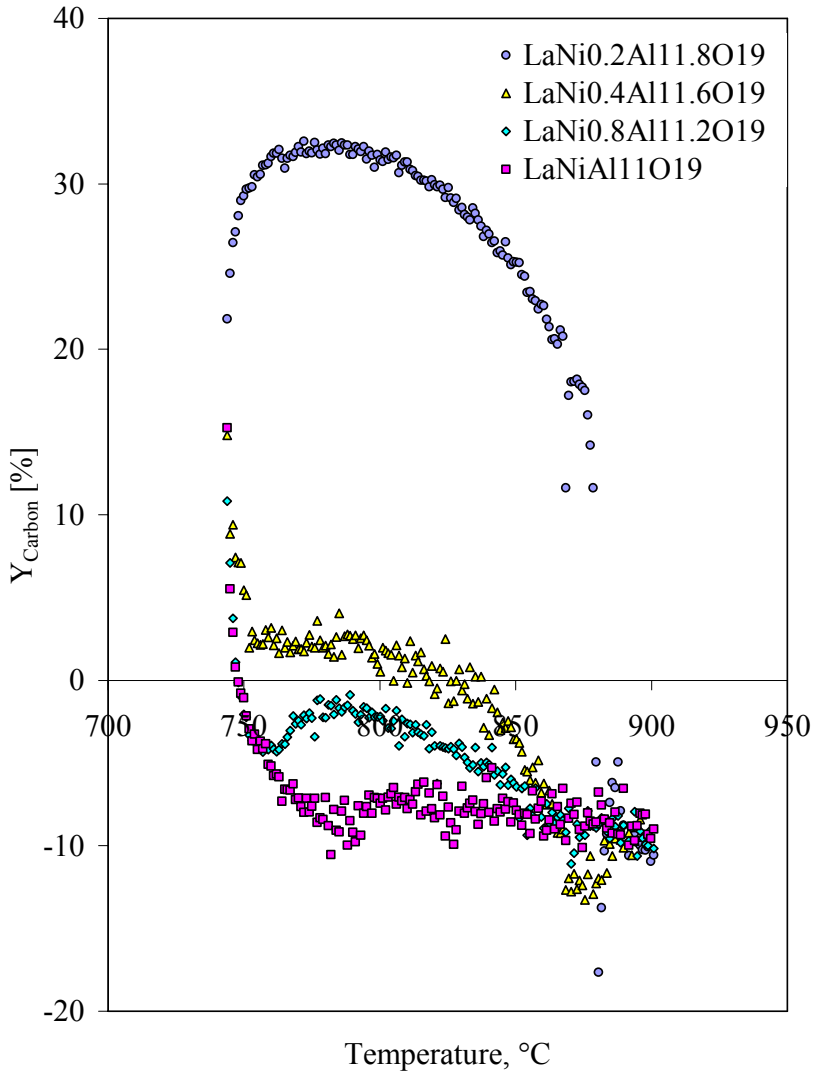

Figure A1. Y_{Carbon} residuals for the n-tetradecane temperature programmed reaction over $LaNi_yAl_{12-y}O_{19-\delta}$ series catalysts.

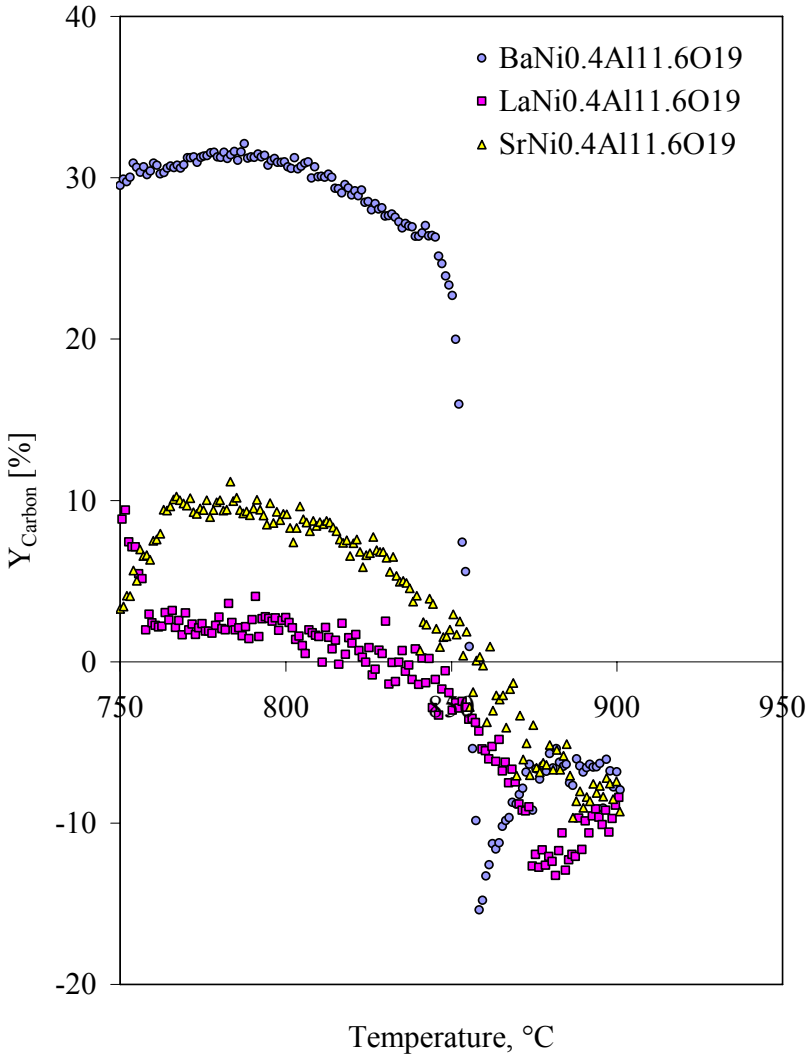

Figure A2. Y_{Carbon} residuals for the n-tetradecane temperature programmed reaction over $M_INi_{0.4}Al_{12-y}O_{19-\delta}$ series catalysts.

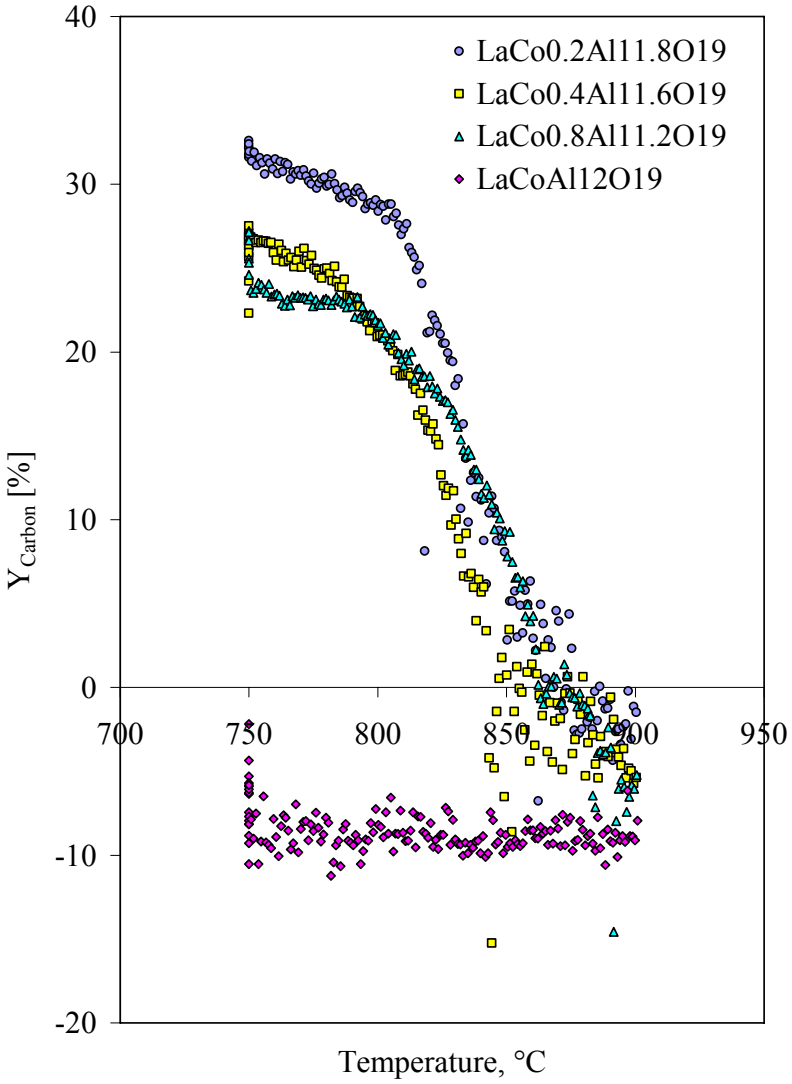

Figure A3. Y_{Carbon} residuals for the n-tetradecane temperature programmed reaction over $LaCo_yAl_{12-y}O_{19-\delta}$ series catalysts.

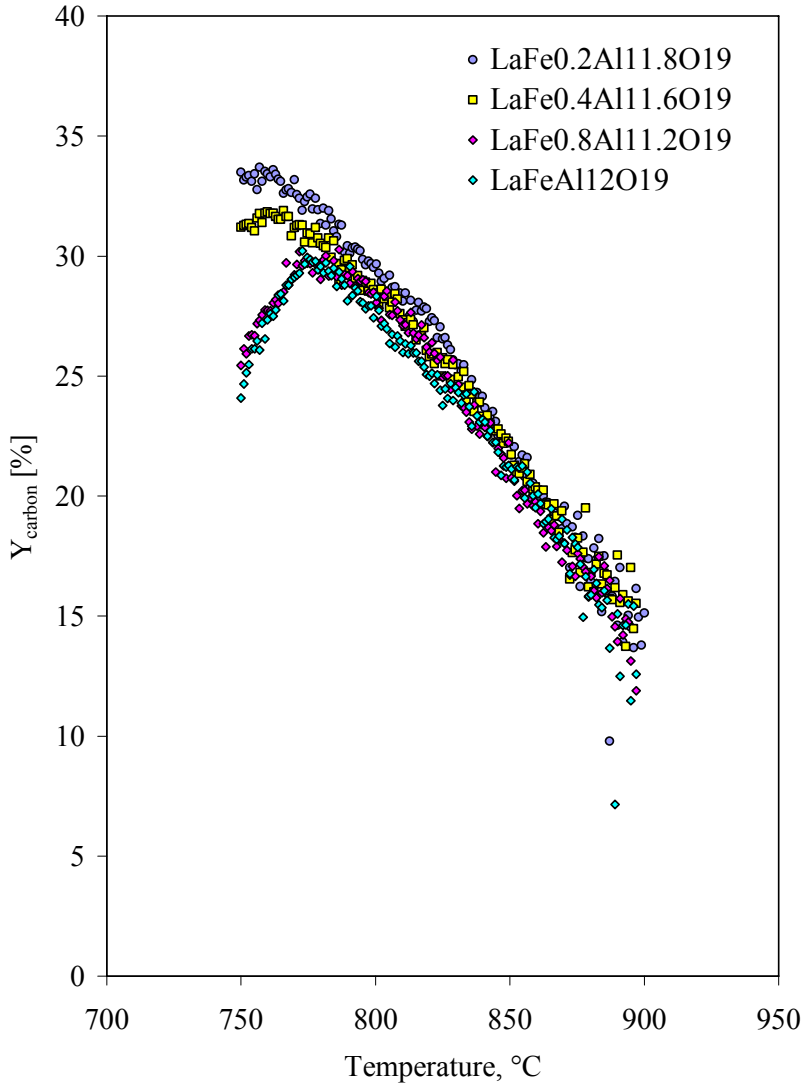

Figure A4. Y_{Carbon} residuals for the n-tetradecane temperature programmed reaction over $LaFe_yAl_{12-y}O_{19-\delta}$ series catalysts.

Sample Yield Calculations:

$$F_{T,o} = \frac{0.0201\frac{\text{Total mol in}}{\text{min}} \times 0.7961\frac{\text{mol } N_2 \text{in}}{\text{Total mol}}}{0.7230\frac{\text{mol } N_2 \text{out}}{\text{Total mol}}} = 0.0221\frac{\text{Total mol out}}{\text{min}}$$

$$Y_{H_2} = \frac{2 \times 0.0810\frac{\text{mol } H_2}{\text{Total mol}} \times 0.0221\frac{\text{Total mol out}}{\text{min}}}{30 \times 0.0217\frac{\text{mol n - } C_{14}H_{30}}{\text{Total mol}} \times 0.0201\frac{\text{Total mol feed in}}{\text{min}}} \times 100 = 27.4\%$$

$$Y_{CO} = \frac{0.0862\frac{\text{mol CO}}{\text{Total mol}} \times 0.0221\frac{\text{Total mol out}}{\text{min}}}{14 \times 0.0217\frac{\text{mol } C_{14}H_{30}}{\text{Total mol}} \times 0.0201\frac{\text{Total mol feed in}}{\text{min}}} \times 100 = 31.2\%$$

$$Y_{CO_2} = \frac{0.0972\frac{\text{mol } CO_2}{\text{Total mol}} \times 0.0221\frac{\text{Total mol out}}{\text{min}}}{14 \times 0.0217\frac{\text{mol } C_{14}H_{30}}{\text{Total mol}} \times 0.0201\frac{\text{Total mol feed in}}{\text{min}}} \times 100 = 35.2\%$$

$$Y_{CH_4} = \frac{0.0106\frac{\text{mol } CH_4}{\text{Total mol}} \times 0.0221\frac{\text{Total mol out}}{\text{min}}}{14 \times 0.0217\frac{\text{mol n - } C_{14}H_{30}}{\text{Total mol}} \times 0.0201\frac{\text{Total mol feed in}}{\text{min}}} \times 100 = 3.8\%$$

$$Y_{Carbon} = 100 - (Y_{CO} + Y_{CO_2} + Y_{CH_4}) = 100 - (31.2 + 35.2 + 3.8) = 29.8\%$$

Sample Dispersion Calculation:

$$\text{Dispersion} = \frac{4.84\ \text{ml}\ H_2\ (\text{ads})}{\text{g catalyst}} \times \frac{4.64 \times 10^{-3}\ \text{mol}\ H_2(\text{STP})}{\text{mL}\ H_2} \times \frac{2\ \text{mol H}}{1\ \text{mol}\ H_2} \times \frac{58.7\ \text{g Ni}}{\text{mol Ni}} = 0.025$$

Mass Spectrometer Calibration Data:

Calibration of the mass spectrometer was performed on 8/04/2006. The calibration was performed utilizing an automated calibration method within the 'Gas Works' software package which changes the relative sensitivity of the Faraday cup for each component of the calibration gases. After calibration the standards were re-analyzed on a normalized basis as a check of calibration.

Mass Spectrometer Calibration Report for 08/04/2006

Cal Gas Name	Gas	% in mix	Old calibration factor	New calibration factor	% Change	Standard Check	% error
FPL FUEL MIX	CO2	15.2	1.19868	1.19493	-0.31	15.1937	-0.04
FPL FUEL MIX	CH4	9.9	0.65252	0.65666	0.63	9.9114	0.11
FPL FUEL MIX	H2	9.85	0.50067	0.50298	0.46	9.8602	0.10
FPL FUEL MIX	N2	65.05	0.99050	0.9916	0.11	64.9700	-0.12
FPL Air	N2	78.08	0.98760	0.9898	0.22	78.0615	-0.02
FPL Air	O2	20.947	0.83631	0.83274	-0.43	20.9299	-0.08
FPL Air	Ar	0.934	1.52603	1.52842	0.16	0.9371	0.33
FPL CO	CO	9.66	1.08122	1.10229	1.95	9.685286	0.26
FPL CO	He	90.34	0.13905	0.1389	-0.11	90.22968	-0.12

Mass Flow Controller Calibration Data:

NETL Calibration Report
Mass Flow Meter / Controller

Calibration Date: October 18, 2005
Operator: S. Clingenpeel
Calibration Gas: N2
Process Gas: AIR
Test Data File: C:\Program Files\COMPASS for molbox\data\FTC-125\2005_291_000.dat
Project: B-25, Room 201 FPL

Device Under Test		Reference	
Manufacturer	BROOKS INSTRUMENT	Manufacturer	DH Instruments Inc.
Model	5850I	Model	Molbox1-AG
Tag/SN	FTC-125/SN: 0102090216762001	SN	398/884
ID	1204084/Inlet Press: 100 psig	ID	0000000119/1202431
Flow Range	0.000 to 2000.000 sccm @ 0.00C	Range	0-5000 sccm
Output Range	0.000 to 5.000 V		
Tolerance	1 %DUTFS		
Inlet Pressure	100 psig (+/- 2.5 psig)		

Calibration Data (As Found)

Ref Flow (sccm @ 0.00C)	DUT Flow (sccm @ 0.00C)	DUT Output (V)	%Rdg Error	%FS Error	Temp	Press (psi)
0.0000	1.240	0.0030	N/A	0.062	24.749	14.160
202.06	200.0	0.5000	-1.017	-0.103	24.770	14.790
402.80	399.8	0.9990	-0.745	-0.150	24.780	15.400
601.70	600.0	1.500	-0.283	-0.085	24.790	15.980
798.83	800.0	2.000	0.147	0.059	24.794	16.540
995.41	1000.	2.500	0.461	0.229	24.804	17.080
1191.3	1200.	3.000	0.727	0.433	24.814	17.600
1388.2	1400.	3.500	0.848	0.589	24.820	18.110
1585.9	1600.	4.000	0.889	0.705	24.830	18.620
1784.6	1800.	4.500	0.863	0.770	24.840	19.110
1979.2	1992.	4.981	0.665	0.658	24.847	19.580

DUT upstream of reference.
Inlet Pressure 100 psig (+/- 2.5 psig).
This "As-Found" data report matches the previous calibration inlet pressure and temperature parameters.

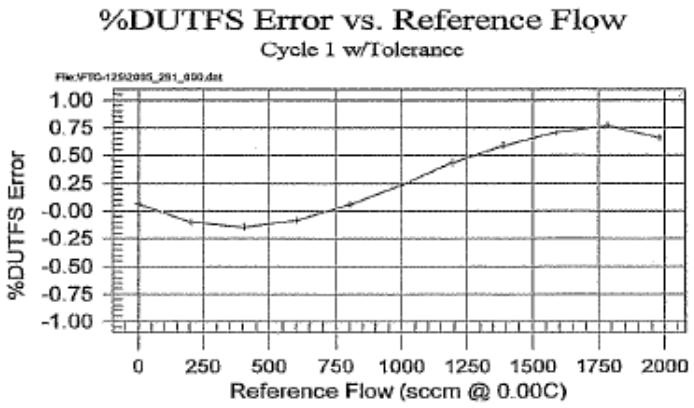

NETL Calibration Report
Mass Flow Meter / Controller

Calibration Date: October 18, 2005
Operator: S. Clingenpeel
Calibration Gas: N2
Process Gas: AIR
Test Data File: C:\Program Files\COMPASS for molbox\data\FTC-425\2005_291_001.dat
Project: B-25, Room 201 FPL

Device Under Test		Reference	
Manufacturer	BROOKS INSTRUMENT	Manufacturer	DH Instruments Inc.
Model	5850I	Model	Molbox1-AG
Tag/SN	FTC-425/SN: 0103100245067001	SN	398/884
ID	1204794/Inlet Press: 80 psig	ID	0000000119/1202431
Flow Range	0.000 to 2000.000 sccm @ 70.00F	Range	0-5000 sccm
Output Range	0.000 to 5.000 V		
Tolerance	1 %DUTFS		
Inlet Pressure	80 psig (+/- 2.5 psig)		

Calibration Data (As Left)

Ref Flow (sccm @ 70.00F)	DUT Flow (sccm @ 70.00F)	DUT Output (V)	%Rdg Error	%FS Error	Temp	Press (psi)
0.0000	0.000	0.000	N/A	0.000	24.369	14.160
205.65	200.5	0.5010	-2.516	-0.259	24.379	14.760
407.17	400.0	1.000	-1.762	-0.359	24.390	15.320
606.91	600.0	1.500	-1.139	-0.346	24.398	15.870
804.86	800.0	2.000	-0.604	-0.243	24.408	16.390
1002.0	1000.	2.500	-0.200	-0.100	24.419	16.890
1199.5	1200.	3.000	0.040	0.024	24.430	17.390
1397.6	1400.	3.500	0.172	0.120	24.439	17.870
1596.7	1600.	4.000	0.208	0.166	24.450	18.340
1707.9	1711.	4.277	0.169	0.145	24.459	18.600
1706.7	1709.	4.272	0.125	0.107	24.469	18.600

DUT upstream of reference.
Inlet Pressure: 80 psig (+/- 2.5 psig).
Full scale flow of 2000 sccm could not be achieved at 80 psig inlet pressure.

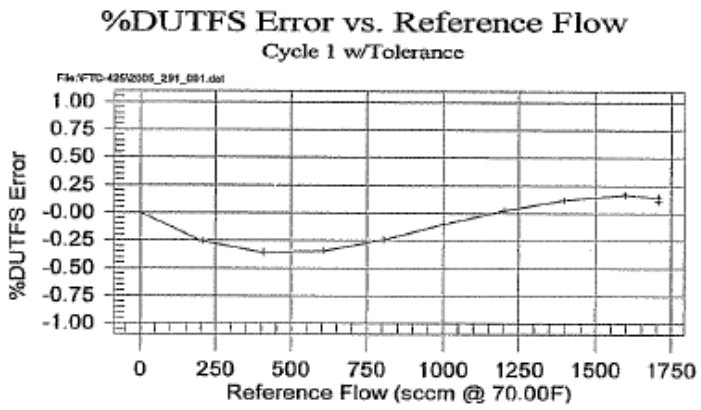

NETL Calibration Report
Mass Flow Meter / Controller

Calibration Date: October 18, 2005
Operator: S. Clingenpeel
Calibration Gas: N2
Process Gas: AIR
Test Data File: C:\Program Files\COMPASS for molbox\data\FTC-425\2005_291_000.dat
Project: B-25, Room 201 FPL

Device Under Test		Reference	
Manufacturer	BROOKS INSTRUMENT	Manufacturer	DH Instruments Inc.
Model	5850I	Model	Molbox1-AG
Tag/SN	FTC-425/SN: 0103100245067001	SN	398/884
ID	1204794/Inlet Press: 100 psig	ID	0000000119/1202431
Flow Range	0.000 to 2000.000 sccm @ 0.00C	Range	0-5000 sccm
Output Range	0.000 to 5.000 V		
Tolerance	1 %DUTFS		
Inlet Pressure	100 psig (+/- 5 psig)		

Calibration Data (As Found)

Ref Flow (sccm @ 0.00C)	DUT Flow (sccm @ 0.00C)	DUT Output (V)	%Rdg Error	%FS Error	Temp	Press (psi)
0.0000	0.4000	0.0010	N/A	0.020	23.541	14.160
204.16	200.1	0.5000	-2.000	-0.204	23.563	14.790
404.29	400.0	1.000	-1.062	-0.215	23.588	15.390
601.90	600.0	1.500	-0.316	-0.095	23.610	15.970
797.50	800.0	2.000	0.314	0.125	23.626	16.520
992.73	1000.	2.500	0.732	0.363	23.638	17.050
1187.6	1200.	3.000	1.041	0.618	23.660	17.570
1383.3	1400.	3.500	1.211	0.837	23.677	18.070
1578.9	1600.	4.001	1.359	1.073	23.699	18.570
1777.9	1800.	4.499	1.223	1.087	23.719	19.060
1947.8	1967.	4.917	0.974	0.949	23.740	19.470

DUT upstream of reference.
Inlet Pressure: 100 psig (+/- 5 psig).
This "As-Found" data report matches the previous calibration inlet pressure and temperature parameters.